

Chapter 1 Introduction

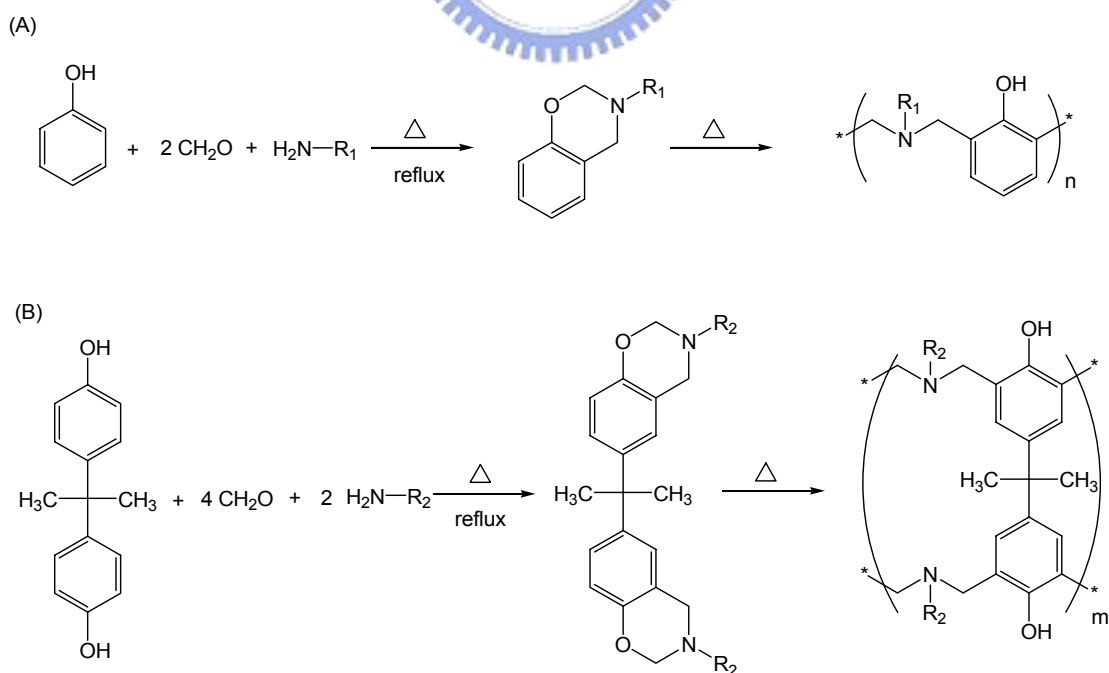
1.1 Overview on Benzoxazines and Polybenzoxazines (PBZZs)

The novel phenolic resins are based on benzoxazine structures, which were first synthesized by Holly and Cope [1]. These structures were not recognized as phenolic resin precursors until Schreiber [2] reported in 1973 that a hard and brittle phenolic material was formed from benzoxazine precursors. No further details about structures and properties were included. Riess *et al.* [3] studied synthesis and reactions of monofunctional heterocyclic compound of this kind at 1986. They found that only oligomer phenolic structures could be obtained because the thermo-dissociation of the monomer was always competing with the chain propagation. Polyfunctional benzoxazine monomer has been used as modifier for coating and encapsulation. Ning and Ishida [4] synthesized bifunctional benzoxazine precursor to overcome the low degree of cure of the compounds prepared by Riess *et al.* Furthermore, samples with high mechanical integrity were obtained, and the synthetic method consists of a few simple steps and can easily provide different phenolic structures with wide design flexibility.

1.1.1 Syntheses of Benzoxazines and Thermal Curing of Polybenzoxazines

In phenolic chemistry, both the ortho- and para- position on the benzene ring are reactive toward electrophilic substitution reactions due to the directing effect of the hydroxyl group. Benzoxazine, a class of heteroatomic ring compounds [5] derived from various phenols, formaldehyde, and primary amines, [1,6,7] are also deems to show multiple reactivities of the benzene ring due to directing effect of both the alkoxy and alkyl groups connected to the benzene ring as shown in Scheme 1-1. Benzoxazine polymerizes via a thermally induced ring-opening reaction that neither requires catalyst nor releases any condensation byproduct and form a phenolic-like

structure by a Mannich base bridge (-CH₂-NR-CH₂-) [8-10]. The free ortho- position on a benzoxazine benzene ring has been reported to have high reactivity toward thermal and phenol-initiated ring-opening polymerizations, forming a phenolic Mannich base polymer structure. Furthermore, the free para- position has also shown reactivity toward a similar type of polymerization [3,11]. Even the meta- positions are reactive under severe curing conditions, albeit with much less reactivity [12-14]. A systematic study of the regioselectivity of the benzoxazine benzene ring revealed quantitatively that both the free ortho- and the para- positions of the aromatic amine-based benzoxazine benzene ring showed high reactivities toward thermal polymerization, possibly resulting in a crosslinked structure. This result opened a new insight into the thermosetting benzoxazine field. In addition, the ring-opening polymerization can also be catalyzed by acidic catalysts that permit a wide curing temperature. In the presence of acidic catalysts [15], the curing temperature can be reduced from 160-220 °C to about 130-170 °C and increase the application range.



Scheme 1-1. The synthesis and thermal curing of (A) monofunctional benzoxazines and (B) difunctional benzoxazines

1.1.2 Features of Polybenzoxazines

In recent years, thermosetting PBZZs have been actively studied because of their excellent physical and mechanical properties and high thermal stability. These new materials, belonging to the addition-cure phenolics family were developed to combine the thermal properties and flame retardance of phenolics and the mechanical performance and molecular design flexibility of advanced epoxy systems. The PBZZs overcome several shortcomings of conventional novolac and resole-type phenolic resins, while retaining their benefits. PBZZ resins are expected to replace traditional phenolics, polyesters, vinyl esters, epoxies, cyanate esters and polyimides in many respects. [16] The molecular structure of PBZZ offers superb design flexibility that allows properties of the cured material to be controlled for specific requirements of a wide variety of individual requirements. The physical and mechanical properties of these new PBZZs are shown to compare very favorably with those of conventional phenolic and epoxy resins. The resin permits development of new applications by utilizing some of their unique features such as [8,17-19]:

- ◆ Near zero volumetric change upon polymerization
- ◆ No release of volatiles during curing
- ◆ Low melting viscosity (for benzoxazine)
- ◆ High glass transition temperature (T_g)
- ◆ High thermal stability (T_d)
- ◆ Low CTE
- ◆ Low water absorption
- ◆ Good mechanical properties
- ◆ Excellent electrical properties

1.2 Polymer Miscibility and Interactions

Polymer blend phase behavior can be predicted or analyzed by inserting the binary interaction model into the thermodynamic framework of either the Flory-Huggins theory or an appropriate equation-of-state theory. It is useful for evaluation of isothermal phase boundaries, miscibility maps, or phase separation by using the simplicity of the Flory-Huggins theory and equation-of-state. Recently, several polymer theoretical equations of state are available [21-23], and some have been applied to polymer solutions and blends [24-26]. However, the role of polymer interaction in determining the phase behavior of polymer blends is fascinating from a number of concentrations. Polymer interactions are usually meaning "strong," specific, and orientation dependent. In polymer blends, most it has been widely concerned with the following intermolecular or inter-segment forces:

- (a) Strong dipoles
- (b) Hydrogen bonds
- (c) Charge transfer complexes
- (d) Ionic interactions in ionomers



Although a few studies of miscibility in blends where polymer segments interact through charge transfer complexes and ionic forces have appeared, by far the most common and important systems involving strong interactions are (at the time of writing) those involving hydrogen bonds and/or strong dipole interactions. Hildebrand and Scott [27] considered that molecules with “dipoles capable of forming hydrogen bonds or bridges - are so exceptional in their behavior as to require separate consideration.” We concerned with miscibility in polymer mixtures that is a result of hydrogen bond formation.

Polymer miscibility is based on the assertion that the free energy of mixing can be

written in the following form:

$$\frac{\Delta G_m}{RT} = \frac{\Phi_A}{M_A} \ln \Phi_A + \frac{\Phi_B}{M_B} \ln \Phi_B + \chi \Phi_A \Phi_B + \frac{\Delta G_H}{RT} \quad (1-1)$$

The segmental interaction parameter χ is the “physical” interaction parameter and subscripts A and B refer to the blend components, while the ΔG_H term reflects free energy changes corresponding to specific interactions, most commonly, but not necessarily, hydrogen bonds. Nevertheless, hydrogen bonds are not easily characterized. There are two common experimental ways being able to characterized hydrogen bonds within polymers:

(a) *Thermodynamic*: Measurements depend upon thermodynamic changes in a system as a whole and can be related to molecular properties through the analyses of statistical mechanics, and these results are often model dependent and sensitive to he various assumptions that have to made.

(b) *Spectroscopic*: Spectroscopy techniques can aid in the evolution of miscibility, specifically when the interactions induce a change in the material physical properties (e.g. glass transition temperature); such as a change can be measured by radiative energy, including spectroscopy of solid-state or liquid nuclear magnetic resonance (NMR), Fourier-transform infrared spectroscopy (FT-IR), Raman, XPS and others.

1.3 Reference Review

1.3.1 Syntheses of various Benzoxazines and Polybenzoxazines

In **1994**, Ishida et al. [28] synthesized the B-m type benzoxazine and discussed the solvent effect on the precursor composition. The solvent polarity increase, the reaction between the benzoxazine structures and the free phenol structures becomes easier. Thus, there are less benzoxazine rings present at the end of the reaction, and the chance of forming oligomeric structures in the precursor becomes higher as the solvent polarity increase. Dimerization of benzoxazine of the same reaction nature had been documented in the literature [29]. It showed that we may able to control the extent of such reaction by adjusting the solvent polarity. Furthermore, the dioxane is the most suitable solvent for synthesizing benzoxazines and preventing the chance of forming oligomeric structures. In **2001**, Takeichi et al. [19] successfully prepared novel benzoxazine monomers containing a propargyl ether group as the cross-link site. Ring-opening polymerization of oxazine ring and cross-linking of propargyl ether group occurred at almost the same temperature range, with the exotherm maximum on DSC at 230 °C for monofunctional and 249 °C for bifunctional monomer. Polybenzoxazines derived from the novel monomers exhibited significantly improved thermal properties than the typical polybenzoxazines. The T_g of the novel polybenzoxazines increased by ca. 100-140 °C than the typical polybenzoxazines. The storage moduli of PP-appe and PB-appe were maintained constant up to temperature higher by ca. 100 °C than those of PP-a and PB-a. The onset of the decomposition by 5% weight loss was increased by ca. 20-40 °C than the typical polybenzoxazines. The char yield of the novel polymers increased by ca. 22-29% more than the typical polybenzoxazines, suggesting the superior thermal stability of the novel polybenzoxazine. In **2003**, Takeichi et al. [30] synthesized two novel benzoxazine

monomers containing allyl groups: 3-allyl-3,4-dihydro-2H-1,3-benzoxazine (P-ala) and bis(3-allyl-3,4-dihydro-2H-1,3-benzoxazinyl)isopropane (B-ala). Their DSC exhibit two exotherms at ca. 145 °C and at ca. 220 °C which correspond to allyl and oxazine thermal polymerization, respectively. Both monomers undergo thermal cure with the formation of thermosets having excellent thermomechanical properties. These thermosets exhibit higher T_g (ca. 300 °C), maintain their storage moduli at higher temperature, and have better thermal stability than the corresponding polybenzoxazines without allyl groups.

1.3.2 Polymer Blending of Polybenzoxazines

In 2001, Takeichi et al. [31] reported that phase separation occurred when a B-a type benzoxazine monomer was blended with soluble poly(imide-siloxane)s with and without pendent hydroxyl groups (structures PISi-OH and PISi, respectively) were prepared from the reaction 2,2'-bis(3,4-dicarboxylphenyl)hexafluoropropane dianhydride with α,ω -bis(aminopropyl)dimethylsiloxane oligomer (PDMS; molecular weight=5000) and 3,3'-dihydroxybenzidine or 4,4'-diaminodiphenyl ether. The presence of poly(imide-siloxane)s lowered the temperature for the ring opening reaction of benzoxazine. For a blend of benzoxazine with PISi(OH), one T_g was observed in a high-temperature range and one T_g was observed in a lower temperature range due to PDMS. The appearance of only one T_g in a high-temperature range was due to the formation of an AB-crosslinked polymer between polybenzoxazine and PISi(OH). However, for PISi two T_g 's were observed in a high-temperature range due to the phase separation between polybenzoxazine and poly(imide-siloxane) because of the formation of a semi-IPN. In both cases, T_g in a high temperature range due to polybenzoxazine increased with the incorporation of a small amount of

poly(imidesiloxane)s. The tensile modulus decreased and the elongation increased inversely with increased poly(imide-siloxane)s content, showing the toughening effect of the incorporated poly(imide-siloxane). The thermal stability of polybenzoxazine was enhanced with increased poly(imide-siloxane) content. In **2002**, Ishida et al. [32] studied the hydrogen-bonded network structure for polybenzoxazines is investigated by FT-IR with model dimer systems. It is shown that the simpler structures of asymmetric dimers well simulate the hydrogen bonded network structure between polymer chains while the structures of symmetric dimers reflect the hydrogen bonding scheme related to the end-groups of polymer chains. It is confirmed that the amine functional group in the Mannich bridge is greatly responsible for the distribution of hydrogen bonding species. Bisphenol A/methylamine-based polymer (B-m) mainly consists of $\text{—OH} \cdots \text{N}$ intramolecular hydrogen bonding while bisphenol A/aniline-based polymer (B-a) has a large amount of intermolecular hydrogen bonding and relatively weak hydrogen bonding groups in the polymer network structure.

In **2001**, Ishida et al. [33] studied the polymer blends composed of polybenzoxazine and poly(ϵ -caprolactone) (PCL). Hydrogen-bond formation between the hydroxyl groups of polybenzoxazine and the carbonyl groups of PCL was evident from the FTIR spectra. Only one glass transition temperature (T_g) value was found in the composition range (low PCL content) investigated, and the T_g value of the resulting blend appeared to be higher in the blend with a greater amount of PCL. In **2003**, Zheng et al. [34] studied the polymer blends composed of polybenzoxazine and poly(ethylene oxide) (PEO). Before curing, the B-a/PEO blends displayed the single and composition-dependant glass transition temperatures in the entire blend composition, and the equilibrium melting point depression was also observed in the

blends. The miscibility was mainly ascribed to the contribution of entropy to mixing free energy since the molecular weight of B-a type benzoxazine is rather low. However, phase separation occurred after curing reaction at the elevated temperature, which was confirmed by differential scanning calorimetry (DSC) and scanning electronic microscopy (SEM). Furthermore, the investigation by FTIR spectra via model compounds indicates that the phenolic hydroxyl groups could not form the favorable intermolecular hydrogen bonding interactions at the elevated temperatures (e.g. the curing temperatures), i.e. the phenolic hydroxyl groups existed mainly in the non-associated form in the system.



References

- [1] Holly, F. W.; Cope, A. C. *J. Am. Chem. Soc.* **1944**, *66*, 1875.
- [2] Scheriber, H. Ger, *Offen.* 2225504, **1973**; *Offen.* 2323936, **1973**.
- [3] Riess, G.; Schwob, J. M.; Guth, G.; Roche, M.; Lande, B. in “Advances in Polymer Science” (Eds B. M. Culbertson and J. E. Mcgrath), Plenum, New York, **1986**.
- [4] Ning, X.; Ishida, H. *J. Polym. Sci., Polym. Phys. Ed.* **1994**, *32*, 921.
- [5] Ishida, H. *J. Appl. Polym. Sci.* **1995**, *58*, 1751.
- [6] Burke, W. J.; Murdoch, K. C.; Ec, G. *J. Am. Chem. Soc.* **1954**, *76*, 1677.
- [7] Burke, W. J.; Glennie, E. L. M.; Weatherbee, C. *J. Org. Chem.* **1964**, *24*, 909.
- [8] Ishida H, Sanders DP. *Macromolecules* **2000**, *33*, 8149.
- [9] Laobuthee A, Chirachanchai S, Ishida H, Tashiro K. *J. Am. Chem. Soc.* **2001**, *123*, 9947.
- [10] Dunkers, J.; Ishida, H. *J. Polym. Sci. Part A: Polym. Chem.* **1999**, *37*, 1913.
- [11] Shen, S. B.; Ishida, H. *J. Appl. Polym. Sci.* **1996**, *61*, 1595.
- [12] Cid, J. A.; Wang, Y. X.; Ishida, H. *Polym. Polym. Comp.* **1999**, *7*, 409.
- [13] Russel, V.; Koenig, J. L.; Low, H. Y.; Ishida, H. *J. Appl. Polym. Sci.* **1998**, *70*, 1401.
- [14] Russel, V.; Koenig, J. L.; Low, H. Y.; Ishida, H. *J. Appl. Polym. Sci.* **1998**, *70*, 1413.
- [15] Dunkers, J.; Ishida, H. *J. Polym. Sci. Part A: Polym. Chem.* **1999**, *37*, 1913.
- [16] Nair, C. P. R. *Prog. Polym. Sci.* **2004**, *29*, 401.
- [17] Ishida, H.; Rodriguez, Y. *Polymer* **1995**, *36*, 3151.
- [18] Ishida, H.; Low, H. Y. *Macromolecules* **1997**, *30*, 1099.
- [19] Agag, T.; Takeichi, T. *Macromolecules* **2001**, *34*, 7257.

- [20] Flory, P. J.; Orwoll, R. A.; Vrij, A. *J. Am. Chem. Soc.* **1964**, *86*, 3515.
- [21] Sanchez, I. C.; Lacombe, R. H. *J. Polym. Sci.: Polym. Lett. Ed.* **1977**, *15*, 71.
- [22] Dee, G. T.; Walsh, D. J. *Macromolecules* **1988**, *21*, 811.
- [23] Nies, E.; Stroecks, A. *Macromolecules* **1990**, *23*, 4088.
- [24] Flory, P. J. *J. Am. Chem. Soc.* **1965**, *87*, 1833.
- [25] Sanchez, I. C.; Lacombe, R. H. *Macromolecules* **1978**, *11*, 1145.
- [26] Jain, R. K.; Simha, R. *Macromolecules* **1984**, *17*, 2663.
- [27] Hildebrand, J. H.; Scott, R. L. *The Solubility of Nonelectrolytes*, 3rd Edition, American Chemical Society Monograph Series, **1950**.
- [28] Ning, X.; Ishida, H. *J. Polym. Sci., Part A: Polym. Chem.* **1994**, *32*, 1121.
- [29] Burke, W. J.; Glennie E. L. M.; Bauer W. N. Jr. *J. Org. Chem.* **1965**, *30*, 3423.
- [30] Agag, T.; Takeichi, T. *Macromolecules* **2003**, *36*, 6010.
- [31] Takeichi, T.; Agag, T.; Zeidam, R. *J. Polym. Sci., Part A: Polym. Chem.* **2001**, *39*, 2633.
- [32] Kim, H. D.; Ishida, H. *J. Phys. Chem. A* **2002**, *106*, 3271.
- [33] Ishida, H.; Lee, Y. H. *J. Polym. Sci., Part B: Polym. Phys.* **2001**, *39*, 736.
- [34] Lu, H.; Zheng, S. *Polymer* **2003**, *44*, 4689.

Chapter 2

2.1 Overview on Low Dielectric Constant Materials for IC Applications

Continuing improvement in device density and performance has significantly impacted the feature size and complexity of the wiring structure for on-chip interconnects. As the minimum device dimensions reduce beyond 250 nm, the increase in propagation delay, crosstalk noise and power dissipation of the interconnect structure become limiting factors for ultra-large-scale integration (ULSI) of integrated circuits [1-3]. The impact due to interconnect scaling on performance can be examined by evaluating the RC delay of multilevel interconnects. While interconnect dimensions continue to decrease with scaling, the RC delay will increase approximately with the square of the scaling factor, assuming that the materials of the interconnect remain the same. As scaling proceeds beyond the 250-nm node [4], the interconnect delay will exceed the gate delay of the microprocessor assuming no change in the system architecture. There are other scaling issues, including increase in crosstalk noise and power dissipation, which will further degrade the interconnect performance. The increase in the number of metal layers to meet the increase in wiring requirements due to scaling presents additional concerns of manufacturing yield and cost for future interconnects.

Another important factor that governs the speed of integrated circuits is the resistance of interlayer metal. Table 2-1 lists the electrical resistivity of different metals [2]. It is apparent that copper has much lower resistivity than that of aluminum. Considering this situation, semiconductor industries have been fully transitioning toward using Cu instead of Al in IC applications for many years.

As semiconductor technology advances, both the speed and packing density of chips steadily increase with greater integration of functionality. As a result, the R and

C of the interconnect structure rise dramatically with smaller metal lines and reduced wire spacing. The global interconnect RC delay becomes the limiting factor to overcome, issue such as noise tolerance, power dissipation, and electro-migration become increasingly important and must be tackled [5]. The time, which is related to the resulting signal delay is given by equation (2-1).

$$\tau = RC \quad (2-1)$$

and call the RC the time delay of signals. R is the line resistance and C is the line capacitance of the used structure. Furthermore, Equation (2-2) can be used to estimate the RC delay.

$$RC = 2\rho\varepsilon\varepsilon_0\left(\frac{4L^2}{P^2} + \frac{L^2}{T^2}\right) \quad (2-2)$$

R : total line resistance, C : total line capacitance, ρ : metal resistivity, ε : dielectric constant, ε_0 : permittivity of free space, L : line length, P : the distance between two conducting lines, T : metal thickness.

To reduce the number of metal layers, one must reduce R and C through the introduction of new materials. New interconnected metals, such as copper, help to lower resistivity, while low k materials assist in reducing capacitance C . Since copper is about 35% lower in resistivity than aluminum, replacing aluminum with copper will reduce the RC delay by approximately 35 %. Changing the dielectric from SiO_2 ($k \sim 4$) to a relatively ideal low k dielectric ($k \sim 2$) can reduce the capacitance by 50 %. Combined with changing aluminum to copper, chip speeds can operate approximately three times faster. Therefore, that is why so many researches have been done in order to reduce the dielectric constant value of materials after replacing the aluminum process with copper process.

Table 2-1. Electrical Resistivities of Metals

Metal	Melting point (°C)	Resistivity (ρ) at 293 K ($10^{-8} \Omega\text{m}$)
Tungsten (W)	3422	5.28
Aluminum (Al)	660	2.65
Copper (Cu)	1084	1.678
Silver (Ag)	961	1.587

2.1.1 Requirements for interlayer and intermetal dielectrics

Since the reduction of RC delay can be achieved by introducing a low permittivity polymer into the interconnected structure. Heat resistant, nonpolar or slightly polar polymers are potential candidates for IMD in future devices. Therefore, many polymers have been investigated to prove their utility as IMD materials. The dielectric constant of the investigated polymers runs from $k=3.6$ for common low-stress polyimides to $k=1.9$ in the case of poly(tetrafluoroethylene) as demonstrated in Table 2-2.

In addition to dielectric constant and thermal stability, there are a large number of additional issues, which must be addressed before a new material can be used as intermetal dielectric [7]. These important issues include moisture uptake, purity, adhesion to Si, SiO₂, Al, Cu and other inorganic materials, planarization behavior, plasma etching behavior and others. And these requirements for low dielectric constant polymers are summarized in Table 2-3.

Table 2-2. Dielectric Constant of Some Low k Polymer Materials [6]

Polymer	Dielectric constant
Nonfluorinated aromatic polyimide ^a	3.2-3.6
Fluorinated polyimide ^b	2.6-2.8
Poly(phenyl quinoxaline) ^b	2.8
Poly(acrylene ether oxazole) ^b	2.6-2.8
Poly(arylene ether) ^b	2.9
Poly(benzoxazole) ^b	2.6-3.0
Poly(quinoline) ^b	2.8
Silisesquioxane ^b	2.8-3.0
Divinysiloxane-benzocyclobutane ^b	2.7
Polyindane ^b	2.6
Parylene N ^a	2.6
Poly(norbornene) ^b	2.4
Perfluorocyclobutane ^b	2.4
Fluorinated (arylene ether) ^b	2.4-2.7
Poly(naphthalene) N ^a	2.4
Parylene AF ^a	2.2
Poly(naphthalene) F ^a	2.2
Poly(tetrafluoroethylene) ^a	1.9
Teflon ^a	1.9

^aCVD depositable

^bOnly spin-on depositable

Table 2-3. Properties Required for New Intermetal Dielectrics [1-3,7]

Property	Value
Dielectric constant	< 3 (preferably <2.5)
Dissipation factor at 1 MHz	< 0.005
Thermal stability: 1% weight loss in N ₂ atmos.	> 425°C
Moisture absorption	< 1%
Adhesion (to metal, self-adhesion)	Pass tape test after thermal cycles to 450°C
Coefficient of thermal expansion	< 50 ppm
Resistance to solvents, photoresist strippers	
Etch rate	> 3 nm/s
Etch selectivity	Oxygen plasma resistance
Stress	< ±100 MPa
Gap-fill	No voids at 0.35 μm, aspect ratio = 2
Planarization	> 80% (regional)
Tensile modulus	> 1 GPa
Tensile strength	> 200 MPa
Elongation-at-break	> 5%
T _g	> 400°C
Reliability of metal, when surrounded by dielectric material	
Non-corrosive	
Crack free	
Environmental, health, safety	
Thermal conductivity	
Thickness uniformity within wafer (3σ)	< 10%
Thickness uniformity wafer to wafer (3σ)	< 5%
Cost at 4–7% solids content	< 1.2 \$/g
Metal content	ppb level
Shelf life	6 Months
Thermal shrinkage after curing	< 2.5%
Gas and moisture permeability	
Hardness	
Density	
Dielectric breakdown	> 1 MV/cm
Step coverage	> 80%
Number of particles >0.3 μm	< 0.08/cm ²
Throughput	
CMP compatibility	
Transmission at 300 nm	

2.1.2 Dielectric Constant and Bonding Characteristics

Fluorinating polymers and forming porous structures are two major directions that have been followed in the course of developing materials that have low dielectric constant materials [1,8-10]. First, it is necessary to either incorporate atoms and bonds that have a lower polarizability, or else to lower the density of atoms and bonds in the material, or both in order to reduce the k value of materials [11]. With regard to the first effect, there are several components to the polarizability that must be minimized in reducing the dielectric constant. The polarization components usually considered are the electronic, atomic, and orientational responses of the material. The latter two components constitute the nuclear response and are important at lower frequencies ($< 10^{13} \text{ s}^{-1}$), while the electronic response dominates at higher frequencies. At typical device operating frequencies, currently 10^9 to 10^{10} s^{-1} , all three components contribute to the dielectric constant, and should be minimized for optimum performance.

Some typical electronic polarizabilities and the associated bond enthalpies are shown in Table 2-4. The data indicates that single C–C and C–F bonds have the lowest electronic polarizability, making fluorinated and nonfluorinated aliphatic hydrocarbons potential candidates for low k application. Incorporation of fluorine atoms is particularly effective in lower the polarizability due to their high electronegativity, which leads to tight binding of electrons. Conversely, the higher electronic polarizability results in less tightly bound electrons. For example, materials containing a large number of carbon double and triple bonds can be expected to have a large polarization due to the increased mobility of the π electrons. Conjugated carbon double bonds in aromatic structures are a common source of extensive electron delocalization leading to higher electronic polarizability.

Table 2-4. Electronic Polarizability and Bond Enthalpies [8]

Bond	Polarizability (\AA^3) ^a	Ave. bond energy (kcal/mole) ^b
C—C	0.531	83
C—F	0.555	116
C—O	0.584	84
C—H	0.652	99
O—H	0.706	102
C=O	1.020	176
C=C	1.643	146
C≡C	2.036	200
C≡N	2.239	213

2.1.3 Porous Low Dielectric Materials

Since the dielectric constant of gases is not much different from that of vacuum ($k \sim 1$); the incorporation of free space or pores is an attractive approach to decrease the dielectric constant of films. This is done on a submolecular level by using bulky groups such as fluorenyl in the repeating units of polymers to decrease packing density and increase free volume [1,11,12]. Increment tables for calculation of dielectric constants indicate that this should result in lower dielectric constants.

Foamed films with pores in the 10 nm range have been successfully demonstrated to exhibit quite low dielectric constants. Aerogels or xerogels with SiO₂ as matrix with porosities above 90% and dielectric constants close to 1 have been reported [13-17]. However, large volumes of solvent must be removed to obtain such extremely porous structures. Since the pores must not be interconnected, the diffusion of the solvent or solvent vapor has to proceed through the matrix material. Control of

the process without shrinkage and formation of macroscopic cracks is quite difficult. To be used for interconnect fabrication for circuits with minimum feature sizes below 250 nm (preferably below 100 nm to ensure future applicability of the processes and materials), the pores should not be much larger than 10 nm in diameter. In addition, they should be regular with a narrow size distribution, and they must not be interconnected. A rather intriguing methodology was developed by a group at IBM Almaden Research Center. This approach takes advantage of the phase separation of block copolymers, which results in the formation of spherical domains of the minor component at certain compositions under appropriate conditions of films formation [18-21]. To this end, polyimides or poly(phenylquinoxaline)s with thermally labile blocks or grafts from poly(propylene oxide) [18,22,23], poly(methyl methacrylate) [18], polystyrene [24], poly(α -methylstyrene) [25], and polyesters [26] were prepared. Up to 30% (volume fraction) of the labile blocks were incorporated into the films. Carefully heating the films result in degradation of the thermally labile blocks, which leave pores behind which ideally are identical in shape and volume to the space previously occupied by the labile polymer blocks. The greatest challenge in the future will be to reduce the pore size at an even distribution while maintaining the strength within a range acceptable for mechanical and electronic applications.

2.2 Overview on Cyclodextrins

2.2.1 Structural Features of Cyclodextrins

Cyclodextrins (CDs) are a family of naturally occurring, water-soluble oligosaccharides forming a bucket-shaped macrocycle and made up of glucopyranose units, which adopt a 4C_1 chair conformation. The most common members which are produced on an industrial scale contain six, seven, or eight units and are named α -, β -, and γ -CDs, respectively [27-29]. The three major cyclodextrins are crystalline, homogeneous, nonhygroscopic substance, which are torus-like macro-rings. The α -cyclodextrin (Schardinger's α -dextrin, cyclomaltohexaose, cyclohexaglucan, cyclohexaamylose, α -CD, ACD, C6A) comprises six glucopyranose units, β -CD (Schardinger's β -dextrin, cyclomaltoheptaose, cycloheptaglucan, cycloheptaamylose, β -CD, BCD, C7A) comprises seven such units, and γ -CD (Schardinger's γ -dextrin, cyclomaltooctaose, cyclooctaglucan, cyclooctaamylose, γ -CD, GCD, C8A) comprises eight such units. The most important characteristics of the CDs are summarized in Table 2-5 [30]. The practically important, industrially produced CDs are α -, β -, and γ -CDs.

As a consequence of the conformation of the glucopyranose units, all secondary hydroxyl groups are situated on one of the two edges of the ring, whereas all the primary ones are placed on the other edge. The ring, in reality, is a cylinder, or better said a conical cylinder, which is frequently characterized as a doughnut or wreath-shaped truncated cone. The cavity is lined by the hydrogen atoms and the glycosidic oxygen bridges, respectively. The nonbonding electron pairs of the glycosidic oxygen bridges are directed toward the inside of the cavity producing a high electron density there and lending to it some Lewis base characteristics.

The C_2 -OH group of one glucopyranoside unit can form a hydrogen bond with

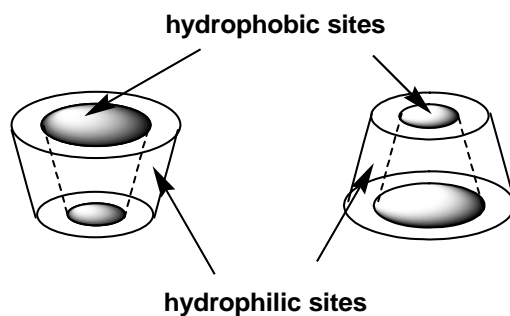
the C₃-OH group of the adjacent glucopyranose unit. In the CD molecule, a complete secondary belt is formed by these H bonds, therefore, the β-CD is a rather rigid structure. This intramolecular hydrogen bond formation is probably the explanation for the observation that β-CD has the lowest water solubility of all CDs. The hydrogen-bond belt is incomplete in the α-CD molecule, because one glucopyranose unit is in a distorted position. Consequently, instead of the six possible H-bonds, only four can be established fully. The γ-CD is a noncoplanar, more flexible structure, therefore, it is the most soluble of the three CDs.

Scheme 2-1 shows a sketch of the characteristic structural features of CDs. On the side where the secondary hydroxyl groups are situated, the diameter of the cavity is larger than on the side with the primary hydroxyls, since free rotation of the latter reduces the effective diameter of the cavity. The approximate dimensions of CDs are shown schematically in Scheme 2-2. The driving force of the complex formation, the substitution of the high enthalpy water molecules in the CD cavity, is weaker in the case of larger CDs, therefore, their utilization as inclusion complexing agents will probably remain rather restricted.

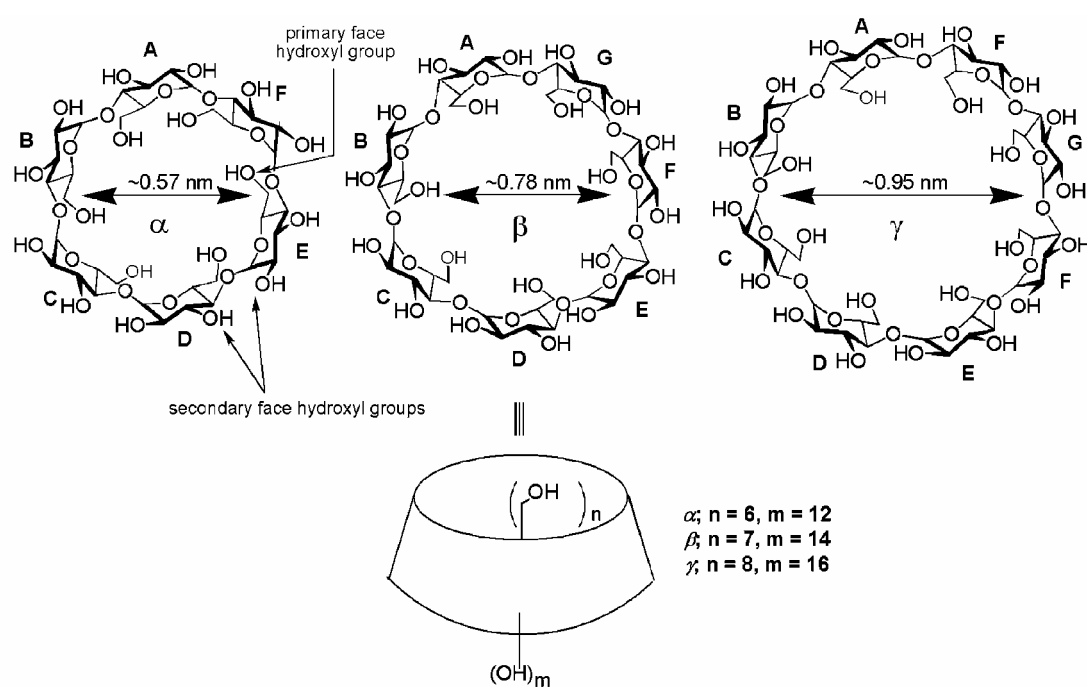
Table 2-5. Characteristics of α-, β-, and γ-CDs [30]

	α	β	γ
no. of glucose units	6	7	8
mol wt	972	1135	1297
solubility in water, g 100 mL ⁻¹ at room temp	14.5	1.85	23.2
[α] _D 25 °C	150 ± 0.5	162.5 ± 0.5	177.4 ± .5
cavity diameter, Å	4.7–5.3	6.0–6.5	7.5–8.3
height of torus, Å	7.9 ± 0.1	7.9 ± 0.1	7.9 ± 0.1
diameter of outer periphery, Å	14.6 ± 0.4	15.4 ± 0.4	17.5 ± 0.4
approx volume of cavity, Å ³	174	262	427
approx cavity volume in 1 mol CD (ml)	104	157	256
in 1 g CD (ml)	0.10	0.14	0.20
crystal forms (from water)	hexagonal plates	monoclinic parallelograms	quadratic prisms
crystal water, wt %	10.2	13.2–14.5	8.13–17.7
diffusion constant at 40 °C	3.443	3.224	3.000
hydrolysis by <i>A. oryzae</i> α-amylase	negligible	slow	rapid
V _{max} value, min ⁻¹	5.8	166	2300
relative permittivity (on incorporating the toluidinyl group of 6- <i>p</i> -toluidinyl naphthalene 2-sulfonate) at pH = 5.3, 25 °C	47.5	52.0	70.0
(on incorporating the naphthalene group)	^a	29.5	39.5
pK (by potentiometry) at 25 °C	12.332	12.202	12.081
partial molar volumes in solution mL mol ⁻¹	611.4	703.8	801.2
adiabatic compressibility in aqueous solutions mL (mol ⁻¹ bar ⁻¹) × 10 ⁴	7.2	0.4	-5.0

^a Naphthalene group is too bulky for the α-CD cavity.



Scheme 2-1. Schematic representation of the hydrophobic and hydrophilic regions of a CD cylinder.

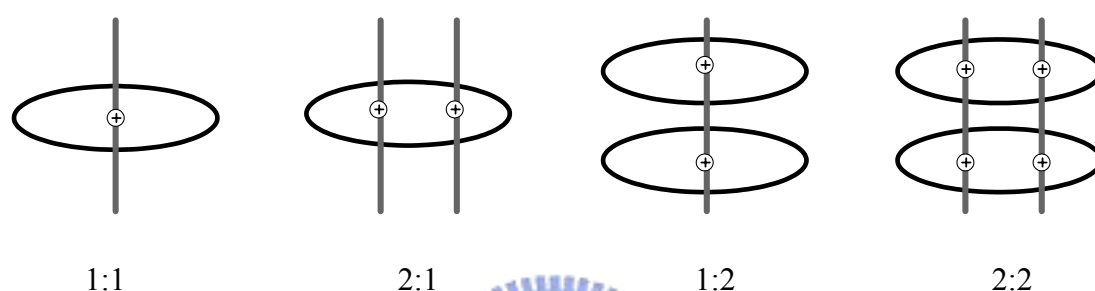


Scheme 2-2. Schematic representations of the most commonly encountered CDs

2.2.2 CD Inclusion Complexes

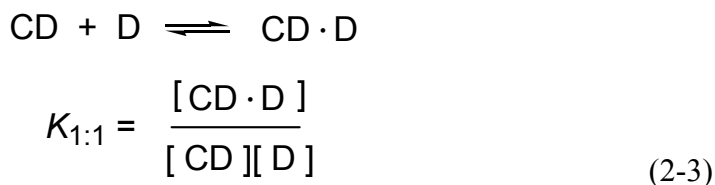
In an aqueous solution, the slightly apolar cyclodextrin cavity is occupied by water molecules which are energetically unfavored (polar-apolar interaction), and therefore can be readily substituted by appropriate “guest molecules” which are less polar than water. The dissolved cyclodextrin is the “host” molecule, and the “driving

force” of the complex formation is the substitution of the high-enthalpy water molecules by an appropriate “guest” molecule. One, two, or three cyclodextrin molecules contain one or more entrapped “guest” molecules. Most frequently the host:guest ratio is 1:1, and this is the essence of “molecular encapsulation”. It is the simplest and most frequent case. However, 2:1, 1:2, 2:2, or even more complicated associations, and higher order equilibria exist, almost always simultaneously as shown in Scheme 2-3 [31].



Scheme 2-3. Schematic representations of various host-guest stoichiometries

Furthermore, the formed inclusion complexes can be isolated as stable crystalline substances. Upon dissolving these complexes, an equilibrium is established between dissociated and associated species, and this is expressed by the complex stability constant K_a . The association of the CD and guest (D) molecules, and the dissociation of the formed CD/guest complex is governed by a thermodynamic equilibrium.



2.2.3 Two Types of Crystal Structures: Channel-type and Cage-type

CDs are easily dissolved in water and crystallize with their cavities filled only by water molecules. For the crystallization of an inclusion complex of a CD, one has to add the guest molecule in many fold molar excess to form the complex because the dissociation constants are in the molar to minimum molar range, indicating weak affinities. If CDs are crystallized either as hydrate or as inclusion complex, the molecules are arranged within the crystal lattice in one of two modes described as cage and channel structures according to the overall appearance of the formed cavities [32,33].

(a) Channel-Type Structures [33-34]

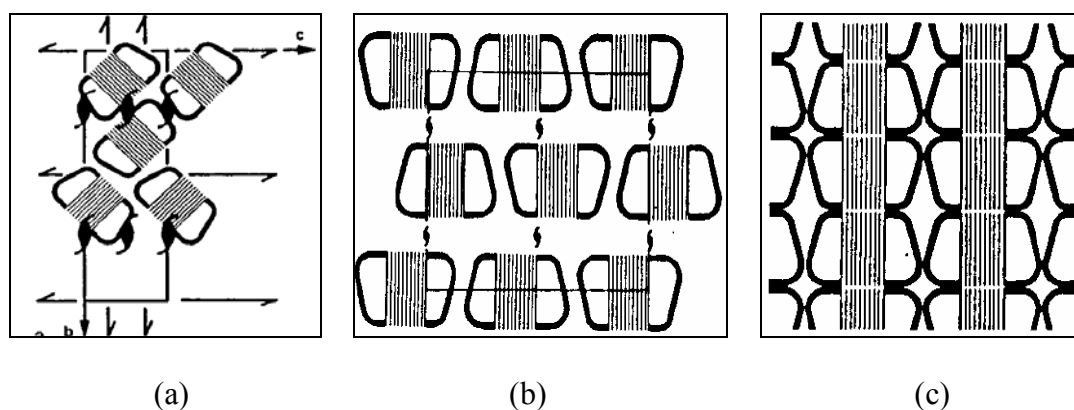
In channel-type complexes, CD molecules are stacked on top of each other like coins in a roll, and the now linearly aligned cavities form “infinite” channels in which the guest molecules are embedded (Scheme 2-4c). The stacks of CD are stabilized by hydrogen bonds either between O₂-H/O₃-H and O₆-H sides producing head-to-tail patterns, or between O₂-H/O₃-H and O₂-H/O₃-H on one side and between O₆-H and O₆-H on the other side leading to head-to-head arrangement. In general, in one particular crystal structure only one type of stack is formed. In γ -CD complexed with small organic molecules, however, a unique situation is encountered because head-to-tail and head-to-head orientations alternate within the same stack, with three stacked γ -CD molecules forming the repeating unit along the stack axis. Another related packing motif is frequently observed with β -CD in which the stack consists of β -CD dimers hydrogen bonded with their O₂-H/O₃-H sides. They form basket-like units in which guest molecules are accommodated. The dimers are then stacked and interact with their O₆-H sites to form the channel structure. It goes without saying that the channels are not always straight, and frequently the individual CD molecules are

tilted with respect to the channel axis. Only in cases where a crystallographic symmetry axis coincides with the channel axis the CD macrocycle is exactly perpendicular to the channel (symmetry) axis.

2. Cage-Type Structures in Herringbone and Brick Motifs [33-34]

In crystal structures belonging to the cage type, the cavity of one CD molecule is blocked off on both sides by adjacent CDs, thereby leading to isolated cavities in which the guest molecules are not in contact with each other. With the cage-type structures, two different categories are encountered, depending on the packing of the CD molecules. In one, CDs are packed crosswise in herringbone fashion, Scheme 2-4a; this packing motif is observed for α -CD to δ -CD if cocrystallized with water, and if α -CD is cocrystallized with krypton and with small molecules such as iodine, methanol, or propanol. As to β -CD, the cage-type packing is observed with small alcohols, whereas complexes with larger alcohols and other guest molecules prefer the channel type. With γ -CD, cage-type packing is only observed with water, and all other guest molecules induce the channel form [35]. The other cage-type packing is observed when α -CD is complexed with para-disubstituted benzene derivatives [36] or with a dimethyl sulfoxide/methanol [37] mixture (Scheme 2-4b). The obtained packing motif is reminiscent of bricks in a wall; the α -CD molecules are arranged in layers, and adjacent layers are laterally displaced so that the cavity of each α -CD is closed on both sides by molecules in adjacent layers. Besides α -CD, this brick-type packing is also observed with β -CD. It can form a different brick-type packing motif, in which dimer “baskets” are stabilized intermolecularly by hydrogen bonding between O₂-H/O₃-H sides and arranged in layers which are displaced laterally. In fact, this brick-type pattern can be considered as a variety of the channel motif in which

every second unit is displaced with respect to the channel axis so that the channel is disrupted and individual cages are produced. For the β -CD dimer, all kinds of different forms of this variety have been observed, from truly channel to truly brick-type packing.



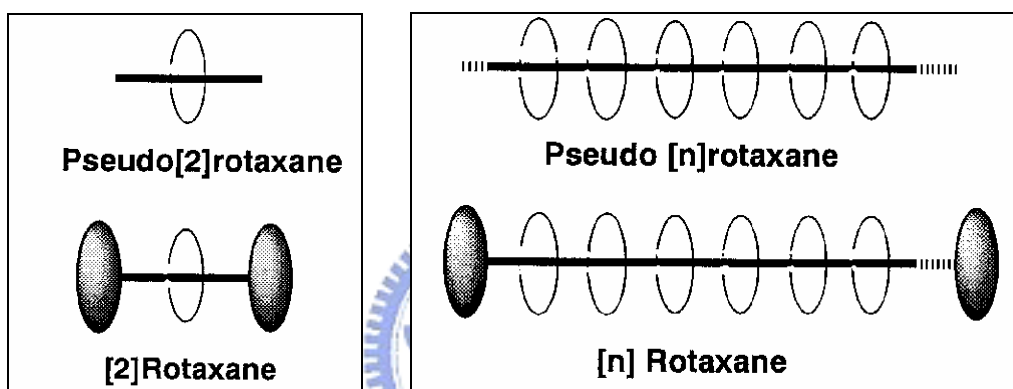
Scheme 2-4. Schematic representations of cage-type: (a) and (b), channel-type: (c)

2.2.4 Rotaxanes and Pseudorotaxanes

In recent years, with increasing recognition of the roles played by specific noncovalent interactions in biological systems and chemical processes, the science of noncovalent assemblies- often called supramolecular science- has aroused considerable interest [38]. Rotaxanes are the compounds consisting of noncovalent entities called “rotor” and “axle” [39]. Scheme 2-5 illustrates them schematically. Initially, attempts were made to prepare them by statistical methods, so that the yields were necessarily very low [40–41]. Recently, methods have been proposed for their more efficient synthesis, with renewed interest in their unique structure and properties.

If in a rotaxane consisting of rings and a chain molecule the ends of the latter are not blocked by bulky substituents, the rings can slip off the chain. In this case, the

rotaxane is called pseudo-rotaxane. The rotaxane containing a single ring is referred to as [2] rotaxane, and that containing $n+1$ rings ($n \geq 1$) as [n]rotaxane as shown in Scheme 2-5 [42]. When n is arbitrarily large, the rotaxane is named polyrotaxane, and the rings in rotaxanes are conventionally called “beads”. In principle, a rotaxane can be obtained by end-capping an axle containing one or more rings with large substituents in ordered environments of noncovalent templating forces, in such a way that the order originally created by weak interactions is retained [43].



Scheme 2-5. Schematic representations of rotaxane and polyrotaxane

2.3 Reference Review

2.3.1 Low Dielectric Constant Materials

In **1994**, Usami et al. [44,45] reported that the dielectric constant of the SiOF can be changed from 3.7 to 3.0 by controlling the fluorine concentration. The effect of fluorine addition on SiO₂ films properties deposited by using electron cyclotron resonance (ECR) plasma CVD was investigated as a function of the SiF₄/O₂ gas flow ratio. The chemical bonding structure of the films was evaluated by FT-IR, fluorine concentration by XPS, and film thickness and refractive index by ellipsometer. In **1994**, Hougham et al. [11] reported that the effect of fluorine incorporation on dielectric properties has been studied for a series of polyimides in order to distinguish between several contributing mechanisms to the generally observed decrease in the relative permittivity. Using low-frequency capacitance measurements after exhaustive in situ drying, in conjunction with refractive index measurements, the overall decrease in dielectric constant was semiquantitatively assigned between changes in the three modes of polarization via the use of fluorine/hydrogen and symmetric/asymmetric analogs. These results suggest that replacement of hydrogen with fluorine always lowers the dielectric constant increment due to the electronic mode of polarization, has little effect on the atomic increment, and in the case of asymmetric fluorine substitution, results in an increase in the orientation increment.

In **2001**, Carter et al. [46] reported the thin-film nanofoams of 6FXDA/6FDAm polyimide, with pores in the nanometer size range, has been demonstrated. 6FXDA/6FDAm/poly-(propylene oxide) polyimide copolymers were made, cured to effect solvent removal with annealing at 310 °C under argon, and subsequently transformed into a porous structure by heating at 250 °C in air. The initial annealing at 310 °C allowed for solvent removal and the development of

microphase separation in the polyimide matrix as evidenced by DMTA, SAXS, and TEM measurements. After pore generation, these nanofoam films could be subjected to further thermal treatments, even above the polyimide T_g , with only a small amount of pore collapse. With the incorporation of air pores, a lowering of the bulk dielectric constant of thin-film polyimide from 2.56 to 2.27 was accomplished, yielding new, low dielectric constant materials with pore stability in excess of 300 °C. In **2002**, Yang et al. [47] studied that triblock polymers, poly(ethylene oxide-*b*-propylene oxide-*b*-ethylene oxide) (PEO-*b*-PPO-*b*-PEO), are used as molecular templates in poly(methyl silsesquioxane) (MSQ) matrixes to fabricate nanoporous organosilicates for low dielectric constant applications. The results show that aggregation of block copolymers in the MSQ matrix can be prevented with the fast solvent evaporation which accompanies spin casting. Solid-state NMR shows that the triblock copolymer microphase-separates from the MSQ during a curing step, resulting in polymer domain size in the range of 3-15 nm, depending upon the polymer composition and loading percentage. When the films are heated to 500 °C, extremely small pores (2-6nm) are generated, which are studied by small angle neutron scattering and positronium annihilation lifetime spectroscopy. These materials attain ultralow dielectric constants ($k \approx 1.5$) with good electrical and mechanical properties.

2.3.2 Complex Formation of Cyclodextrins with Hydrophilic Polymers

In 1995, Harada et al. [48] studied that β -Cyclodextrin (β -CD) and γ -cyclodextrin (γ -CD) formed inclusion complexes with poly-(propylene glycol)s (PPG) of various molecular weights to give stoichiometric compounds in crystalline states. α -Cyclodextrin (α -CD) did not form complexes with PPG of any molecular weight. β - and γ -CD did not form complexes with the low molecular weight analogs,

such as propylene glycol, di(propylene glycol), and tri(propylene glycol). The yields of the complexes of β - and γ -CD with PPG increased with increasing molecular weight (M_w) of the PPG and reached a maximum at about M_w 1000; yield decreased with a further increase in the M_w . They were isolated and found to be 2:1 (monomer unit:CD). The complexes were characterized by IR, ^1H NMR, ^{13}C NMR, ^{13}C CP/MAS NMR, and ^{13}C PST/MAS NMR spectra and X-ray (powder), thermal, and elemental analyses. Complex formation of CDs with PPG derivatives has also been studied. The structures of the complexes are discussed. Complex formation of p-CD with atactic and isotactic PPG has been compared. In **2000**, Brown et al. [49] studied a novel route to the formation of large aggregates, with associated rheological enhancement, is provided by formation of inclusion complexes between a telechelic polymer and a second polymer containing appropriate receptor groups. The main focus of this paper describes such complexes between an adamantane end-capped poly(ethylene oxide) (PEO) ($M_w = 10^4 \text{ gmol}^{-1}$) with a polymer of β -cyclodextrin ($M_w = 3.5 \times 10^4 \text{ gmol}^{-1}$) as studied by light scattering. There is a pronounced broadening of the width of the particle size distribution with increasing concentration of end-capped polymer, accompanied by a strong increase in the average relaxation time. Viscosity enhancement in the system was measured on the same samples. Newtonian behavior was observed in the shear rate range $0.017\text{-}90 \text{ s}^{-1}$. Light scattering experiments (static and dynamic) were also made on the telechelic PEO itself. Light scattering shows the presence of a slowly relaxing component which dominates the scattering and this reflects large structures (radius 80 nm) created by interchain association to form a loose network, albeit at low concentration. Static and time-resolved fluorescence experiments show that there is no detectable tendency for “micellization” of the adamantane groups.

In **2003**, Ogoshi et al. [50] reported that CDs(α -, β -, γ -CD) could be dispersed in the silica gel matrix at a nanometer level because of the hydrogen-bonding interaction between hydroxyl moieties of CD and residual silanol groups of silica gel. It is known that, β -CD forms a strong host-guest complex with 1-adamantanol in an aqueous solution. Thus, the organic polymer modified with an adamantane group at the side chain (ADA-PAA) and silica gel hybrids could be prepared by complexation of β -CD with ADA-PAA. β -CD played a role as a compatibilizer between ADA-PAA and silica gel to obtain transparent and homogeneous polymer hybrids. The evidence of the host-guest complex formation was confirmed by a fluorescence technique using a dansyl group. Furthermore, transparent and homogeneous CD-polymer complex/silica gel hybrids were prepared utilizing CDs formed polyrotaxane-type inclusion complexes with polymers, such as poly(ethyleneglycol) and polyisobutylene. In **1998**, Ritter et al. [51] synthesized a new water-soluble semi-rotaxane monomer consisting of threaded 2,6-dimethyl- β -cyclodextrin on a 3-*O*-(11-acryloylaminoundecanoyl)cholic acid guest component. This new monomer complex was polymerized in water as a solvent in the presence of a free radical redox initiator, yielding a side-chain polyrotaxane. Two main fractions of the resulting polymeric product were isolated by extraction with water. About 50 wt.-% of the polymer material contains approximately 40 mol-% of noncovalently anchored cyclodextrin with regard to the amount of side-chain units. This fraction is not soluble in water. Additionally, a smaller water-soluble fraction with a significantly lower degree of polymerization was isolated bearing nearly one cyclodextrin on each side-chain unit.

References

- [1] Maier, G. *Prog. Polym. Sci.* **2001**, 26, 3.
- [2] Nalwa, H. S., editor. "Handbook of Advanced Electronic and Photonic Materials and Devices, Volume 4." San Diego: Academic Press, **2001**.
- [3] Treichel, H.; Ruhl, G.; Ansmann, P.; Wurl, R.; Muller, C. H.; Dietlmeier, M. *Microelectronic Eng.* **1998**, 40, 1.
- [4] Peters, L. *Semicond. Int.* **1998**, 10, 64.
- [5] Lin, X. W.; Pramanik, D. *Solids State Technol.* **1998**, 10, 63.
- [6] Nalwa, H. S., editor. "Handbook of Low and High Dielectric Constant Materials and Their Applications, Volume 1." San Diego: Academic Press, **2001**.
- [7] Singer, P. *Semicond, Int*, **1996**, 5, 88.
- [8] Ho, P. S.; Leu, J.; Lee, W. W. In *Low Dielectric Constant Materials for IC Applications*; New York: Springer, **2002**.
- [9] Yang, P.; Zhao, D.; Chmelka, B. F.; Stucky, G. D. *Chem. Mater.* **1998**, 10, 2033.
- [10] Hedrick, J. L.; Carter, K.R.; Cha, H. J.; Hawker, C. J.; DiPietro, R. A.; Labadie, J. W.; Miller, R. D.; Russel, T. P.; Sanchez, M. I.; Volksen, W.; Yoon, D. Y.; Mecerreyes, D.; Jerome, R.; McGrath, J. E. *Reactive & Functional Polymers* **1996**, 30, 43.
- [11] Hougham, G.; Tesoro, G.; Viehbeck, A.; Chapple-Sokolg, J. D. *Macromolecules* **1994**, 27, 5964.
- [12] Hougham, G.; Tesoro, G.; Shaw, J. *Macromolecules* **1994**, 27, 3642.
- [13] Bruschi, P.; Stucki, F.; Baumann, T.; Kluge-Weiss, P.; Bruhl, B.; Niemeyer, L.; Strumpler, R.; Ziegler, B.; Mielke, M. *J. Appl. Phys.* **1993**, A57, 329.
- [14] Hrubesh, L.W.; Keene, L. E.; Latorre, V. R. *J. Mater. Res.* **1993**, 8, 1736.
- [15] Ramos, T.; Roderick, K.; Maskara, A.; Smith, D. M. *Mater. Res. Soc. Symp.*

- Proc.* **1997**, 443, 91.
- [16] Cho, C. C.; Gnade, B.; Smith, D. M. *US Pats.* 5 470 802, 5 494 858, 5 504 042, 5 523 615, **1995**.
- [17] Smith, D. M.; Anderson, J. M.; Cho, C. C.; Johnston, G. P.; Jeng, S. P. *Mater. Res. Soc. Symp. Proc.* **1995**, 381, 261.
- [18] Hedrick, J. L.; Labadie, J. W.; Russell, T. P.; Hofer, D.; Wakharkar, V. *Polymer* **1993**, 34, 4717.
- [19] Hedrick, J. L.; Carter, K. R.; Labadie, J. W.; Miller, R. D.; Volksen, W.; Hawker, C. J.; Yoon, D. Y.; Russell, T. P.; McGrath, J. E.; Briber, R. M. *Adv. Polym. Sci.* **1998**, 141, 1.
- [20] Hedrick, J. L.; Labadie, J. W.; Volksen, W.; Hilborn, J. G. *Adv. Polym. Sci.* **1999**, 147, 61.
- [21] Carter, K. R. *Mater. Res. Soc. Symp. Proc.* **1997**, 476, 87.
- [22] Charlier, Y.; Hedrick, J. L.; Russell, T. P.; Jones, A.; Volksen, W. *Polymer* **1995**, 36, 987.
- [23] Hedrick, J. L.; Russell, T. P.; Labadie, J. W.; Lucas, M.; Swanson, S. *Polymer* **1995**, 36, 2685.
- [24] Hedrick, J. L.; Hawker, C. J.; DiPietro, R.; Jerome, R.; Charlier, Y. *Polymer* **1995**, 36, 4855.
- [25] Hedrick, J. L.; DiPietro, R.; Charlier, Y.; Jerome, R. *High Perform. Polym.* **1995**, 7, 133.
- [26] Hedrick, J. L.; Russell, T. P.; Sanchez, M.; DiPietro, R.; Swanson, S.; Meccerreyes, D.; Jerome, R. *Macromolecules* **1996**, 29, 3642.
- [27] Engeldinger, E.; Armspach, D.; Matt, D. *Chem. Rev.* **2003**, 103, 4147.
- [28] Douhal, A. *Chem. Rev.* **2004**, 104, 1955.

- [29] Rekharsky, M. V.; Inoue, Y. *Chem. Rev.* **1998**, *98*, 1743.
- [30] Szejtli, J. *Chem. Rev.* **1998**, *98*, 1743.
- [31] Lindoy, L. F.; Atkinson, I. M. In *Self-assembly in Supramolecular Systems*; Cambridge: UK, **2000**.
- [32] Saenger, W. *Israel J. Chem.* **1985**, *25*, 43.
- [33] Saenger, W.; Jacob, J.; Gessler, K.; Steiner, T.; Hoffmann, D.; Sanbe, H.; Koizumi, K.; Smith, S. M.; Takaha, T. *Chem. Rev.* **1998**, *98*, 1787.
- [34] Takahashi, K.; *Chem. Rev.* **1998**, *98*, 2013.
- [35] Lindner, K., Saenger, W. *Biochem. Biophys. Res. Commun.* **1980**, *92*, 933.
- [36] Saenger, W.; Beyer, K.; Manor, P. C. *Acta Crystallogr. Sect. B.* **1976**, *32*, 120.
- [37] Harata, K. *Bull. Chem. Soc. Jpn.* **1978**, *51*, 1644.
- [38] Lehn, J. M. *Angew Chem. Int. Ed. Engl.* **1992**, *29*, 1304.
- [39] Schill, G. *Catenanes Rotaxanes and Knots*, Academic Press: New York, **1971**.
- [40] Agam, G.; Graiver, D.; Zilkha, A. *J. Am. Chem. Soc.* **1976**, *98*, 5206.
- [41] Harrison, I. T.; Harrison, S. *J. Am. Chem. Soc.* **1967**, *89*, 5723.
- [42] Harada, A. *Adv. Polym. Sci.* **1997**, *133*, 141.
- [43] Anelli, P. L.; Ashton, P. R.; Ballardini, R.; Balazani, V.; Delgado, M.; Gandolfi, M. T.; Goodnow, T. T.; Kaifer, A. E.; Philp, D.; Pietraszkiewicz, M.; Prodi, L.; Reddington, M. V.; Slawin, A. M. Z.; Spencer, N. Stoddart, J. F.; Vicent, C.; Williams, D. J. *J. Am. Chem. Soc.* **1992**, *114*, 193.
- [44] Usami, T.; Shimokawa, K.; Yoshimaru, M. *Jpn. J. Appl. Phys.* **1994**, *33*, 408.
- [45] Mei, Y. J.; Chang, T. C.; Chang, S. J.; Pan, F. M.; Chen, M. S. K.; Tuan, A.; Chou, S.; Chang, C. Y. *Thin Solid Films* **1997**, *308-309*, 501.
- [46] Carter, K. R.; DiPietro, R.A.; Sanchez, M. I.; Swanson, S.A. *Chem. Mater.* **2001**, *13*, 213.

- [47] Yang, S.; Mirau, P. A.; Pai, C. S.; Nalamasu, O.; Reichmanis, E.; Pai, J. C.; Obeng, Y. S.; Seputro, J.; Lin, E. K.; Lee, H. J.; Sun, J.; Gidley, D. W.. *Chem. Mater.* **2002**, *14*, 369.
- [48] Harada, A.; Okada, M.; Li, J.; Kamachi, M. *Macromolecules* **1995**, *28*, 8406.
- [49] Sandier, A.; Brown, W.; Mays, H.; Amiel, C. *Langmuir* **2000**, *16*, 1634.
- [50] Ogoshi, T.; Chujo, Yoshiki. *Macromolecules* **2003**, *36*, 654.
- [51] Noll, O; Ritter, H. *Macromol. Chem. Phys.* **1998**, *199*,791.



Chapter 3

Thermal Properties and Hydrogen Bonding in Polymer Blend of Polybenzoxazine/Poly (N-vinyl-2-pyrrolidone)

Abstract

The thermal properties and hydrogen bonding behavior of polybenzoxazine (B-a type)/poly (N-vinyl-2-pyrrolidone) (PVP) blends were investigated by using differential scanning calorimetry (DSC) and Fourier transform infrared spectroscopy (FTIR). The DSC result shows a single glass transition temperature (T_g) over the entire compositions, indicating that the amorphous phase of polybenzoxazine (PBZZ) is totally miscible with PVP. In addition, a large positive deviation based on Kwei equation was observed in the T_g versus composition diagram, implying that strong hydrogen bonding interaction exists between the hydroxyl group of PBZZ and the carbonyl group of PVP. The FTIR analysis also provides positive evidence for the hydrogen bonding interaction existing between these two polymers. The equilibrium constants, including self- and inter-association hydrogen bonding, were determined from appropriate low molar mass mixtures, which can be used to predict the miscibility behavior and hydrogen bonding interaction of analogous polymers. The strength of hydrogen bonding interaction is found in the order of: inter-association between PBZZ hydroxyl and PVP carbonyl ($\text{OH} \cdots \text{O}=\text{C}$) > self-association between PVP hydroxyl ($\text{OH} \cdots \text{OH}$) > A_1 inter-association between PBZZ hydroxyl and the Mannich-based bridge ($\text{OH} \cdots \begin{array}{c} \text{N}-\text{C} \\ | \\ \text{C} \end{array}$).

3.1 Introduction

Syntheses and characterizations of PBZZ have been widely described recently by Ishida and co-workers [1-4]. Its structure is similar to phenolic resin through thermal self-curing of the heterocyclic ring opening reaction that neither requires catalyst nor releases any condensation byproduct [5]. These PBZZ resins were found to possess several outstanding properties such as near-zero shrinkage after curing, high thermal stability and low water absorption [6]. Furthermore, the PBZZ has high glass transition temperatures even though it has relatively low crosslinking density [7].

The most important specific interaction of polymer blends is the hydrogen bonding, which is the driving force responsible for many miscible polymer pairs [8-10]. The PBZZ possess the hydroxyl group that is expected to form intermolecular hydrogen bonding with other polymers with a proton-acceptor. Since PVP [11-12] is a water-soluble tertiary amide and a Lewis base that possesses good biocompatibility and several medical applications. The PVP contains carbonyl group that is known as a strong proton acceptor for several polymers with proton donor [13-14]. Chemical structures of PBZZ and PVP are shown in Scheme 3-1. Thermal properties and hydrogen bonding behavior of PBZZ/PVP blends will be discussed in this study.

In order to better understand the hydrogen bonding interaction of the pure PBZZ and the PBZZ/PVP blend systems, a series of model compounds shown in Scheme 3-2 are used to simulate the miscibility behavior of analogous hydrogen bonded polymer blends [8,15]. In this blend system, these equilibria can be described by four different constants: two self-association equilibrium constants describing the formation of hydrogen bonded dimer (K_2) and multimers (K_B) of the PBZZ hydroxyls, inter-association equilibrium constants (K_A and K_C) between PBZZ hydroxyl and PVP

carbonyl, and the inter-molecular interaction between hydroxyl and Mannich-based bridge both of pure PBZZ, respectively. Blend of 4-isopropylphenol (IPP)/1-ethyl-2-pyrrolidinone (EPr) has been employed to simulate the PBZZ/PVP blend. In addition, an extra inter-association hydrogen bonding can be attributed to the hydroxyl group of IPP and the Mannich based bridge (-CH₂-NAr-CH₂) (which replaced by using N,N-dimethylaniline (DMA)) both of pure PBZZ. We use these model compounds to determine the self- and inter-association equilibrium constants by using the hydroxyl stretching region in infrared spectroscopy based on classical Whetsel/Lady (W&D) and Coggeshall/Saier (C&S) methods, respectively. Therefore, the self- and inter-association hydrogen bonding interactions of this blend system can be represented by Scheme 3-3.

3.2 Experimental

3.2.1 Materials

Benzoxazine (B-a type) based on bisphenol-A, formaldehyde, and aniline was synthesized according to Scheme 3-4. Poly (N-vinyl-2-pyrrolidone) (PVP) used in this study was purchased from Aldrich of USA with the $M_w=58,000$. 4-isopropyl phenol (IPP), 1-ethyl-2-pyrrolidone (EPr), and N,N-dimethylaniline (DMA) were purchased from Acros Chemical Company of USA.

3.2.2 Blend Preparations

Blends of benzoxazine/PVP with several different compositions were prepared by solution blending. The polymer mixture was stirred and dissolved in N,N-Dimethylformamide (DMF), then the solution was allowed to evaporate slowly at 50 °C for 1 day. Afterwards, it was cured at 180 °C for 4hr under vacuum to ensure total curing of the benzoxazine.



3.2.3 Differential Scanning Calorimetry (DSC)

A DSC from Du-Pont (DSC-2010) measured the glass transition temperature (T_g) of the blends. The samples were preheated with a scan rate of 20 °C/min from 30 °C to 260 °C and maintained at 260 °C for 2 min. The measurement was made using 5-10 mg sample on a DSC sample after the cell was cooled to 100 °C (below each polymer blend's T_g) slowly and then cooled to 30 °C quickly from the melt of the first scan. The second scan rate was 20 °C/min from 30 to 300 °C and T_g was taken as the midpoint of the heat capacity transition between the upper and lower points of deviation from the extrapolated liquids and glass lines.

3.2.4 Infrared Spectroscopy

FT-IR measurement was recorded on a Nicolet Avatar 320 FT-IR spectrophotometer, 32 scans were collected with a spectral resolution of 1cm^{-1} . Infrared spectra of the polymer blends were obtained using the conventional NaCl disk method. The chloroform solution containing the blend was cast onto a NaCl disk and dried under condition similar to that used in the bulk preparation. The film used in this study was thin enough to obey the Beer-Lambert law. The sample chamber was purged with nitrogen during process of measurement in order to maintain sample films drying. For the sample in solution form, a sealed cell with NaCl windows and 0.2mm sample thickness was used. A single optical path was used to study the intra- and inter-association equilibrium constants between model compounds of IPP, EPr, and DMA. All model compound solutions in the absorption range obey the Beer-Lambert law. Cyclohexane (CHEX) was selected as the solvent because of it is low polar and does not form any interaction with model compounds in the study.

3.3 Results and Discussion

3.3.1 Glass Transition Temperature Analysis

All the PBZZ/PVP blends were subjected to DSC measurements for the purpose of examining microscopic miscibility. Figure 3-1 shows the DSC thermograms of PBZZ/PVP blends showing only one T_g from all compositions. A single T_g strongly implies that blends of PBZZ and PVP are miscible over the entire composition ranges. Figure 3-2 shows the dependence of the T_g on the composition of these miscible blends. The maximum T_g deviation is obtained when blend composition at PBZZ/PVP =60/40 (weight ratio). Kwei equation [16] describes the effect of T_g hydrogen bonding interaction between polymers as shown in equation (3-1):

$$T_g = \frac{W_1 T_{g1} + kW_2 T_{g2}}{(W_1 + kW_2)} + qW_1 W_2 \quad (3-1)$$

where W_1 and W_2 are weight fractions of the components, T_{g1} and T_{g2} represent the component glass transition temperatures. Both k and q are fitting constants. In general, the parameter q may be considered as a measurement of the specific interaction in a polymer blend system. When the intermolecular interaction is stronger than intramolecular interaction in a binary blend, the value of q will be positive; otherwise, q will be negative. When the q value is larger, it represents that the interaction is stronger than the self-interaction of the blend. In case of no any interaction existed between components, the q value will be equal to zero and its T_g behavior can be described by the Gordon-Taylor equation [17] as show in equation (3-2).

$$T_g = \frac{W_1 T_{g1} + kW_2 T_{g2}}{(W_1 + kW_2)} \quad (3-2)$$

As shown in Figure 3-1, the PBZZ is completely miscible with PVP in the amorphous phase and results in positive T_g deviation. After the “best fitting” by the Kwei equation, $k=1$ and $q=75$ were obtained. In this study, a large positive q value of

75 indicates that a strong intermolecular interaction exists between PBZZ and PVP. This result can also explain why T_g s of these blends are all higher than their respective mother polymers as shown in Figure 3-1.

3.3.2 Fourier Transfer Infrared Spectroscopy Analysis

FTIR spectroscopy has been successfully applied in polymer blends possessing intermolecular interaction through hydrogen bonding [18-20]. Figure 3-3 shows the infrared spectra of the carbonyl stretching measured at room temperature ranging from 1620 cm^{-1} to 1730 cm^{-1} of various PBZZ/PVP blends. The pure PVP gives a broad carbonyl absorption peak at 1680 cm^{-1} [21-22]. After adding the PBZZ into the PVP system, the carbonyl stretching frequency is split into two bands at 1680 cm^{-1} and 1660 cm^{-1} , corresponding to the free and the hydrogen-bonded carbonyl groups, respectively. This free carbonyl band (1680 cm^{-1}) gradually shifts into the hydrogen-bonded carbonyl (1655 cm^{-1}) with increasing of the PBZZ content in the blend. These two carbonyl bands can be fitted well to the Gaussian function and the fraction of the hydrogen-bonded carbonyl group can be calculated according to equation (3-3) [23].

$$f_b^{C=O} = \frac{A_b / 1.3}{A_b / 1.3 + A_f} \quad (3-3)$$

A_f and A_b denote peak areas corresponding to the free and the hydrogen-bonded carbonyl groups. The absorptions, ratio $\varepsilon_2/\varepsilon_1 = 1.3$, was taken from previous infrared studies in hydroxyl-carbonyl inter-association [24]. Table 3-1 summarizes results from the curve fitting, indicating that the hydrogen-bonded fraction of the carbonyl group increases with increasing the PBZZ content as would be expected.

3.3.3 The Self-Association of Hydroxyl Groups of PBZZ

According to the Painter-Coleman Association Model [8], we designate 2, B, C, and A as dimers of PBZZ, multimers of PBZZ, Mannich based bridge and PVP units, respectively, and K_2 , K_B , K_C and K_A as their corresponding association equilibrium constants.

In this study, we choose the 4-isopropylphenol (IPP) to replace the PBZZ unit because the pure PBZZ is not soluble in cyclohexane (CHEX). In addition, the CHEX does not exhibit fundamental vibrational frequencies in the hydroxyl ($3100\text{-}3700\text{ cm}^{-1}$) or carbonyl ($1600\text{-}1800\text{ cm}^{-1}$) stretching regions of the infrared spectrum. Hence CHEX is a suitable solvent to characterize the vibrational frequency change of infrared spectrum. The self-association of hydroxyl groups can be analyzed from the infrared spectra of IPP/CHEX mixtures by increasing from 0.00125M to 0.5M. Infrared spectra were recorded using the standard KBr unit liquid cell (0.2mm), and the infrared bands had absorbance below 1 cm^{-1} . These overtone and combination bands were eliminated by spectral subtraction in the spectra of the more dilute solutions. The hydroxyl stretching region with low concentration of 0.01M is shown in Figure 3-4. After subtracting the contribution of the CHEX, the resultant difference in spectrum is essentially the pure IPP at a given dilution without any interaction. By reducing the concentration of IPP below 0.01M, the same result was presented. Contrary, by increasing the concentration of IPP above 0.01M, the effect of self-interaction of dimers and multimer becomes noticeable; especially the multimers one as shown in Figure 3-5.

In order to calculate the self-association equilibrium constant [5,25], we need to measure the fraction of free monomers in the dilute solution of a given concentration of IPP. The intensity (absorbance) of the isolated hydroxyl band (at 3620 cm^{-1}), I , is

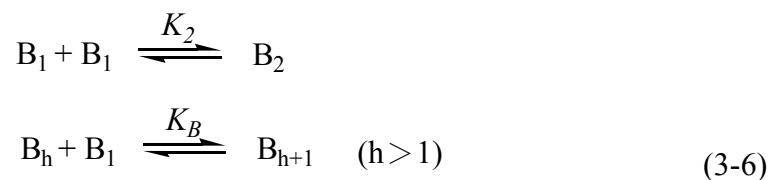
related to absorptivity coefficient, ε , the concentration, c , and the path length, l , using the Beer-Lambert law, $I = c \cdot \varepsilon \cdot l$. The value of absorptivity coefficient (ε) is determined by plotting $(I/c \cdot l)$ versus c , the value of $\varepsilon = 31.1$ is obtained through equation (3-4) and illustrated in Figure 3-6.

$$\lim_{c \rightarrow 0} \left| \frac{I}{c \cdot l} \right| = \varepsilon \quad (3-4)$$

The experimental fraction of free monomer, f_m^{OH} and the value of $\varepsilon (= I/c \cdot l)$, at any given concentration of IPP was calculated by equation (3-5) and summarized in Table 3-2. When the concentration of the IPP is increased; the fraction of free hydroxyl group is decreased gradually.

$$f_m^{OH} = \frac{I}{I_0} \quad (3-5)$$

There are two equilibrium constants that can describe the self-association of IPP containing hydroxyl groups, the formation of dimers (K_2) and the formation of multimers complex (K_B) as shown in equation (3-6).



Where B_1 , B_2 and B_h represent the hydroxyl group, hydroxyl/hydroxyl dimers and hydroxyl/hydroxyl multimers of PBZZ, respectively.

Finally, we used equation (3-7) [8] to obtain the best fit of K_2 and K_B for IPP, $K_2 = 28.3 \text{ Lmol}^{-1}$ and $K_B = 72.6 \text{ Lmol}^{-1}$ were obtained as shown in Figure 3-7.

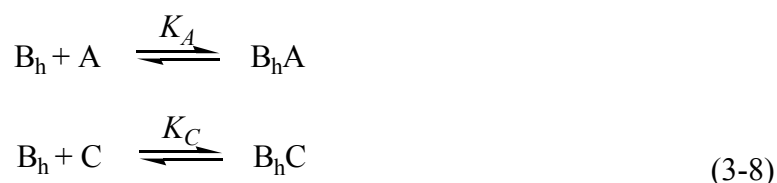
$$f_m^{OH} = \frac{\Phi_{B1}}{\Phi_B} = \left[\left(1 - \frac{K_2}{K_B} \right) + \frac{K_2}{K_B} \left(\frac{1}{(1 - K_B \Phi_{B1})^2} \right) \right]^{-1} \quad (3-7)$$

Where Φ_B is the total volume fraction of B and Φ_{B1} is the volume fraction of

non-hydrogen bonded.

3.3.4 The Equilibrium Constants of Inter-Association

Inter-association is a term that describes the hydrogen bonding association between two different functional groups (which could be located in different molecules or different segments) as shown in equation (3-8).



Where A and C represent the carbonyl group of PVP and the Mannich based bridge of PBZZ, respectively.

In this system, two different types hydrogen bonding are expected to be formed. One is from the hydroxyl group of PBZZ and carbonyl group of PVP, and the other one is from different segments of the PBZZ (the hydroxyl group and the Mannich-based bridge both of PBZZ). We used the several model compounds to describe the behaviors of these polymers.

3.3.4.1 The Inter-Association of Different Molecules

Using a constant dilute concentration (0.02M) of IPP in CHEX, the fraction of free monomer can be assumed as unity. When the EPr is added, the presence of the carbonyl group of EPr is able to form hydrogen bond with the OH group of IPP. Figure 3-8 shows that the intensity (fraction) of the IPP hydroxyl at 3620 cm^{-1} decreases drastically with the increase of the EPr content while the hydrogen bonded hydroxyl shifts to low frequency with increasing EPr content, indicating that more fraction of hydrogen bonding is formed. Base on the equation (3-9), the inter-association dimensionless equilibrium constant can be calculated [5,24-26] for a

given concentration of EPr. Those results are summarized in Table 3-3, and $K_A=594$ Lmol^{-1} is obtained. The mole volume of PBZZ is $129 \text{ cm}^3/\text{mol}$ at room temperature, and the inter-association equilibrium constant $K_A^{Std}=4606$ is calculated and listed in Table 3-3, too.

$$K_A = \frac{1 - f_m^{OH}}{f_m^{OH} (C_A - (1 - f_m^{OH})C_B)} \quad (3-9)$$

Where C_A and C_B denote concentrations of IPP and EPr in molL^{-1} , respectively.

3.3.3.2 The Inter-Association of Different Segments

By using IPP and DMA as model compounds to investigate the inter-association of different segments, their changes of interaction in distinct molar concentrations are plotted in Figure 3-9. Because the concentration of the IPP is diluted, the intensity (fraction) of free hydroxyl group of IPP at 3620 cm^{-1} decreases gradually with increasing DMA content. Furthermore, the hydrogen bonding increases insignificantly in spite of increasing the concentration of DMA. This observation implies that the interaction derived from hydroxyl and Mannich based bridge is very weak or insignificant. The resulted K_C between IPP and DMA also gives same tendency, the K_C value obtained is very small ($< 10 \text{ Lmol}^{-1}$). Since K_A value is significantly greater than K_C , the strong intermolecular interaction due to hydrogen bonding in this system is come from the hydroxyl group of IPP and the carbonyl group of EPr.

3.4 Conclusions

The PBZZ (B-a type) is completely miscible with PVP in the amorphous phase and results in T_g positive deviation based on Kwei equation over entire compositions mainly due to formation of hydrogen bonding between PBZZ hydroxyl and PVP carbonyl. The strength of hydrogen bonding interaction is in the order of inter-association between the hydroxyl group of PBZZ and the carbonyl group of PVP ($K_A=594 \text{ Lmol}^{-1}$) > self-association between the hydroxyl group of pure PBZZ ($K_B=72.6 \text{ Lmol}^{-1}$) > inter-association between the hydroxyl and the Mannich-based bridge of pure PBZZ ($K_C < 10 \text{ Lmol}^{-1}$). This result is consistent with positive q value based on Kwei equation, because the K_A is much higher than K_B and K_C .



References

- [1] Kim, H. J.; Brunovska, Z.; Ishida, H. *Polymer* **1999**, *40*, 1815.
- [2] Agag, T.; Takeichi, T. *Macromolecules* **2001**, *34*, 7257.
- [3] Ishida, H.; Sanders, D. P. *Macromolecules* **2000**, *33*, 8149.
- [4] Kim, H.J.; Brunovska, Z.; Ishida, H. *Polymer* **1999**, *40*, 6565.
- [5] Ishida, H. *J. Appl. Polym. Sci.* **1995**, *58*, 1751.
- [6] Ishida, H.; Low, H. Y. *Macromolecules* **1997**, *30*, 1099.
- [7] Ning, X.; Ishida, H. *J. Polym. Sci., Part B: Polym. Phys.* **1994**, *32*, 921.
- [8] Coleman, M.M.; Painter, P. C. *Prog. Polym. Sci.* **1995**, *20*, 1.
- [9] Motzer, H.R.; Painter, P. C.; Coleman, M. M. *Macromolecules* **2001**, *34*, 8390.
- [10] Prolongo, M.G.; Salom, C.; Masegosa, R. M. *Polymer* **2002**, *43*, 93.
- [11] Schwager, F.; Marand, E.; Davis, R. M. *Macromolecules* **1997**, *30*, 1449.
- [12] Prinos, A.; Dompros, A.; Panayiotou, C. *Polymer* **1998**, *14*, 3011.
- [13] Kuo, S.W.; Chang, F. C. *Macromolecules* **2001**, *34*, 5224.
- [14] Wu, H. D.; Chang, F. C. *Polymer* **2001**, *42*, 555.
- [15] Coleman, M. M.; Xu, Y.; Painter, P. C. *Macromolecules* **1994**, *27*, 127.
- [16] Kwei, T. K. *J. Polym. Sci. Polym. Lett. Ed* **1984**, *22*, 307.
- [17] Gondon, M.; Taylor, J. S. *J. Appl. Chem.* **1952**, *2*, 493.
- [18] Li, D.; Brisson, J. *Polymer* **1998**, *39*, 801.
- [19] Smith, P.; Eisenberg, A. *Macromolecules* **1994**, *27*, 545.
- [20] Mekhilef, N.; Hadhiandreou, P. *Polymer* **1995**, *36*, 2165.
- [21] Kaczmarek, H.; Szalla, A.; Kaminska, A. *Polymer* **2001**, *42*, 6057.
- [22] Lau, C.; Mi, Y. *Polymer* **2002**, *43*, 823.
- [23] Coleman, M. M.; Graf, J. F.; Painter, P. C. "Specific interactions and the miscibility of polymer blends" Lancaster, PA: Technomic Publishing, **1991**.

- [24] Hu, Y.; Motzer, H. R.; Etxeberria, A. M.; Fernandez, B. M. J.; Irin, J. J.; Painter, P. C.; Coleman, M. M. *Macromol. Chem. Phys.* **2000**, *201*, 705.
- [25] Hu, Y.; Painter, P. C.; Coleman, M. M. *Macromol. Chem. Phys.* **2000**, *201*, 470.
- [26] Wang, F. Y.; Ma, C. C.; Hung, Y. C.; Wu, H. D. *Macromol. Chem. Phys.* **2001**, *202*, 2328.



Table 3-1. Curve fitting of fraction of hydrogen-bonding results of the PBZZ/PVP blends at room temperature

PBZZ /PVP	free C=O		H-bonded C=O		f_b (%)
	ν (cm^{-1})	A_f (%)	ν (cm^{-1})	A_b (%)	
80/20	1680.1	56.62	1654.6	43.38	37.08
70/30	1682.2	63.98	1657.5	36.02	30.22
60/40	1682.5	64.98	1658.5	35.02	29.31
50/50	1685.2	68.15	1665.4	31.85	26.45
40/60	1684.2	77.84	1666.0	22.16	17.96
20/80	1682.4	85.71	1662.8	14.29	11.36

f_b = fraction of hydrogen bonding

Table 3-2. IPP/CHEX data

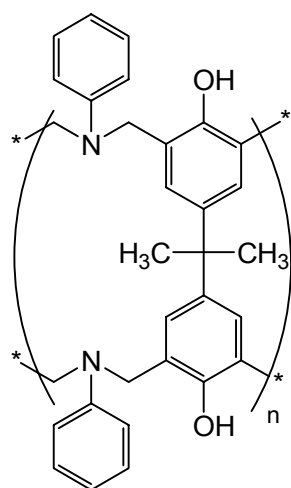
C_{IPP} (M)	$I/c \cdot l$	f_m^{OH}	C_{IPP} (M)	$I/c \cdot l$	f_m^{OH}
0.00125	30.6	0.983	0.08	17.63	0.566
0.0025	30.34	0.975	0.1	15.9	0.511
0.005	29.9	0.961	0.2	10.0	0.321
0.001	29.1	0.935	0.3	7.48	0.240
0.02	27.0	0.867	0.4	6.11	0.196
0.04	23.0	0.739	0.5	4.92	0.158
0.06	19.75	0.635			

Table 3-3. EPr/IPP/CHEX mixture-determination of K_A and K_A^{Std}

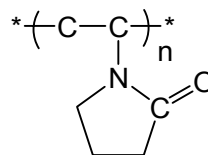
C_{EPr} (M)	C_{IPP} (M)	f_m^{OH}	K_A (Lmol ⁻¹)	K_A^{Std} (dimensionless)
0	0.02	—	594 ^a	4606 ^b
0.02	0.02	0.253	583	4508
0.04	0.02	0.076	562	4346
0.08	0.02	0.029	546	4223
0.10	0.02	0.022	540	4175
0.20	0.02	0.011	522	4033

a, b: extrapolated to $C_{EPr}=0$



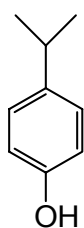


PBZZ (B-a type)

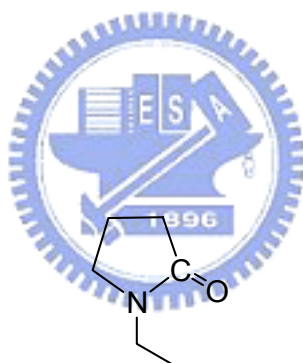


PVP

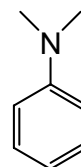
Scheme 3-1. The chemical structures of PBZZ (B-a type) and PVP



4-isopropylphenol
(IPP)

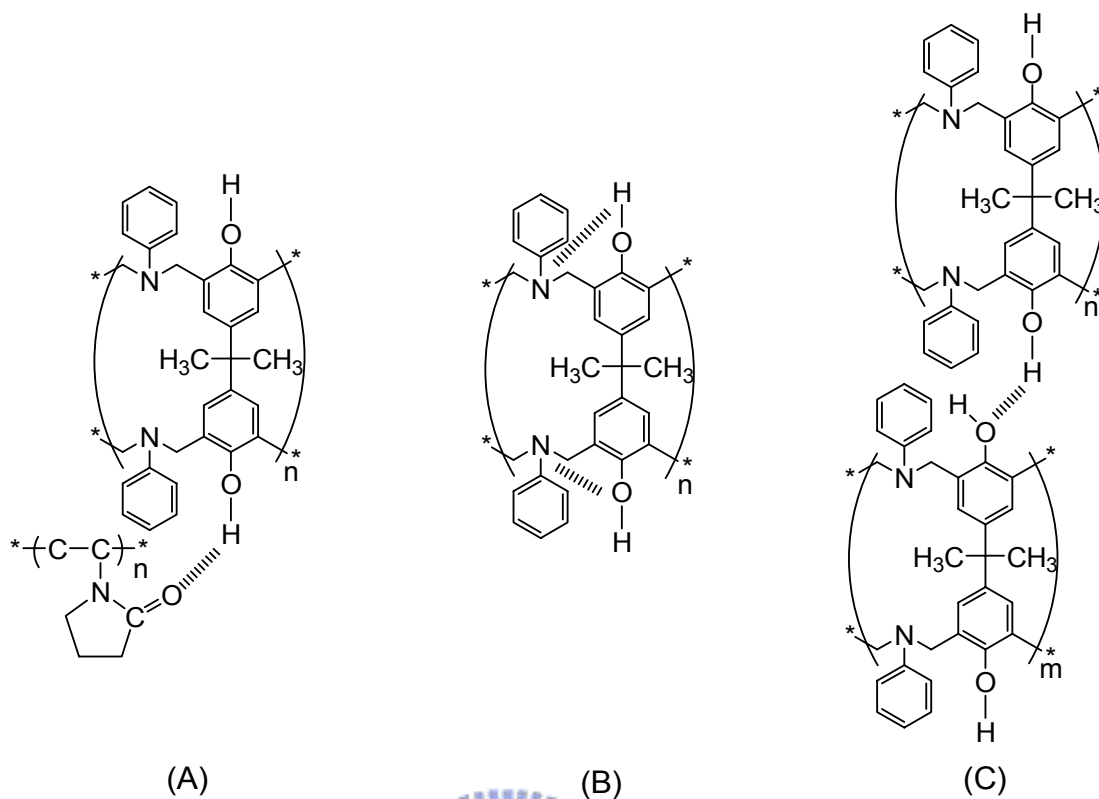


1-ethyl-2-pyrrolidinone
(EPr)



N,N-dimethylaniline
(DMA)

Scheme 3-2. The model compounds used in this study and their chemical structures of IPP, EPr and DMA

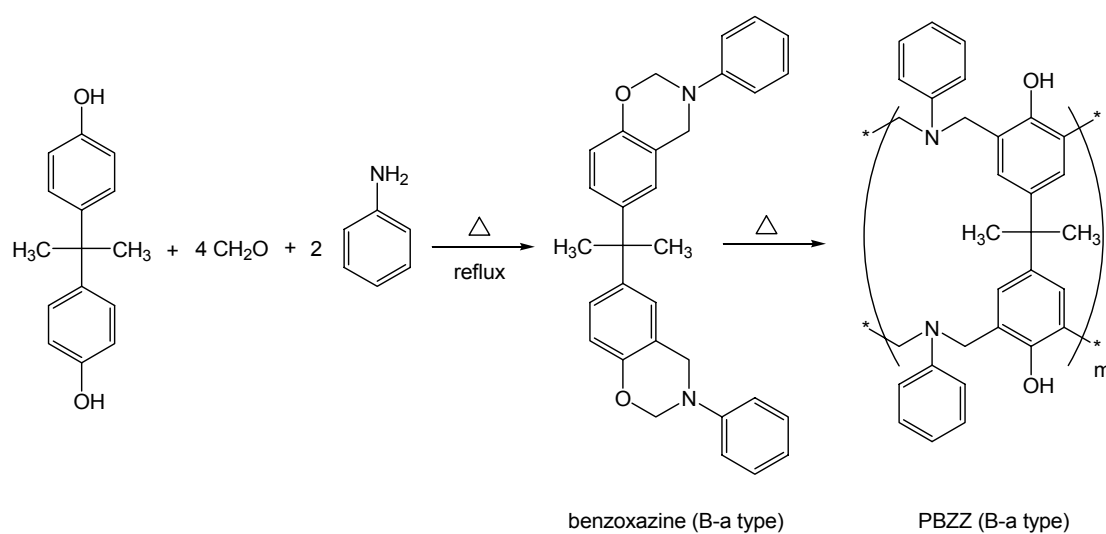


Scheme 3-3. The schematic representation of hydrogen bonding

(A) inter-association of PBZZ/PVP blend

(B) intra-association of the pure PBZZ

(C) inter-association of the pure PBZZ



Scheme 3-4. The chemical reactions of benzoxazine and PBZZ

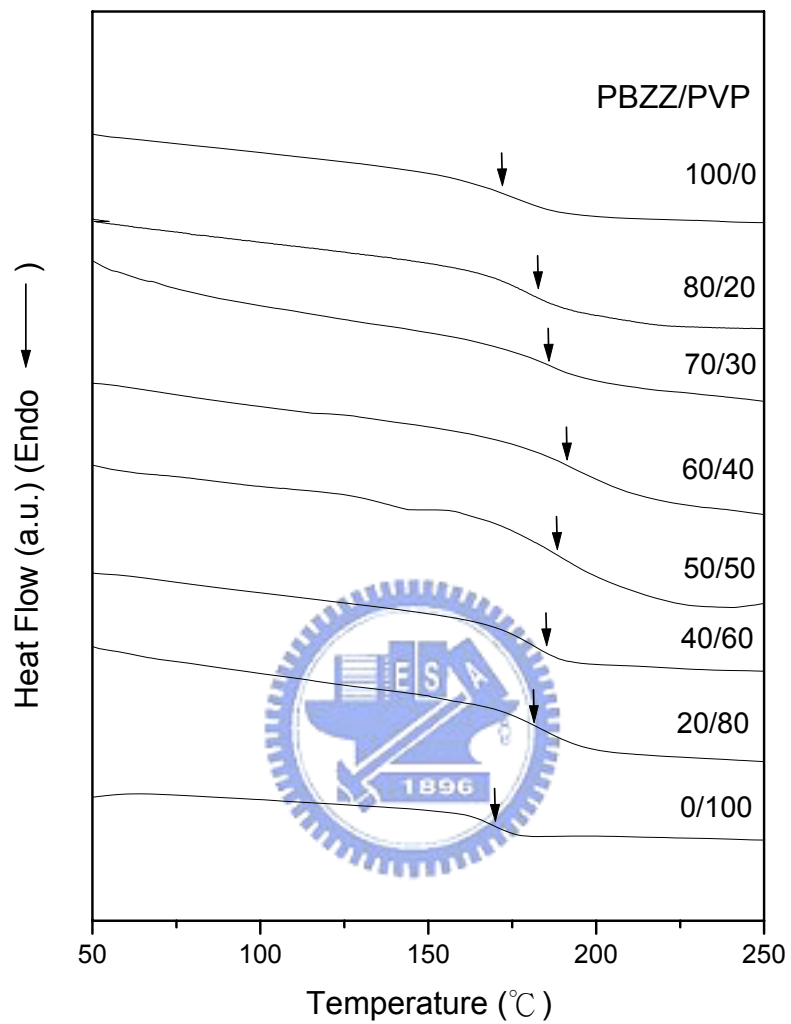


Figure 3-1. The DSC scans of PBZZ /PVP blends with different composition

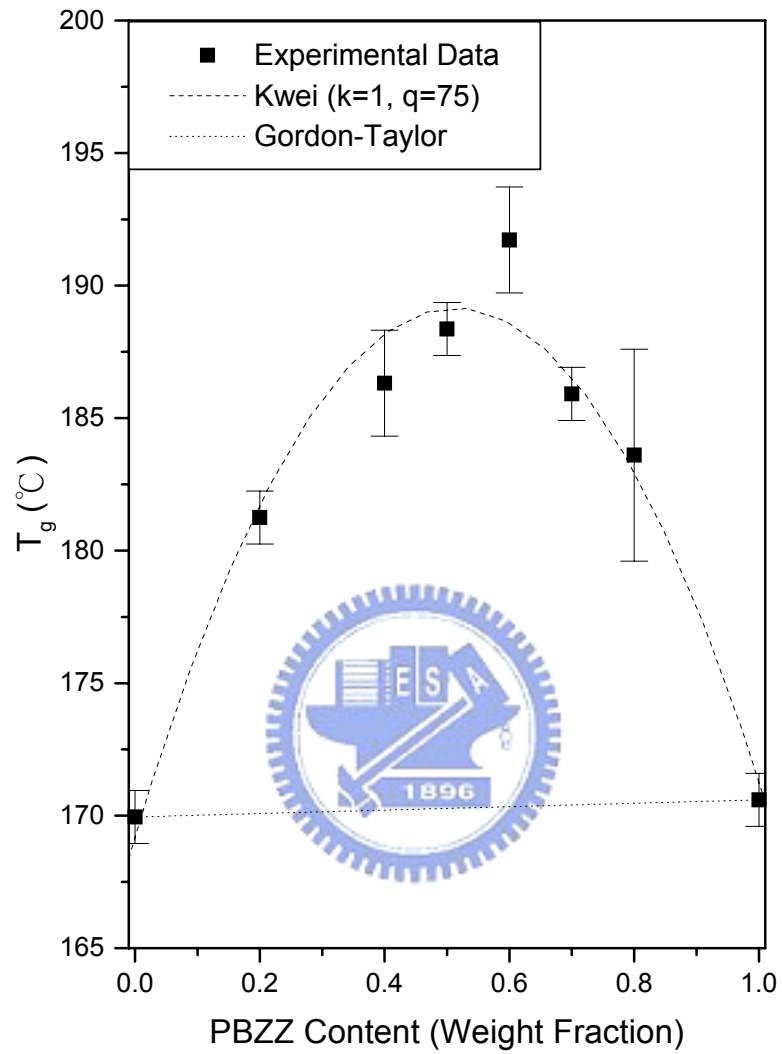


Figure 3-2. T_g versus composition curved base on PBZZ/PVP blends

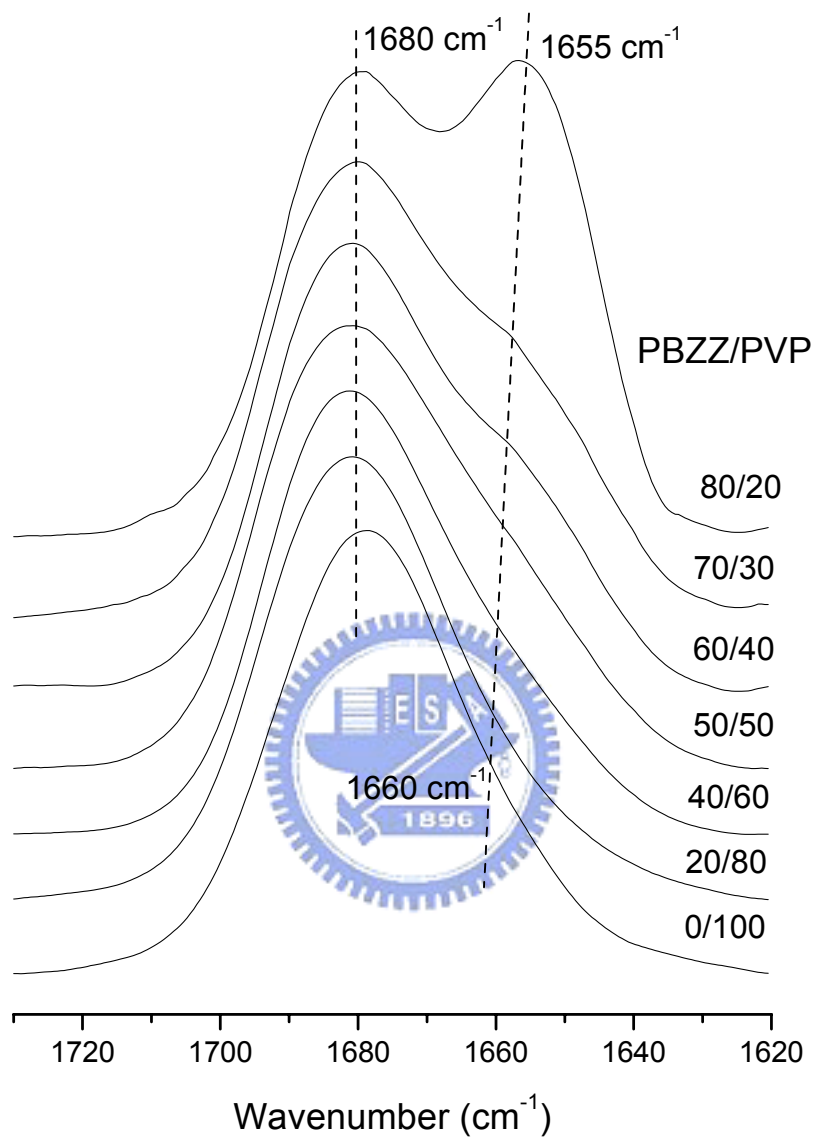


Figure 3-3. FTIR spectra recorded at room temperature between $1620\text{-}1730 \text{ cm}^{-1}$

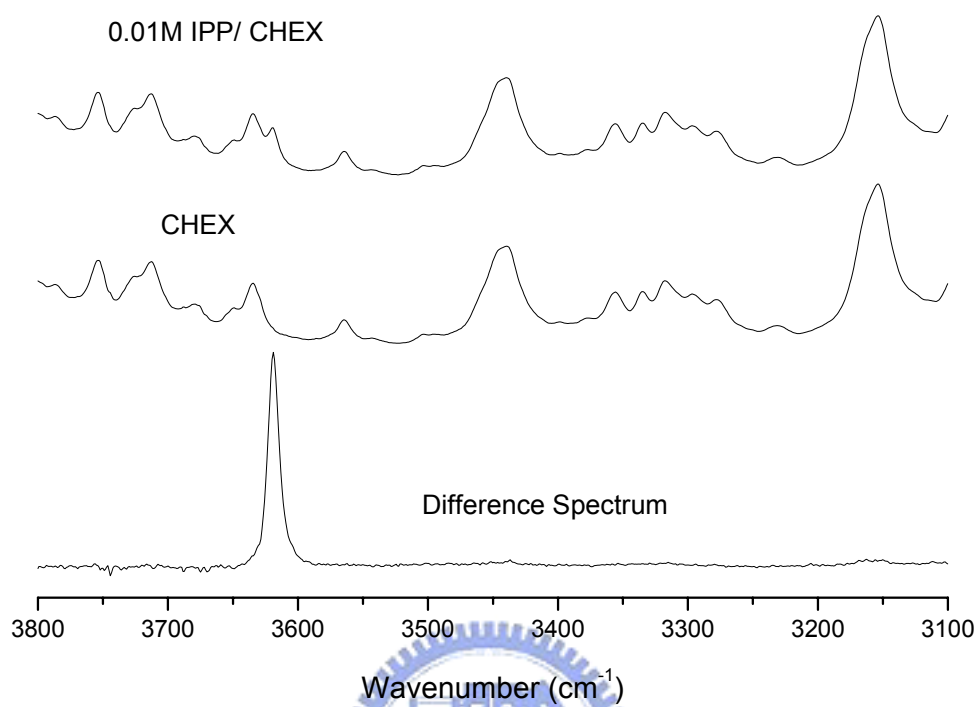


Figure 3-4. Infrared difference spectra of IPP/CHEX solutions recorded at room temperature

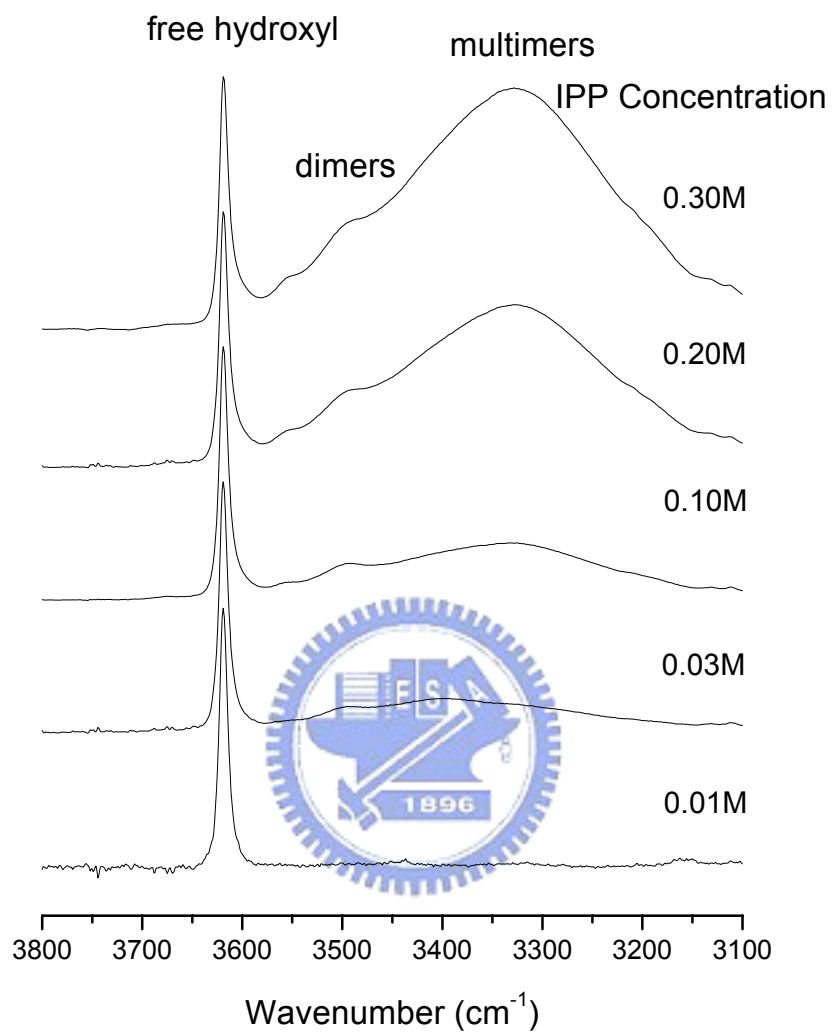


Figure 3-5. Infrared difference spectra of IPP/CHEX solutions with different IPP concentrations recorded at room temperature

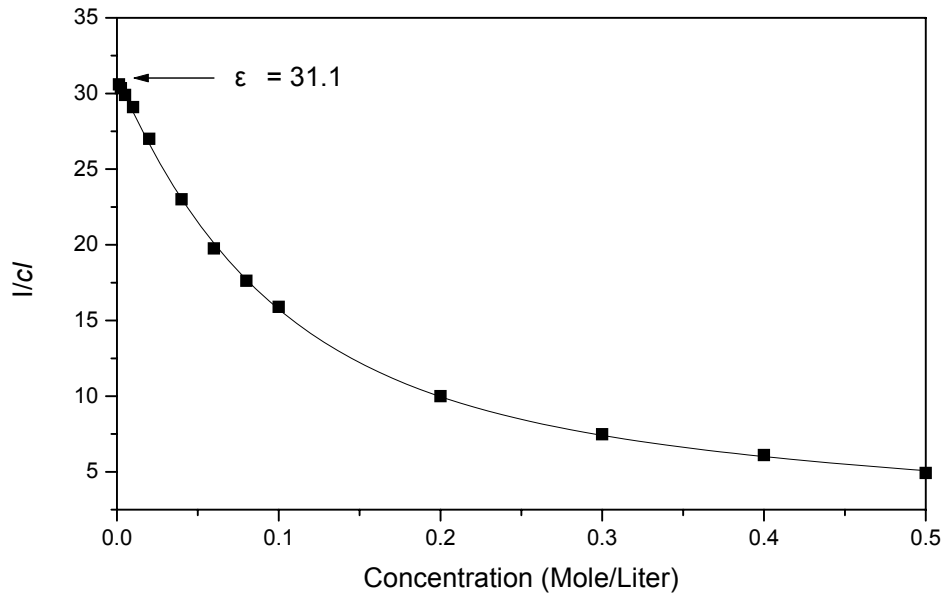


Figure 3-6. Absorptivity coefficient of IPP in cyclohexane at room temperature

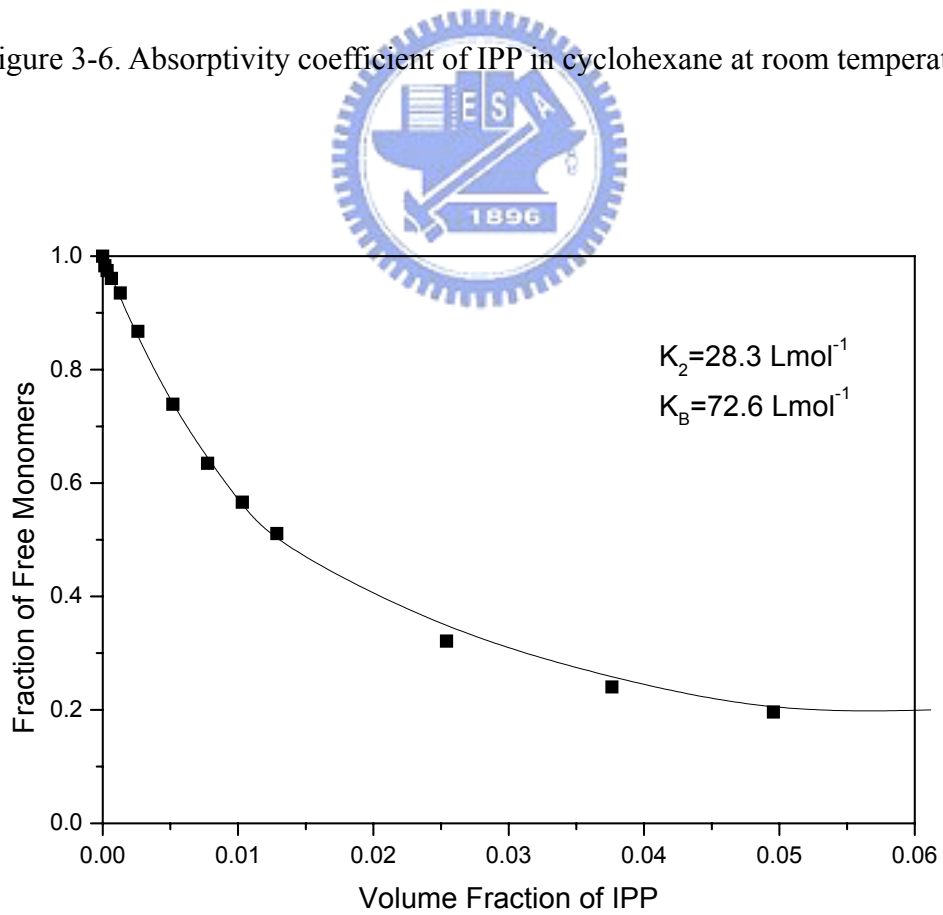


Figure 3-7. K_2 and K_B of IPP in cyclohexane at room temperature

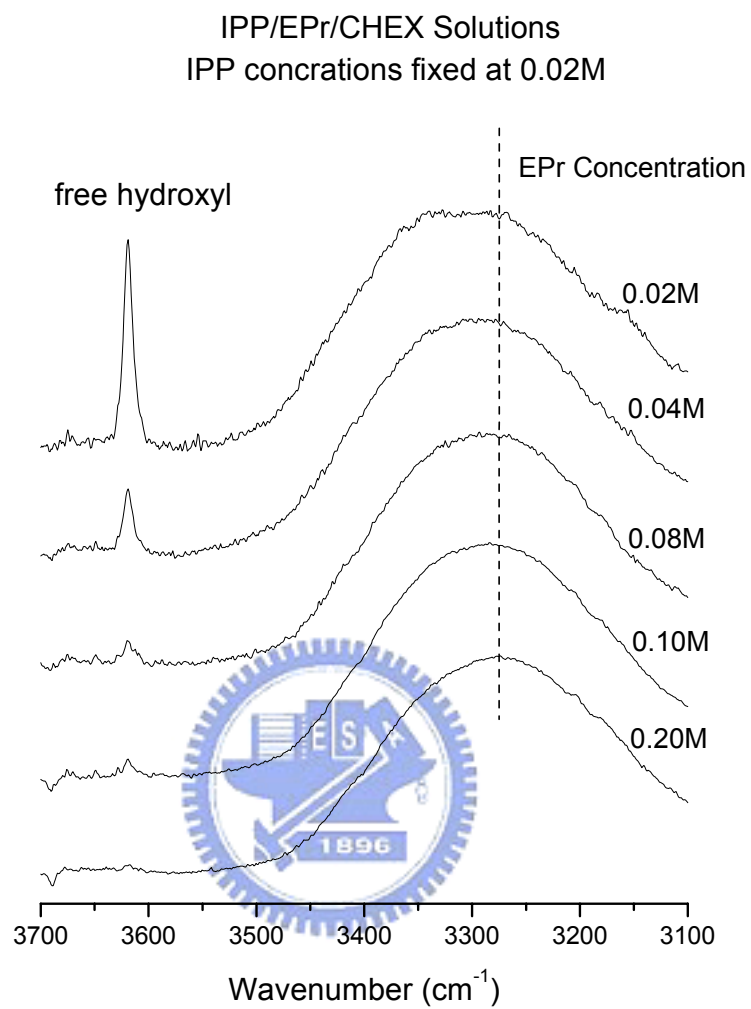


Figure 3-8. Infrared difference spectra of IPP/EPr/CHEX solutions recorded at room temperature

IPP/DMA/CHEX Solutions
IPP concentrations fixed at 0.02M

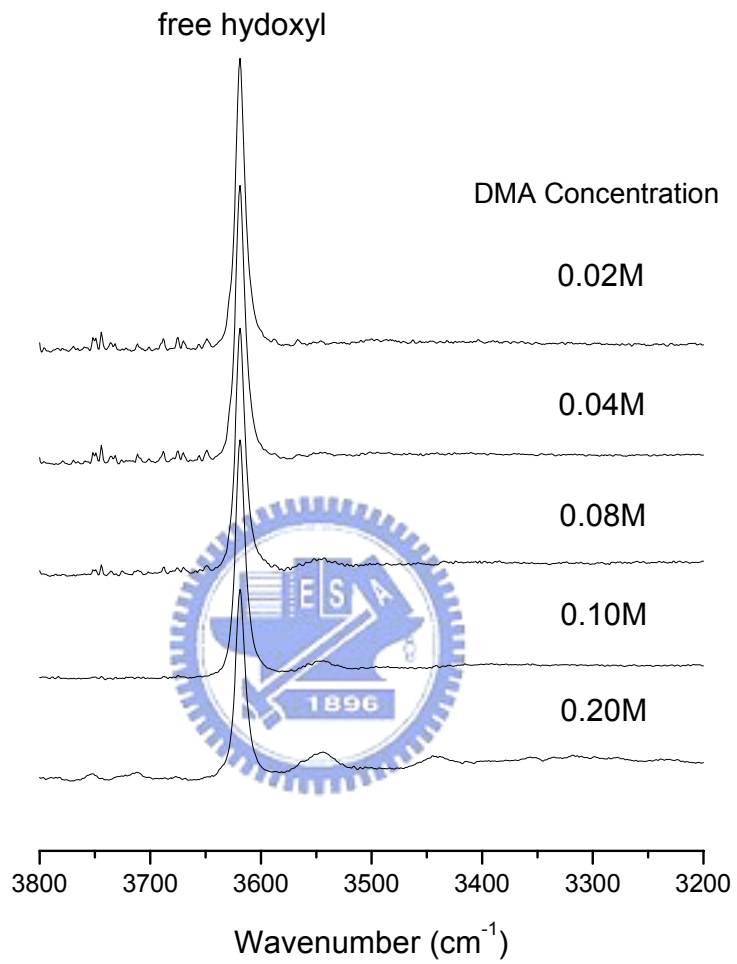


Figure 3-9. Infrared difference spectra of IPP/DMA/CHEX solutions recorded at room temperature

Chapter 4

The Kinetics of B-a and P-a Type Copolybenzoxazine via Ring Opening Process

Abstract

The structure of benzoxazines is similar to phenolic resin through thermal self-curing of the heterocyclic ring opening reaction that neither requires catalyst nor releases any condensation byproduct. These polybenzoxazine resins own several outstanding properties such as high thermal stability and high glass transition temperature. In order to better understand the curing kinetics of this copolybenzoxazine thermosetting resin, dynamic and isothermal differential scanning calorimetry (DSC) measurements were performed. Three models, Kissinger method, Flynn-Wall-Osawa method and Kamal method were used to describe the curing process. Dynamic kinetic activation energies based on Kissinger and Flynn-Wall-Osawa methods are 72.11 and 84.06 KJ/mol, respectively. The Kamal method based on an autocatalytic model results in a total order of reaction between 2.66 and 3.03, depending on curing temperature. Its activation energy and Arrhenius preexponential are 50.3 KJ/mol and 7959, respectively.

4.1 Introduction

The benzoxazine oligomeric products and polybenzoxazine (PBZZ) resins have been investigated recently [1,2]. The benzoxazine can be cured via a thermal ring opening reaction to construct an analogous phenolic structure characterized by a Mannich base bridge ($-\text{CH}_2\text{-NR-CH}_2$) [3]. Furthermore, the preferred reaction site is the position ortho to the hydroxyl functionality on the aromatic ring. In addition, these PBZZ resins were found to possess several outstanding properties such as near-zero shrinkage after curing [4], low water absorption [5] and high thermal stability. Furthermore, the PBZZ has higher glass transition temperature even though it has relatively low crosslinking density [6].

PBZZ can be formed by the heterocyclic curing via ring opening process. Hence, controlling the curing conditions such as temperature and time of the thermal curing process will result in notable difference in thermal properties. In this study, we selected B-a type and P-a type benzoxazines to form random co-PBZZ as shown in Scheme 4-1. The degree of crosslinking depends upon ratio of B-a/P-a benzoxazine, curing temperature and time. Kinetics of polymerization was investigated by using differential scanning calorimetry (DSC) and Fourier transform infrared (FTIR) during isothermal and dynamic curing processes in this study.

4.2 Experimental

4.2.1 Materials

The B-a type benzoxazine based on bisphenol-A, formaldehyde, aniline, and the P-a type based on phenol, formaldehyde, aniline were synthesized according to Scheme 4-2 [7]. Both bisphenol-A and phenol were purchased from SHOWA Chemical Company of Japan. Formaldehyde and aniline were purchased from Aldrich

Chemical Company of USA.

4.2.2 Reactants Preparations

Blend of B-a type and P-a type co-PBZZ with equal molar composition was prepared by solution blending. The monomer mixture was stirred and dissolved in acetone. The solution was allowed to evaporate slowly at 50 °C under vacuum for 1 day and the sample was used for isothermal and dynamic curing experiments. Afterwards, the sample was further post cured at different curing temperatures for 4hr under vacuum to ensure total curing of the co-PBZZ.

4.2.3 Differential Scanning Calorimetry (DSC)

Calorimetric measurements were performed using a TA Instruments Differential Scanning Calorimeter (DSC-2010). Both isothermal and dynamic-heating experiments were conducted under a nitrogen flow of 25 mL/min.

4.2.4 Isothermal Curing

The sample (equal molar ratio of B-a and P-a type benzoxazine) was placed in the Al cell at room temperature and then raised quickly to a preset temperature for each isothermal experimental. The instrument will achieve stability about 60 sec after reaching the setting temperature and data will be recorded immediately. When the DSC exothermic peak reaches the baseline level, the isothermal curing process is completed and the heat of reaction can be measured by integrating the exothermic peak area. Thereafter, the sample is cooled to 30 °C and reheated from 30 °C to 300 °C at a rate of 10 °C/min to determine the residual heat of the unreacted portion. These isothermal curing curves can be used to evaluate kinetic parameters of the curing reaction.

4.2.5 Dynamic Curing

Non-Isothermal experiment was carried out at 1, 5,10 or 20 °C/min from 30

°C to 300 °C and integrate the area of exothermic peak. We assume that the total recorded heat of reaction represents total heat evolved of complete curing at different curing rates.

4.2.6 Glass Transition Temperatures Measurement

The samples was cured at 160, 180, 190, 200 or 210 °C for 4hr in an oven to ensure total curing of the co-PBZZ. Then, all samples preheated with a scan rate of 20 °C/min from 30 °C to 260 °C and maintained at 260 °C for 2 min. The measurement was made using 5-10 mg sample on a DSC sample pan after the cell was cooled to 30 °C quickly from the melt of the first scan. The second scan rate was 20 °C/min from 30 to 300 °C and T_g was taken as the midpoint of the heat capacity transition between the upper and lower points of deviation from the extrapolated liquids and glass lines.

4.2.7 Infrared Spectroscopy

FT-IR measurement was recorded on a Nicolet Avatar 320 FT-IR Spectrophotometer, 32 scans were collected with a spectral resolution of 1 cm^{-1} . Infrared spectra of the copolymers were obtained using the conventional KBr method. The film used in this study was thin enough to obey the Beer-Lambert law. The sample chamber was purged with nitrogen during process of measurement in order to maintain the sample film drying.



4.3 Results and Discussion

4.3.1 Scanning DSC Studies

Figure 4-1 shows the DSC exothermic peaks from different dynamic heating rates [8,9] at 1, 5, 10 and 20 °C/min, respectively. Faster the heating rate results in higher maximum temperature (T_p) since the sample has shorter time to react and to release the heat of reaction. In addition, lower heating rate results in larger exothermic heat per unit weight as would be expected and results are summarized in Figure 4-1. The amount of exothermic heat from the slowest heating rate at 1 °C/min can be considered as the total heat released to completely cure the sample and the total heat (ΔH_{rxn}) is obtained is 439.1 (W/g). The $(dH/dt)_{iso}$ can be calculated from the trace of the isothermal DSC curve. The reaction rate ($d\alpha/dt$) at a pre-set curing temperature can be obtained by equation (4-1):

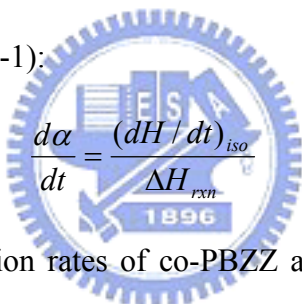

$$\frac{d\alpha}{dt} = \frac{(dH/dt)_{iso}}{\Delta H_{rxn}} \quad (4-1)$$

Figure 4-2 shows the reaction rates of co-PBZZ as a function of curing time for different curing temperatures. All samples were cured without adding any catalyst, and only a single exothermic peak was observed in all DSC curves. In other words, this heterocyclic ring opening curing reaction simply involves a single exothermic chemical process. As would be expected, at a higher curing temperature, the curing rate ($\frac{d\alpha}{dt}$) is higher and the curing time period is shorter. Figure 4-3 illustrates conversion (α) versus isothermal curing time at various curing temperatures. When the curing temperature arising from 160 °C to 220 °C, the conversion increases [10] from 0.35 to 0.93. Figure 4-4 shows plots of reaction rate versus conversion for different curing temperatures. The maximum reaction rate occurring between 20% (180 °C) and 38% (220°C) of conversion. This result confirms that the curing process

follows an autocatalytic model with maximum reaction rate between 20 % and 40 % conversions [11].

4.3.2 Kinetic Analysis

Kinetic analysis can be performed mostly using three kinetic models [12]: Kissinger [13] and Flynn-Wall-Osawa [14] methods are suitable for dynamic kinetic analysis, while the Kamal method [15] is suitable for isothermal kinetic analysis (autocatalytic model).

The extent of reaction, α , is proportional to the heat generated during reaction. The reaction rate is a function of conversion, which can be expressed by the general law as shown in equation (4-2).

$$\frac{d\alpha}{dt} = k(T)f(\alpha) \quad (4-2)$$

where t is the time, $k(T)$ is the rate constant, and $f(\alpha)$ is a function of dependence of conversion. By integrating the above equation, a new equation can be obtained as follow:

$$g(\alpha) = \int_0^\alpha \frac{d\alpha}{f(\alpha)} = k(T)t \quad (4-3)$$

where $g(\alpha)$ is the integrated form of the conversion dependent function.

4.3.2.1 Dynamic Kinetic Method

Non-isothermal can include single heating rate method and multiple heating rate method. The single heating method measures the curing process based on only a single constant rate cycle suitable for the n th-order reaction. Furthermore, these multiple heating rate methods are applicable for both n th-order and autocatalytic reactions. Two such multiple heating rate methods have been proposed by Kissinger [13] and Flynn-Wall-Ozawa [14]. These two methods have been used in this study

instead of other non-isothermal methods because they do not require a prior knowledge of the reaction mechanism to quantify kinetic parameters.

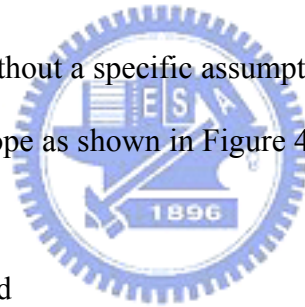
(a) Kissinger Method

Based on the Kissinger method, the activation energy can be obtained while the maximum reaction rate $\frac{d(d\alpha/dt)}{dt}$ is zero under a constant heating rate condition. The resulting relation can be expressed by equation (4-4).

$$\ln\left(\frac{\beta}{T_p^2}\right) = \ln\left(\frac{AR}{E_a}\right) - \frac{E_a}{RT_p} \quad (4-4)$$

where $\beta = dT/dt$ is a constant heating rate, T_p is the maximum exothermic temperature, and R is the universal gas constant. By plotting $\ln\left(\frac{\beta}{T_p^2}\right)$ versus $\frac{1}{T_p}$

gives the activation energy without a specific assumption of the conversion-dependent function, we calculated the slope as shown in Figure 4-5. Therefore, the value of E_a of 72.11 KJ/mol was obtained.



(b) Flynn-Wall-Ozawa Method

Flynn-Wall-Ozawa method is another widespread method used to describe the dynamic kinetic analysis without any assumptions on conversion-dependence function. Its general expression can be represented by equation (4-5).

$$E_a = \frac{-R}{1.052} \frac{\Delta \ln \beta}{\Delta(1/T_p)} \quad (4-5)$$

Plotted $\Delta \ln \beta$ versus $\Delta(1/T_p)$, we can obtain the slope value equal to $\frac{\Delta \ln \beta}{\Delta(1/T_p)}$

by least-squares technique to improve the linear approximation on the temperature integration term at Figure 4-6. Thus, the activation energy of $E_a = 84.06$ KJ/mol was obtained.

4.3.2.2 Isothermal Kinetic Analysis (Autocatalytic Model)

The autocatalytic model is a phenomenological approach developed by Kamal. Since the system is autocatalytic, the reaction rate can be described by the following general expression for autocatalyzed systems:

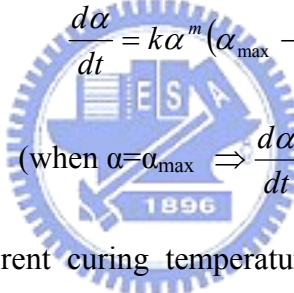
$$\frac{d\alpha}{dt} = k\alpha^m(1-\alpha)^n \quad (4-6)$$

where α is the reaction conversion, k is the kinetic rate constant, m and n are the kinetic exponents of the reaction, and $m+n$ is the overall reaction order.

However, in practice, the curing reaction will be ceased when the reaction conversion reaching the maximum value (α_{\max}). Then, equation (4-6) must be corrected and changed into equation (4-7) [16-18].

$$\frac{d\alpha}{dt} = k\alpha^m(\alpha_{\max} - \alpha)^n \quad (4-7)$$

(when $\alpha = \alpha_{\max} \Rightarrow \frac{d\alpha}{dt} = 0$)



where α_{\max} is based on different curing temperatures. To rearrange and take the nature logarithm of equation (4-7), the equation (4-8) and equation (4-9) are obtained. Using the iteration method to calculate the approximate values of m , n , k are calculated according to equation (4-8) and (4-9). When $|n_{i+1} - n_i| < 0.01$, the iteration will be stopped. Then, the values of m , n , k of different curing temperatures are obtained and results are listed in Table 4-1.

$$\ln\left(\frac{(d\alpha/dt)}{(\alpha_{\max} - \alpha)^n}\right) = \ln k + m \ln \alpha \quad (4-8)$$

$$\ln\left(\frac{(d\alpha/dt)}{k\alpha^m}\right) = n \ln(\alpha_{\max} - \alpha) \quad (4-9)$$

In addition, the rate constant, k , may be described by the Arrhenius expression: ¹⁶

$$k = Ae^{-E_a/RT} \quad (4-10)$$

where A is Arrhenius preexponential factor (or frequency factor), E_a is the energy of activation, R is the universal gas constant, and T is the absolute temperature.

Taking the nature logarithm of equation (4-10), we obtain the equation (4-11). By plotting $\ln k$ versus $1000/T$ for different isothermal curing temperatures, data are shown in Figure 4-7. The activation energy of $E_a=50.3$ KJ/mol and $\ln A=8.982$ ($A=7959$) are obtained.

$$\ln k = \ln A - E_a / RT \quad (4-11)$$

Comparing the three kinetic models, the values of the activation energy can be obtained from both dynamic and isothermal analyses. Hence, it's appropriate to calculate the activation energy and kinetic parameters including m , n and k by using Kissinger, Flynn-Wall-Osawa and Kamal methods in this system.

4.3.3 Glass Transition Temperature Analysis

Figure 4-8 shows traces of DSC thermograms of B-a and P-a type co-PBZZ under various curing temperatures for 4hr. In all conditions, the polymer blend gives only a single glass transition temperature because of similar structure. In addition, increasing the curing temperature, the T_g also increases with increasing the curing temperature until reaching 190 °C or above. Then, the T_g will be remain at a near constant value [19] which is about 173 °C. In the other words, the different curing temperatures affect the degree of curing and results in different glass transition temperatures until the maximum T_g is reached at 173 °C.

4.3.4 Fourier Transfer Infrared Spectroscopy Analysis

The FTIR spectra [20,21] of B-a type and P-a type benzoxazine copolymers

after different temperature treatments were recorded and shown in Figure 4-9(a). The bands of 748 cm^{-1} and 691 cm^{-1} , corresponding to the monosubstituted benzene, are still present even after high temperatures curing. On the contrary, the characteristic absorption band of the oxazine ring at 947 cm^{-1} is disappeared, and the absorption at 1495 cm^{-1} from the trisubstituted benzene ring and at 1236 cm^{-1} from the CH_2 wagging are both decreased. However, a new absorption band appeared at 1478 cm^{-1} due to the tetrasubstituted benzene ring mode. Besides, the absorptions at 1030 and 1230 cm^{-1} corresponding to the symmetric and asymmetric C—O—C bonds of the benzoxazine, disappear after the curing process. Furthermore, a broad hydroxyl bond is form because of the ring opening process as shown in Figure 4-9(b). Based DSC and FTIR results, the ring opening reaction indeed occurs as shown in Scheme 4-1.



4.4 Conclusions

Based on the DSC results, the equal molar mixture of B-a type and P-a type co-PBZZ is completely miscible in the amorphous phase and gives a single glass transition temperature. The product T_g depends upon ratio of B-a/P-a benzoxazine, curing temperature and curing time. The maximum T_g is about 173 °C. The isothermal curing process of the co-PBZZ precursor involves an autocatalytic type curing mechanism. In the dynamic experiments, the activation energy is 72.11 KJ/mol based on Kissinger method and 84.06 KJ/mol based on Flynn-Wall-Ozawa method. Furthermore, in the isothermal experiments, the activation energy and Arrhenius preexponential are 50.3 KJ/mol and 7959 based on Kamal method, and the total order of reaction is between 2.66 and 3.03, depending on the isothermal curing temperature.



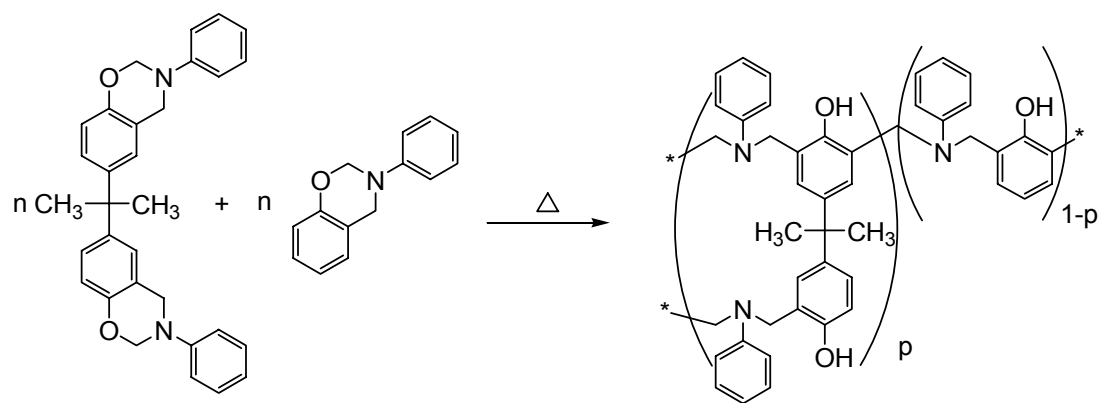
References

- [1] Kim, H. J.; Brunovska, Z.; Ishida, H. *Polymer* **1999**, *40*, 1815
- [2] Kim, H. J.; Brunovska, Z.; Ishida, H. *Polymer* **1999**, *40*, 6565.
- [3] Ishida, H.; Allen, D. J. *J. Polym. Sci. Polym. Phys.* **1996**, *34*, 1019.
- [4] Ishida, H. *J. Appl. Polym. Sci.*, **1995**, *58*, 1751.
- [5] Ishida, H.; Low, H. Y. *Macromolecules* **1997**, *30*, 1099.
- [6] Ning, X.; Ishida, H. *J. Polym. Sci. Polym. Phys.* **1994**, *32*, 921.
- [7] Ning, X.; Ishida, H. *J. Polym. Sci. Polym. Chem.* **1994**, *32*, 1121.
- [8] Zvetkov, V. L. *Polymer* **2001**, *42*, 6687.
- [9] Jost, N.; Koocsis, J. K. *Polymer* **2002**, *43*, 1383.
- [10] Kim, W. G.; Lee, J. Y. *Polymer* **2002**, *43*, 5713.
- [11] Boey, F. Y. C.; Qiang, W. *Polymer* **2000**, *41*, 208.
- [12] Barral, L.; Cano, J.; Lopez, I.; Bueno, L.; Nogueira, P.; ABAD, M. J.; Ramirez, C. *J. Polym. Sci. Polym. Phys.* **2000**, *38*, 351.
- [13] Kissinger, H. E. *Anal. Chem.* **1957**, *29*, 1702.
- [14] Ozawa, T. *J. Therm. Anal.* **1970**, *2*, 301.
- [15] Kamal, M. R. *Polym. Eng. Sci.* **1974**, *27*, 782.
- [16] Fischer, M.; Tran, C. D. *Anal. Chem.*, **1999**, *71*, 953.
- [17] Cole, R. C. *Macromolecules*, **1991**, *24*, 3093.
- [18] Cole, K. C.; Hechler, J. J.; Nobel, D. *Macromolecules* **1991**, *24*, 3098.
- [19] Shen, S. B.; Ishida, H. *J. Polym. Sci. Polym. Phys.* **1999**, *37*, 3257.
- [20] Agag, T.; Takeichi, T. *Macromolecules* **2001**, *34*, 7257.
- [21] Ishida, H.; Sanders, D. P. *Macromolecules* **2000**, *33*, 8149.

Table 4-1. The Values of m , n , k and Total Order of Different Curing Temperature

Curing Temp. (°C)	m	n	k (1/min)	$m+n$
220	1.36	1.67	2.19	3.03
210	1.26	1.70	1.70	2.96
200	1.35	1.55	1.25	2.90
190	1.27	1.46	1.18	2.73
180	1.15	1.52	0.75	2.67
160	1.23	1.43	0.39	2.66

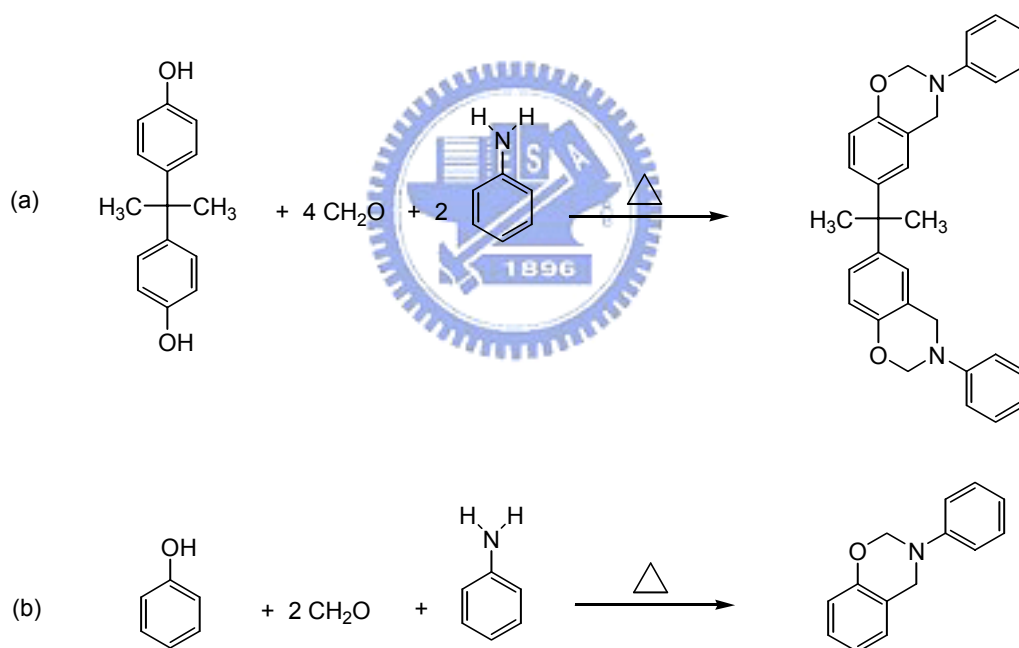




benzoxazine (B-a type)benzoxazine (P-a type)

random co-PBZZ

Scheme 4-1. The ring opening process of B-a type and P-a type co-PBZZ



Scheme 4-2. The chemical reactions of (a) B-a type benzoxazine and (b) P-a type benzoxazine

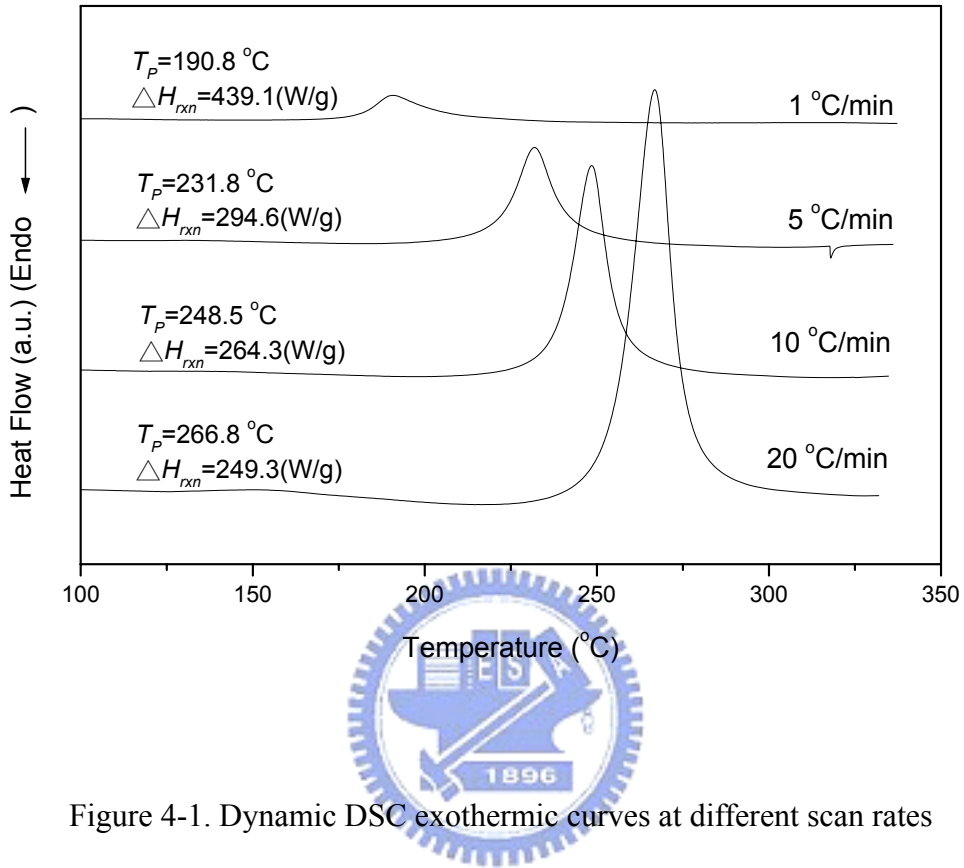


Figure 4-1. Dynamic DSC exothermic curves at different scan rates

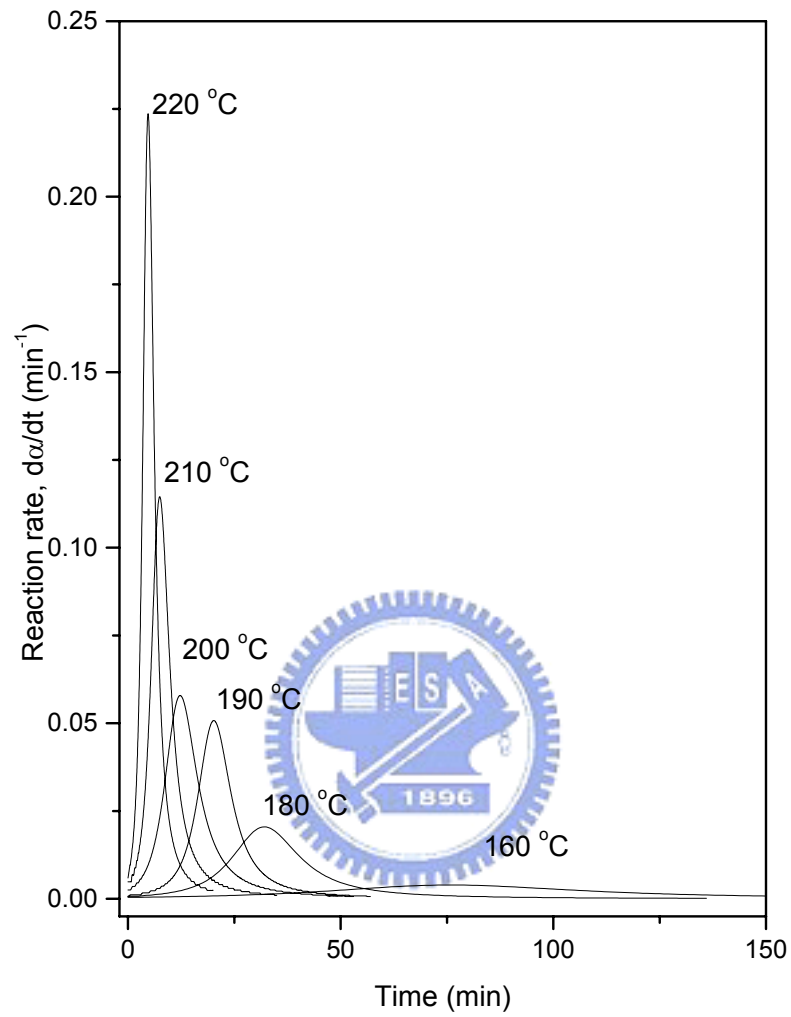


Figure 4-2. Reaction rate versus isothermal curing time at different curing temperatures

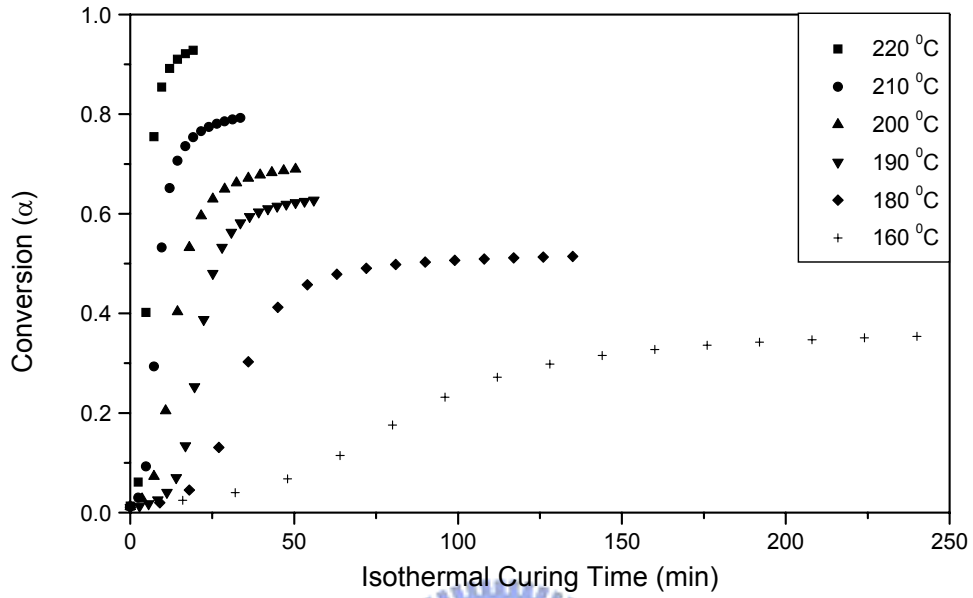


Figure 4-3. Conversion versus isothermal curing time at different curing temperatures



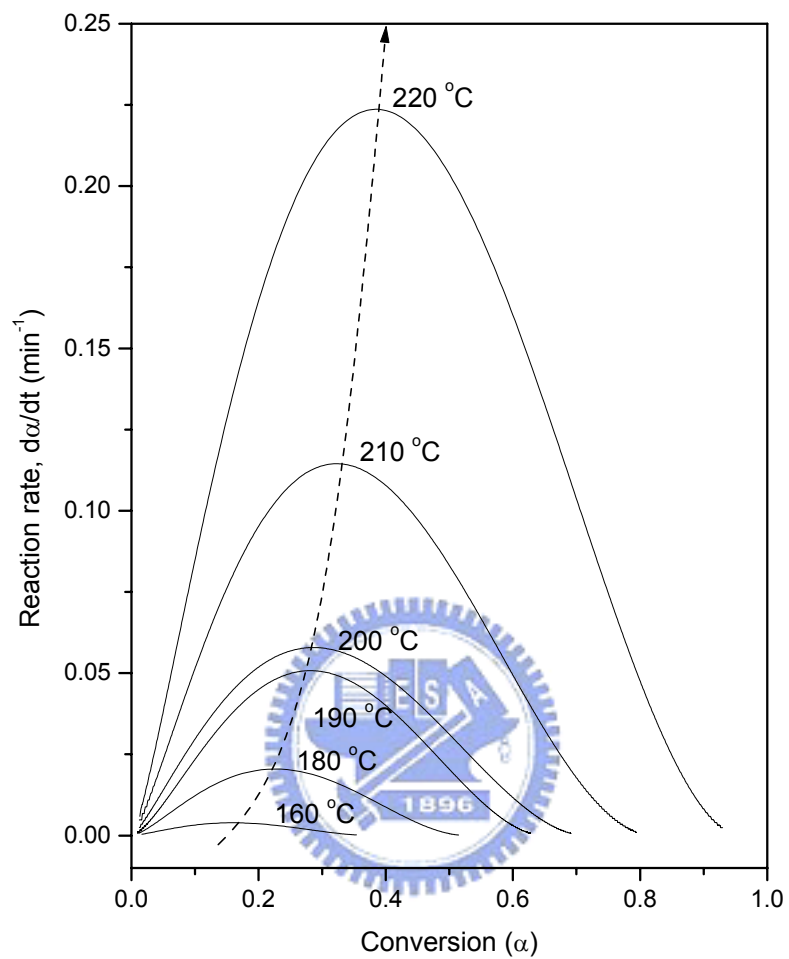


Figure 4-4. The tendency of reaction rate versus conversion

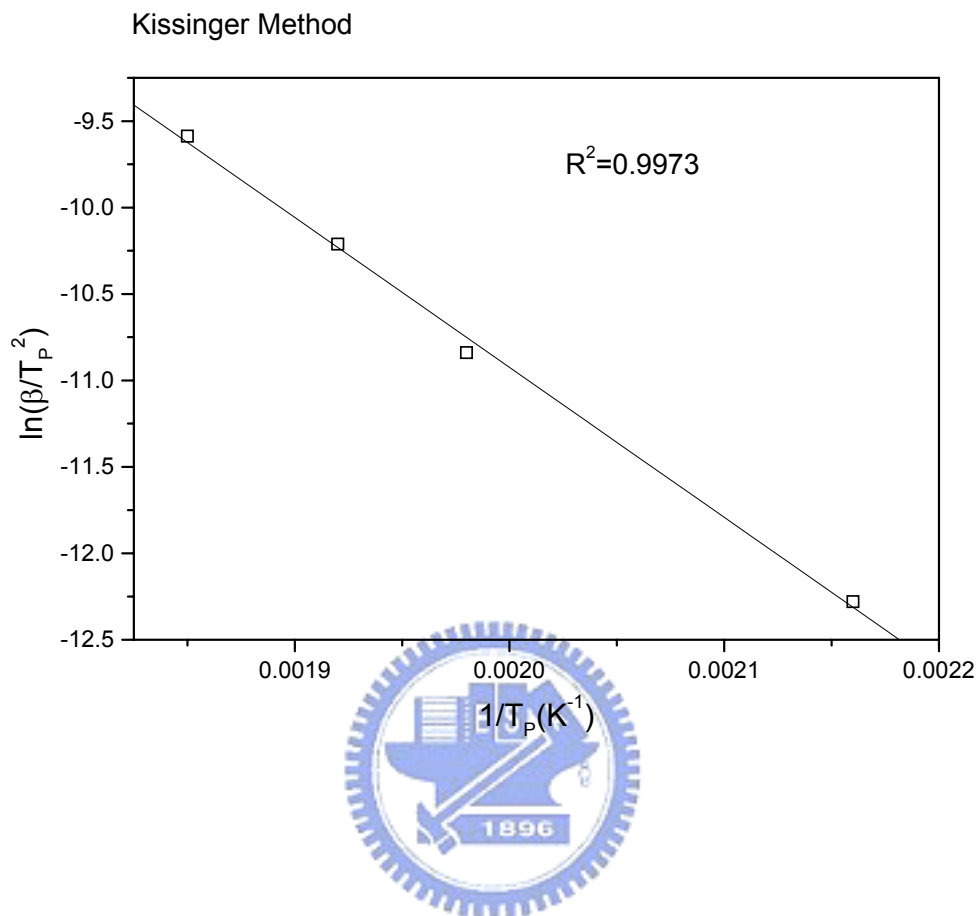


Figure 4-5. Plots for determination of the activation energy of curing reaction by Kissinger method

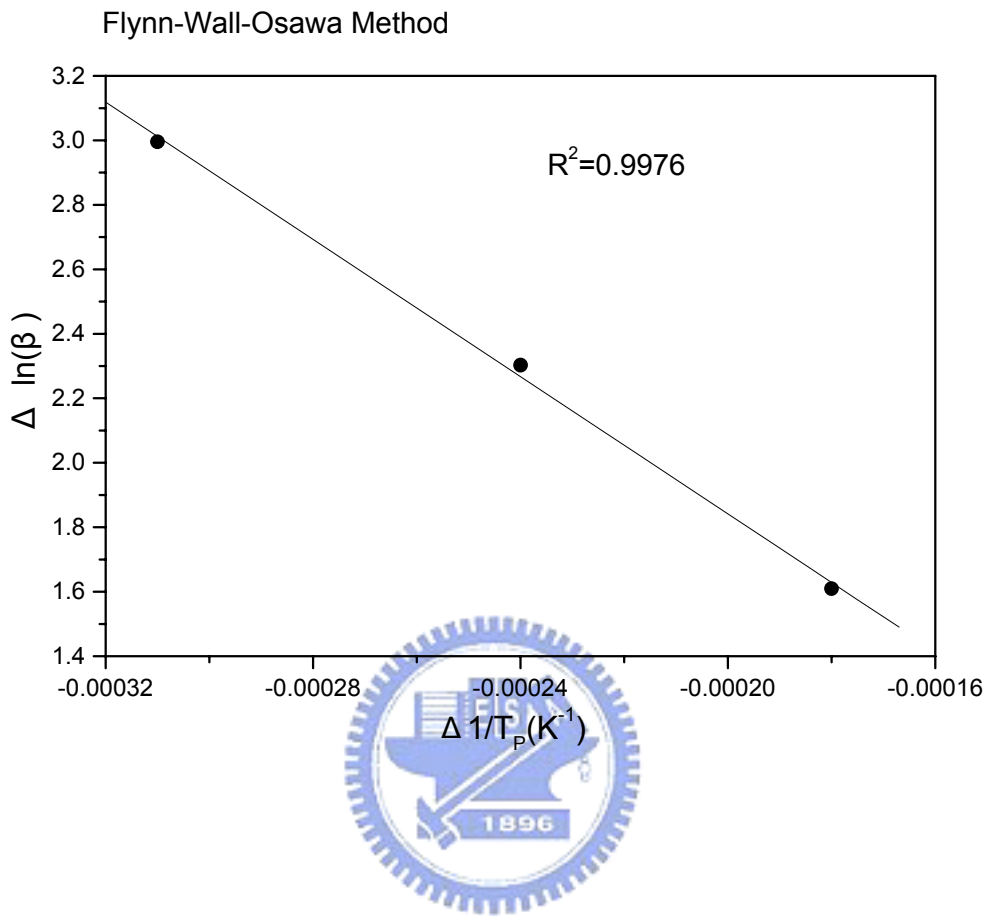


Figure 4-6. Plots for determination of the activation energy of curing reaction by Flynn-Wall-Osawa method

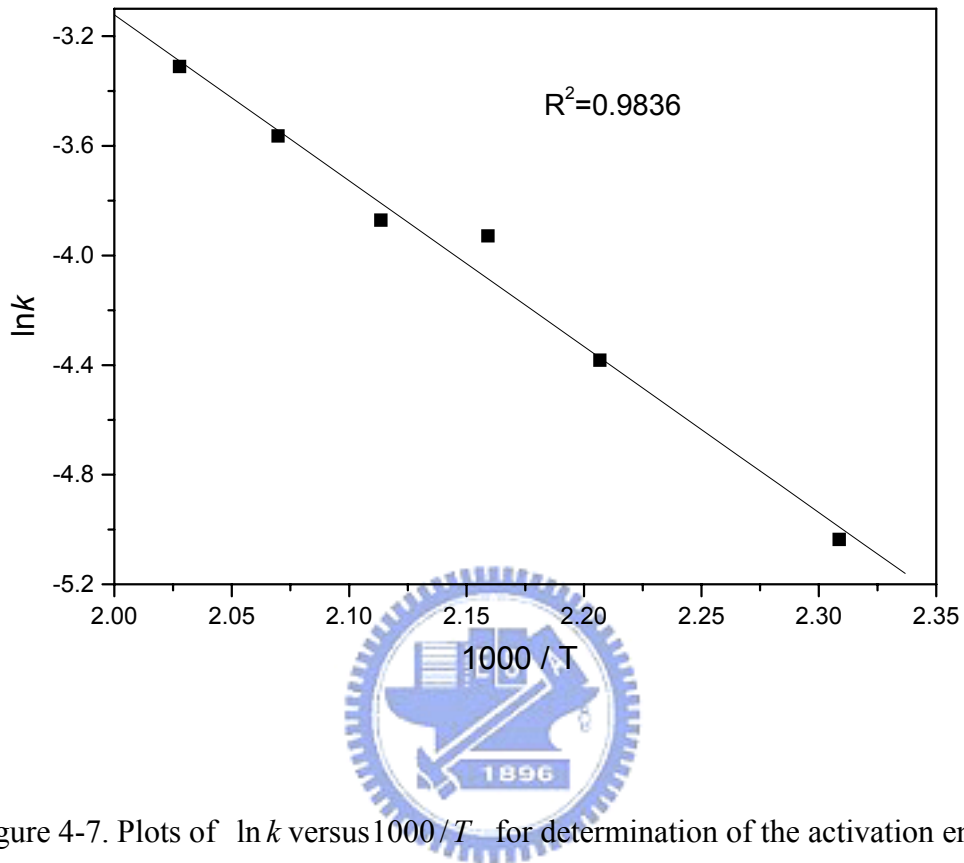


Figure 4-7. Plots of $\ln k$ versus $1000/T$ for determination of the activation energy and Arrhenius preexponential of curing reaction by isothermal method

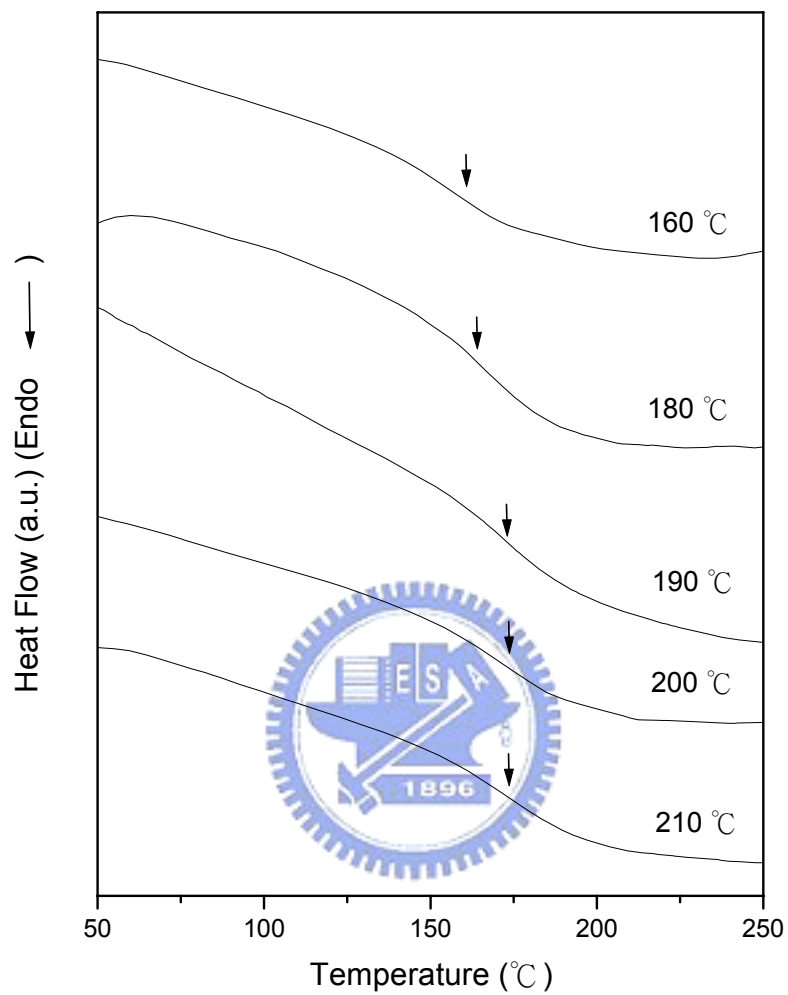


Figure 4-8. The DSC curves at different curing temperatures for 4hr

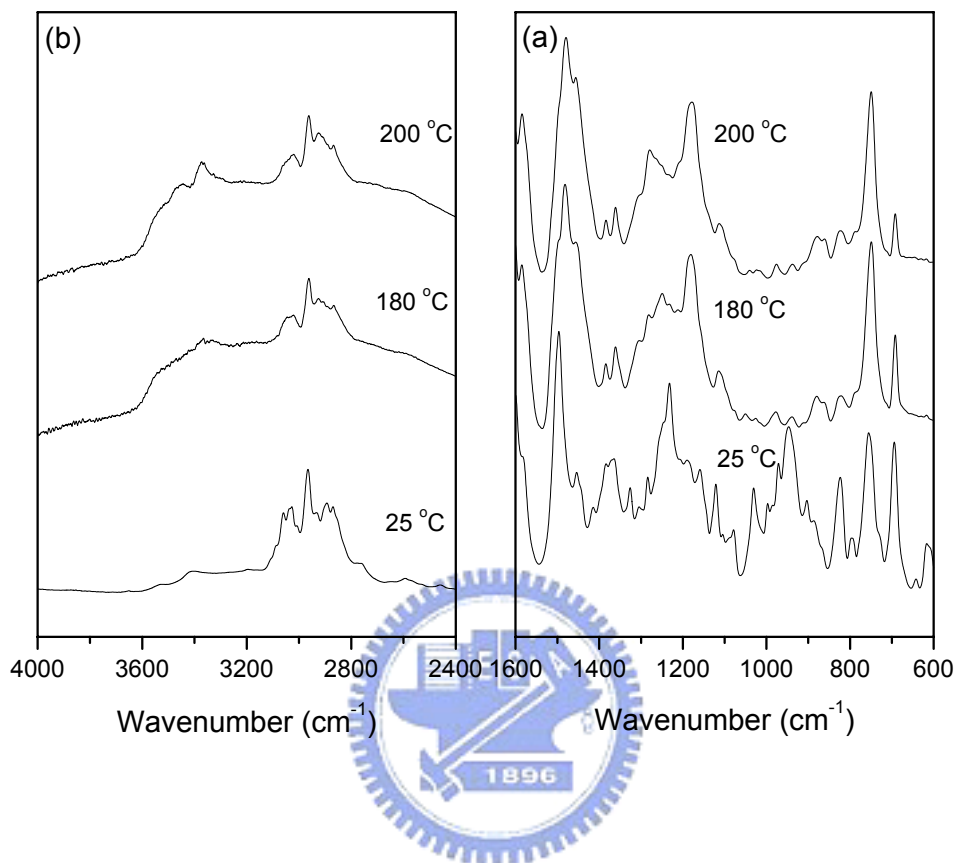


Figure 4-9. FTIR spectra recorded at room temperature between (a) 600-1600 cm^{-1} (b) 2400-4000 cm^{-1}

Chapter 5

Synthesis and Characterization of Fluorinated Polybenzoxazine

Material with Low Dielectric Constant

Abstract

It is well-known that low dielectric materials are used as insulating materials, and the incorporation of fluorinated substitutes into polymer is able to decrease its dielectric constant because of small dipole and the low polarizability of the C—F bond. In this study, a novel structure of the fluorinated benzoxazine (F-1 benzoxazine) has been synthesized by incorporating the trifluoromethyl groups into the monomer, and its structure has been also characterized by $^1\text{H-NMR}$, $^{19}\text{F-NMR}$ and FT-IR. Further, we have prepared the fluorinated copolybenzoxazine (B-a/F-1=1/1) with substantially reduced dielectric constant at $k=2.36$. In addition, this fluorinated copolybenzoxazine possesses high glass transition temperature and high thermal stability, which is suitable for high temperature operation for certain special processes of interlayer dielectrics.

5.1 Introduction

Low dielectric constant materials ($k < 3.0$) have the advantage of facilitating manufacture of higher performance integrated-circuit (IC) devices with decreasing feature size of the chip [1]. However, interlevel dielectric materials must meet stringent material property requirements for successful integration into either the conventional or damascene interconnect structures. These requirements are based on electrical properties, thermal stability, thermomechanical, thermal stress properties, and moisture uptake. The desired electrical properties are low dielectric constant, low dielectric loss, and high breakdown voltage. However, the propagation delay and cross-talk are primary problems which have been concerned in dielectric materials.

Continuing improvement in device's performance has significantly affected its dimensional requirement. These enhancements have to reduce in the wiring pitch and increase in the number of wiring leave to fulfill demands for density and performance improvement, especially at high frequency operations in the hundreds of megahertz or even gigahertz range. As device dimensions shrink to less than $0.18 \mu\text{m}$ process (even $0.13 \mu\text{m}$ or smaller), it is necessary to reduce either the resistance of the metallization or the dielectric constant of the IMD (inter-metal dielectrics) material or both [1,2]. The time, which is related to the resulting signal delay is given by equation (5-1).

$$\tau = RC \quad (5-1)$$

and call the RC the time delay of signals. R is the line resistance and C is the line capacitance of the used structure.

Reducing the resistance-capacitance (RC) [3,4] is needed in order to avoid propagation delay, cross-talk noise, and power dissipation [3]. Equation (5-2) can be used to estimate the RC delay.

$$RC = 2\rho\varepsilon\varepsilon_0\left(\frac{4L^2}{P^2} + \frac{L^2}{T^2}\right) \quad (5-2)$$

R : total line resistance, C : total line capacitance, ρ : metal resistivity, ε : dielectric constant, ε_0 : permittivity of free space, L : line length, P : the distance between two conducting lines, T : metal thickness.

After replacing the aluminum process by the copper process, the metal resistivity has been reduced from $2.650 \times 10^{-8} \Omega\text{m}$ to $1.678 \times 10^{-8} \Omega\text{m}$ [2]. The most feasible approach is to use an insulating material possessing a lower dielectric constant without changing the copper process. In addition to the low dielectric constant, materials must also exhibit high thermal stability (T_g and T_d), low thermal expansion coefficient, low moisture uptake, good chemical stability and electric properties for practical applications [1,3].

Polybenzoxazine (PBZZ) resins were found to possess several outstanding properties such as near-zero shrinkage after curing, high thermal stability and low water absorption [5]. Furthermore, the PBZZ has high glass transition temperature even though it has relatively low crosslinking density [6]. Several methods have been developed to lower the material dielectric constant [1-3]. Fluorinated polymer is a practicable and feasible approach to develop low dielectric materials. It is well-known that the incorporation of fluorinated substitutes into a polymer is able to decrease its dielectric constant because of small dipole and the low polarizability of the C—F bond [1,2,7]. Furthermore, polymer free volume is also increased by replacing methyl groups by trifluoromethyl groups [1].

In this chapter, a series of fluorinated PBZZ possessing desirable properties of low dielectric constant with low RC delay time and high speed logic chip have been synthesized and characterized.

5.2 Experimental

5.2.1 Synthesis of 3-[4-(trifluoromethyl)phenol]-6-(2,2,2-trifluoro-1-(trifluoromethyl)-1-{3-[4-(trifluoromethyl)phenol]-3,4-dihydro-2H-1,3-benzoxazine-6-yl}-ethyl)-3,4-dihydro-2H-1,3-benzoxazine (F-1 benzoxazine)

The F-1 benzoxazine was prepared according to Scheme 5-1. 0.04 mol 37% formaldehyde aqueous solution and 5 mL dioxane were fed into a three-necked flask equipped with nitrogen flow and an ice bath for 10 min. Then, 0.02 mol 4-(trifluoromethyl)aniline dissolved in 5 mL dioxane was added into the reactor slowly by a dropping funnel. The mixture was stirred continuously for 10 min, and 0.01 mol hexafluorobisphenol A in 20 mL dioxane was added. The reaction temperature was raised to 100 °C, and the mixture was allowed to reflux for 24 hr. The solvent was then removed by reducing pressure, and the yellow solid product obtained. The crude product was dissolved in ethyl ether and washed with 1N NaOH and water in sequence for three times. The product solution was dried by magnesium sodium and distilled by reducing pressure, a light yellow solid product, F-1 benzoxazine, in 71% yield was obtained.

5.2.2 Nuclear Magnetic Resonance (NMR)

^1H and ^{19}F NMR spectra were recorded on a Varian Unity Inova 500 FT NMR Spectrometer operating at 500 MHz with chemical shift reported in parts per million (ppm). Deuterium chloroform was used as solvent.

5.2.3 Fourier Transform Infrared Spectroscopy (FT-IR)

FT-IR measurement was recorded on a Nicolet Avatar 320 FT-IR Spectrophotometer, 32 scans were collected with a spectral resolution of 1 cm^{-1} . Infrared spectra of the benzoxazine were obtained using the conventional NaCl method. The film used in this study was thin enough to obey the Beer-Lambert law.

The sample chamber was purged with nitrogen during process of measurement in order to maintain sample film drying.

5.2.4 Reactants Preparations

As shown in Scheme 5-2, blends of B-a/F-1 benzoxazines with different ratio were prepared by solution blending because the mechanical strength of the F-1 PBZZ is too weak to form a film for DEA experiment. The monomer mixture was stirred and dissolved in acetone and the solution was allowed to evaporate slowly at 50 °C for 1 day and cured at 180 °C for 4hr under vacuum to ensure total curing of the co-polybenzoxazine (PBZZ). After curing, a transparent, smooth, stiff and hazel to brown film was obtained.

5.2.5 Dielectric Analysis

Dielectric relaxation data were obtained using a TA instrument (DEA-2970), which was incorporated a parallel plate cell arrangement and a computer-controlled furnace to ensure good electrical contact between the electrodes and the sample. In order to increase the accuracy of measuring dielectric constant, the flat films are required; therefore, we used the automatic scraper to form a flat film. The experiment was conducted under a nitrogen flow 20 mL/min and the thickness of sample was controlled between 0.125 and 0.75 mm. The dielectric constant and dielectric loss were determined with a heating rate of 1 °C/min from 25 °C to 50 °C with scan frequencies ranging from 1 to 10⁵ Hz.

5.2.6 Differential Scanning Calorimetry (DSC)

The calorimetric measurement was performed using a TA Instruments Differential Scanning Calorimeter (DSC-2010) conducted under a nitrogen flow of 25 mL/min. The sample was preheated with a scan rate of 20 °C/min from 30 °C to 260 °C (or 300 °C) and maintained at 260 °C (or 300 °C) for 2 min. The measurement was

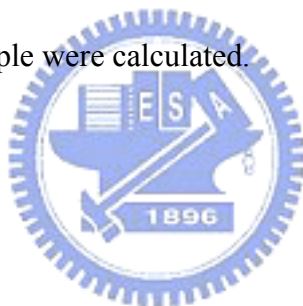
made using 5-10 mg sample in a DSC sample cell by cooling to 30 °C quickly from the melt of the first scan. The second scan rate was 20 °C/min from 30 to 300 °C (or 350 °C) and the T_g was taken as the midpoint of the heat capacity transition between the upper and lower points of deviation from the extrapolated liquids and glass lines.

5.2.7 Thermogravimetric Analysis (TGA)

Thermal stability of the cured sample was investigated by a Du Pont 2050 TGA. The cured sample of 5-10 mg was placed in a Pt cell and heated at a heating rate of 10 °C /min from 30 to 800°C at a nitrogen flow of 90 mL/min.

5.2.8 Water Absorption

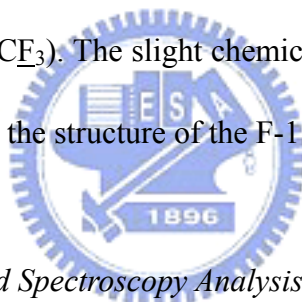
The cured sample was dried under vacuum at 80 °C for 12 hr before placing in the environments of air or water for one day and one week. Then, the percentages of water absorption of cured sample were calculated.



5.3 Results and Discussion

5.3.1 Nuclear Magnetic Resonance Analysis

After the cyclization of oxazine, the characteristic peaks $\text{Ar}-\underline{\text{CH}_2}-\text{N}$ and $\text{N}-\underline{\text{CH}_2}-\text{O}$ can be observed in proton NMR [5,6]. Figure 5-1 shows the ^1H -NMR (CDCl_3 , 500 MHz) spectrum of F-1 benzoxazine: δ 4.65 ppm (4H, $\text{Ar}-\underline{\text{CH}_2}-\text{N}$), δ 5.40 ppm (4H, $\text{N}-\underline{\text{CH}_2}-\text{O}$), δ 6.78~7.52 ppm (14H, Ar). Figures 5-2 (a) and (b) show the ^{19}F -NMR (CDCl_3 , 500 MHz) spectra of monomers of 4-(trifluoromethyl)aniline and hexafluorobisphenol A: δ -61.05 ppm (3F, $\text{NH}_2-\text{Ar}-\underline{\text{CF}_3}$) [8], δ -63.25 ppm (6F, $\text{C}-\underline{\text{CF}_3}$). The ^{19}F -NMR (CDCl_3 , 500 MHz) spectrum of F-1 benzoxazine is shown in Figure 5-3: δ -61.54~-61.66 ppm (6F, $\text{N}-\text{Ar}-\underline{\text{CF}_3}$), δ -63.81~63.94 ppm (6F, $\text{C}-\underline{\text{CF}_3}$). The slight chemical shift (within 1 ppm) observed in ^{19}F -NMR spectrum because the structure of the F-1 benzoxazine ring was formed.



5.3.2 Fourier Transfer Infrared Spectroscopy Analysis

The FT-IR spectrum of F-1 benzoxazine is shown in Figure 5-4. The bands at 755 cm^{-1} and 692 cm^{-1} (referred to monosubstituted benzene) do not appear in comparing with the B-a type benzoxazine [9,10]. However, the same characteristic absorption bands of oxazine ring at 937 cm^{-1} and 1521 cm^{-1} from the trisubstituted benzene ring, and at 1242 cm^{-1} from the CH_2 wagging appear. Besides, the absorptions at 1038 and 1228 cm^{-1} assigned to symmetric and asymmetric $\text{C}-\text{O}-\text{C}$ bonds of the benzoxazine are both present. Based on the NMR and FT-IR results, we confirmed that the F-1 benzoxazine was formed in the study.

5.3.3 Dielectric Constant Analysis

The dielectric constant k is directly related to the polarizability of a material, therefore, it is strongly dependent on its chemical structure [11]. Saturated hydrocarbons are significantly lower polarizable than species that are unsaturated, conjugated, or have polarizable phenyl groups. This effect is demonstrated by comparing the dielectric constants of an aromatic PI with that of the semi-aliphatic PI [11]. In general, the k value can be lowered by breaking off the conjugated system or decreasing the number of phenyl group in the monomer. However, these alterations have to compromise with lower thermal stability. To fluorinate the polymer is one method to solve above-mentioned problems [12]. Fluorine substitution lowers the k value by decreasing the polarizability and the moisture absorption and by increasing the free volume. Substitution of hydrogen with F or $-CF_3$ group decreases the electronic polarizability due to strong electron-withdrawing inductive effect. The bulky $-CF_3$ group is able to reduce efficient molecular packing and increase the free volume. The hydrophobicity introduced by F substitution is important since the moisture, even in small concentrations, strongly affects the dielectric constant due to the large k value of water, 78.5 at 25 °C [2].

In this study, we incorporated fluorine atoms into the backbone of PBZZ. Table 5-1 presents the dielectric constant, and dissipation factor, $\tan \delta$, of co-PBZZ with different B-a/F-1 ratios measured at 10^5 Hz and 298 K. Prior to each measurement, the sample was thoroughly dried under vacuum to reduce the influence of the absorbed moisture on the dielectric constant. Comparing these co-PBZZ mixtures synthesized with different B-a/F-1 weight ratios, the incorporation of fluorinated substitution (F-1 benzoxazine) results in decreasing in the dielectric constant with minimum value of 2.36 (B-a/F-1=1:1). In addition, the dissipation factor

is also a very important property of ILD (interlayer dielectrics) materials [13-15] that less than 0.005 at 1 M Hz is normally required. In this study, those compositions all meet the requirement of dissipation factor. Hence, the fluorination of benzoxazine reduces its dielectric constant with tolerable dissipation factor.

5.3.4 Thermal Properties

Thermal properties of organic polymers with low k dielectrics are another primary concern in process integration. The C–H, C–C, and C–N bonds of aliphatic polymers generally become unstable at temperatures above 400 °C [1-4] even in the nitrogen or vacuum environment. The resulting volatiles may cause delaminating or blistering in the ILD. Only organic materials composed of nonaliphatic C–H, C–C, C–N, and C–S bonds, such as aromatic, crosslinking or ladder structure, is able to resist such elevated temperatures. Unfortunately, material possessing good thermal stability generally tends to have high dielectric constant. The incorporation of fluorine atoms into the benzoxazine structure is able to achieve materials with high thermal stability and low dielectric constant. Fluorination can improve thermal properties partly because the C–F bond is stronger than the C–H bond [1]. More important, it can reduce the dielectric constant due to its lower polarizability structure.

5.3.5 Glass Transition Temperature Analysis

The glass transition temperature is an important property of a dielectric film. Exceeding T_g the polymer may cause a large decrease in Young's modulus and typically results in a shift in the dielectric properties. Hence, a polymer with T_g greater or equal to the highest processing temperature is desirable. All B-a/F-1

co-PBZZ were subjected to DSC measurements for the purpose of examining microscopic miscibility. Figure 5-5 shows the DSC thermograms of all B-a/F-1 co-PBZZ exhibiting only one T_g from all composition. A single T_g strongly implies that all these B-a/F-1 co-PBZZs are homogenous. Figure 5-6 shows the dependence of the T_g on the composition of these copolymers, increasing the F-1 benzoxzine content results in substantial T_g increase than average values. The hydrogen bonding interactions of $O - H \cdots F - C$ [16] and $O - H \cdots O - H$ are expected in these copolymers. Kwei equation [17] describes the effect of hydrogen bonding interaction on T_g between polymers or a copolymer as shown in equation (5-3):

$$T_g = \frac{W_1 T_{g1} + kW_2 T_{g2}}{(W_1 + kW_2)} + qW_1W_2 \quad (5-3)$$

where W_1 and W_2 are weight fractions of the components, T_{g1} and T_{g2} represent the component glass transition temperatures. Both k and q are fitting constants. In general, the parameter q may be considered as a measurement of the specific interaction in a polymer blend system. When the intermolecular interaction is stronger than intramolecular interaction in a binary blend or copolymer, the value of q will be positive; otherwise, q will be negative. When the q value is larger, it represents that the interaction is stronger than the self-interaction of the blend. In case of no interaction existed between components, the q value will be equal to zero and its T_g behavior can be described by the Gordon-Taylor equation [18] as shown in equation (5-4).

$$T_g = \frac{W_1 T_{g1} + kW_2 T_{g2}}{(W_1 + kW_2)} \quad (5-4)$$

As shown in Figure 5-5, the B-a/F-1 co-PBZZs are completely miscible in the amorphous phase and results in positive T_g deviation. After the “best fitting” by the Kwei equation, $k=1$ and $q=141$ were obtained. In this study, a large positive q value of

141 indicates that a strong intermolecular interaction exists between B-a/F-1 co-PBZZ. This result can also explain why T_g s of these copolymers are positively deviated as shown in Figure 5-6. The glass transition temperature increases about 113 °C, from 170.6 °C of the B-a benzoxazine to 283.4 °C (F-1 benzoxazine). The resulted higher T_g makes the high temperature applications possible.

5.3.6 Thermogravimetric Analysis

For organic films, thermal stability is one of the most important requirements for new IMD materials. Unlike aluminum metallization, copper metallization can be achieved by electroplating or electroless plating (chemical reduction) besides PVD and CVD techniques [19-21]. These processes can be conducted at temperatures below 250 °C. Unfortunately, an annealing step is necessary to ensure void free copper deposits. Since this step is performed at temperatures in the range 400-450 °C for up to 1 hr, any low k material must be able to withstand this temperature for several hours.

Table 5-2 shows the weight loss of different compositions of co-PBZZ. The incorporation of fluorinated structure into the backbone of B-a benzoxazine results in noticeable change in thermal stability. The minimum weight loss occurs in the pure F-1 PBZZ structure that can resist high temperature (above 400 °C).

5.3.7 Water Absorption

Since the water possesses large dielectric constant value (78.5 at 25 °C) [2], the water absorption is required to be below 1%. Therefore, the hydrophobic character is required in the low dielectric constant materials. The PBZZ possesses low water absorption ability [5] due to its highly crosslink density and hydrophobic property,

and their percentages of water absorption are listed in Table 5-3. The water absorptions are all below 1%, even under the water environment. The results indicate that the fluorinated co-PBZZs possess an outstanding property of resisting moisture uptake.



5.4 Conclusions

In this study, we have synthesized a series of co-PBZZ with different B-a/F-1 ratios. A single glass transition temperature (T_g) over entire compositions indicates that the amorphous phase of the co-PBZZ is totally miscible and homogeneous. In addition, a large positive deviation based on Kwei equation in the T_g versus composition diagram, implies that strong hydrogen bonding interactions exist within B-a/F-1 co-PBZZ. Furthermore, the fluorination on PBZZ is able to reduce dielectric constant and increase thermal properties. The co-PBZZ with B-a/F-1=1/1 gives low dielectric constant at 2.36 and $\tan \delta$ at 0.0044 which is suitable for insulating applications. Moreover, its thermal properties are also substantially improved over the B-a type PBZZ.



References

- [1] Maier, G. *Prog. Polym. Sci.* **2001**, *26*, 3.
- [2] Nalwa, H. S., editor. "Handbook of Advanced Electronic and Photonic Materials and Devices, Volume 4." San Diego: Academic Press, **2001**.
- [3] Treichel, H.; Ruhl, G.; Ansmann, P.; Wurl, R.; Muller, C. H.; Dietlmeier, M. *Microelectronic Eng.* **1998**, *40*, 1.
- [4] Peters, L. *Semicond Int* **1998**, *21*, 64.
- [5] Ishida, H.; Low, H. Y. *Macromolecules* **1997**, *30*, 1099.
- [6] Ning, X.; Ishida, H. *J Polym. Sci., Part B: Polym. Phys.* 1994, *32*, 921.
- [7] Goodwin, A. A.; Atkinson, J. R.; Hay, J. N.; Mercer, F. W. *Polymer* **1999**, *40*, 1515.
- [8] Bardin, V. V. *J Fluorine Chem.* **1998**, *89*, 195.
- [9] Ishida, H.; Sanders, D. P. *Macromolecules* **2000**, *33*, 8149.
- [10] Agag, T.; Takeichi, T. *Macromolecules* **2001**, *34*, 7257.
- [11] Hougham, G. Tesoro, G.; Viehbeck, A.; Chapple-Sokol J. D. *Macromolecules* **1994**, *27*, 5964.
- [12] Simposon, J. O.; Clair, A. K. S. *Thin Solid Films* **1997**, *308-309*, 480.
- [13] Durstock, M. F.; Rubner, M. F. *Langmuir* **2001**, *17*, 7865.
- [14] Kannurpatti, A. R.; Bowman, C. *Macromolecules* **1998**, *31*, 3311.
- [15] Carter, K. R.; Dipietro, R. A.; Sanchez, M. I.; Swanson, S. A. *Chem. Mater.* **2001**, *13*, 213.
- [16] Thalladi, V. R.; Weiss, H. C.; Blaser, D.; Boese, R.; Nangia, A.; Desiraju, G. R. *J Am. Chem. Soc.* **1998**, *120*, 8702.
- [17] Kwei, T. K. *J Polym. Sci. Poly Lett Ed* **1984**, *22*, 307.

[18] Gondon, M.; Taylor, J. S. *J Appl. Chem.* **1952**, 2, 493.

[19] Singer, P. *Semicond Int* **1999**, 22, 38.

[20] Peters, L. *Semicond Int* **2000**, 23, 108.

[21] Peters, L. *Semicond Int* **2002**, 25, 57.



Table 5-1. The Dielectric Constant and Dissipation Factor of B-a/F-1 co-PBZZ at 298

K & 10^5 Hz

B-a/F-1 (weight ratio)	Dielectric Constant	Dissipation Factor ($\tan \delta$)
1/0	3.56±0.01	0.00206
1/0.05	3.02±0.03	0.00235
1/0.1	2.85±0.02	0.00282
1/0.2	2.76±0.02	0.00287
1/0.5	2.39±0.01	0.00387
1/1	2.36±0.01	0.00440

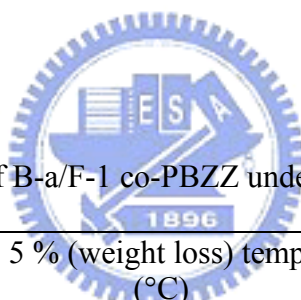


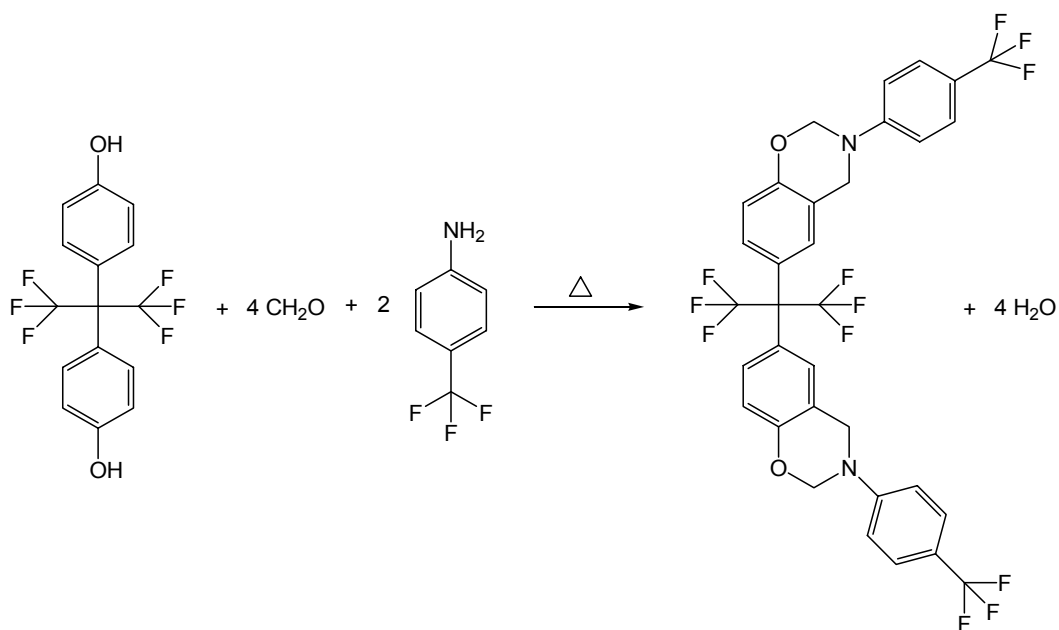
Table 5- 2. The Weight Loss of B-a/F-1 co-PBZZ under N₂ Environment

B-a/F-1 (weight ratio)	5 % (weight loss) temp. (°C)	10 % (weight loss) temp. (°C)
1/0	329.0	363.6
1/0.05	329.9	366.1
1/0.1	346.1	379.7
1/0.2	354.7	400.2
1/0.5	360.5	420.6
1/1	368.6	430.6
0/1	374.4	455.7

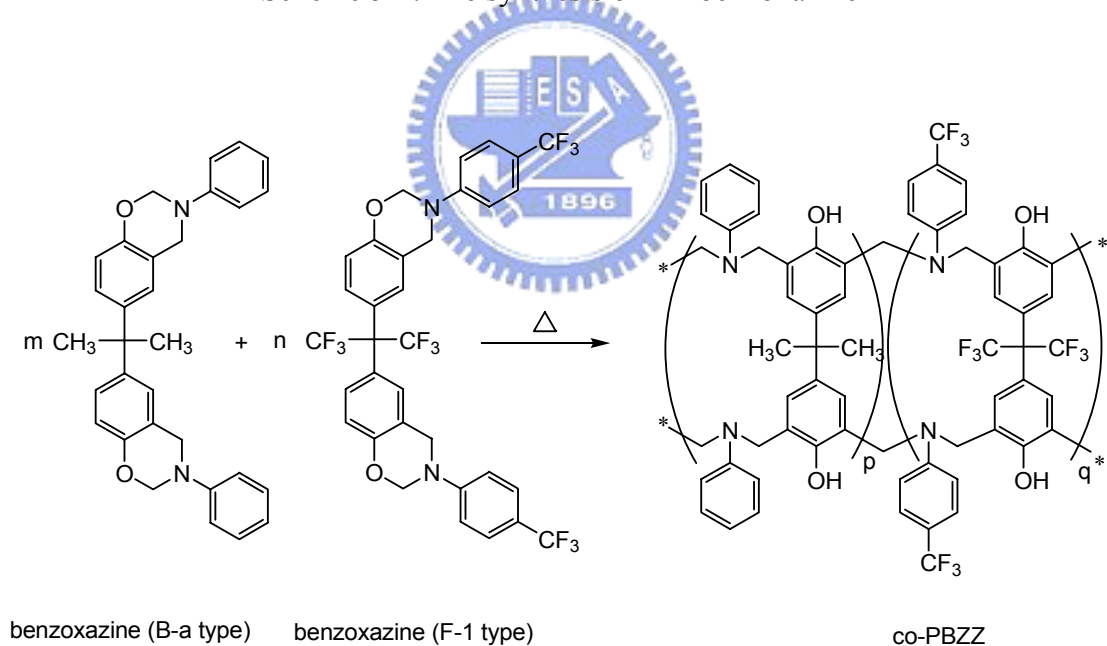
Table 5-3. The Percentages of Water Absorption of B-a/F-1 co-PBZZ at Room Temperature

Environment	B-a/F-1 co-PBZZ water absorption (%)						
	1/0	1/0.05	1/0.1	1/0.2	1/0.5	1/1	0/1
in air 1 day	<0.01	<0.01	<0.01	<0.01	<0.01	<0.01	<0.01
in air 1 week	<0.01	<0.01	<0.01	<0.01	<0.01	<0.01	<0.01
in water 1 day	0.24	<0.01	<0.01	<0.01	<0.01	<0.01	<0.01
in water 1 week	0.70	0.69	0.61	0.64	0.60	0.71	0.52





Scheme 5-1. The synthesis of F-1 benzoxazine



Scheme 5-2. The ring opening process of B-a/ F-1 co-PBZZ

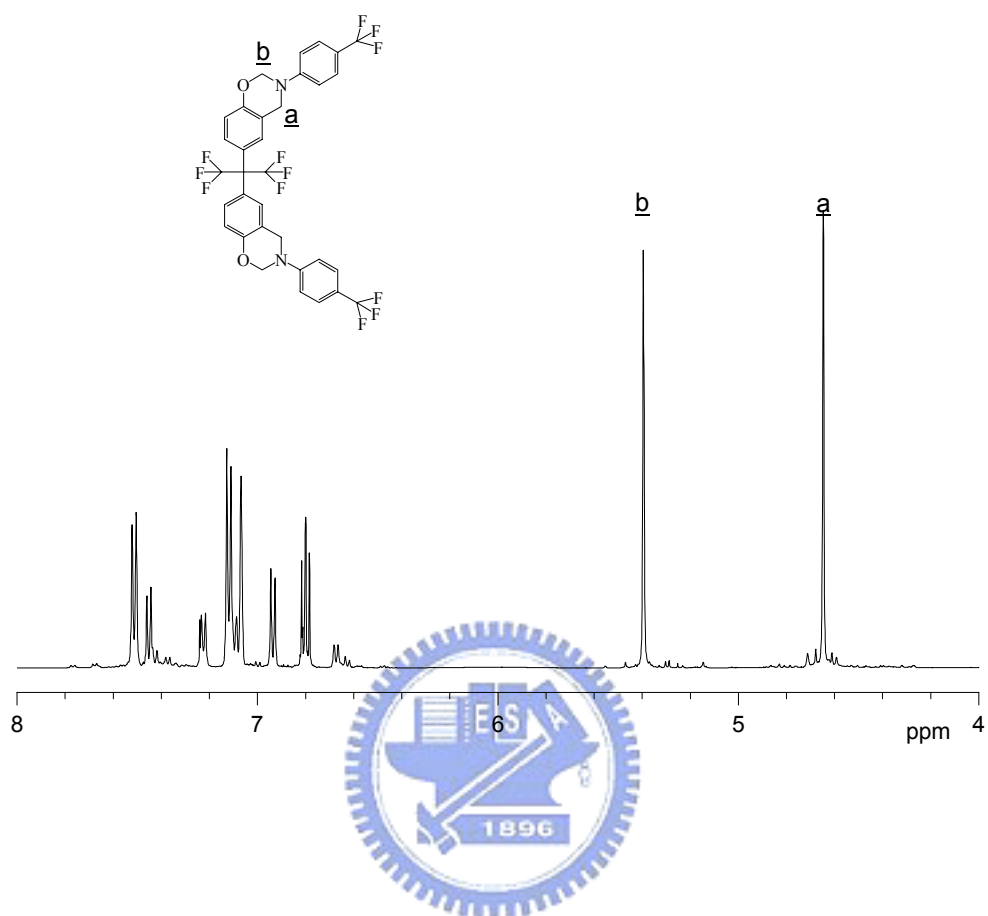


Figure 5-1. The ¹H-NMR spectrum of F-1 benzoxazine

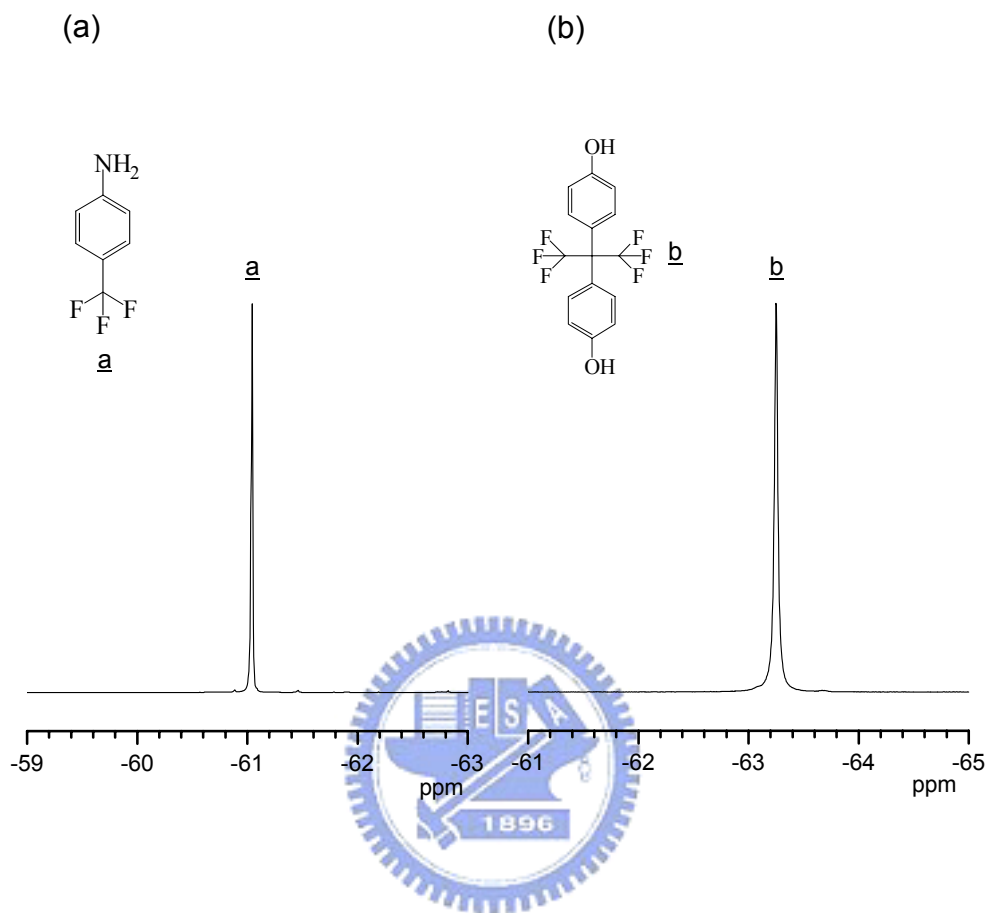


Figure 5-2 The ^{19}F -NMR spectra of (a) 4-(trifluoromethyl)aniline, (b) hexafluorobisphenol A

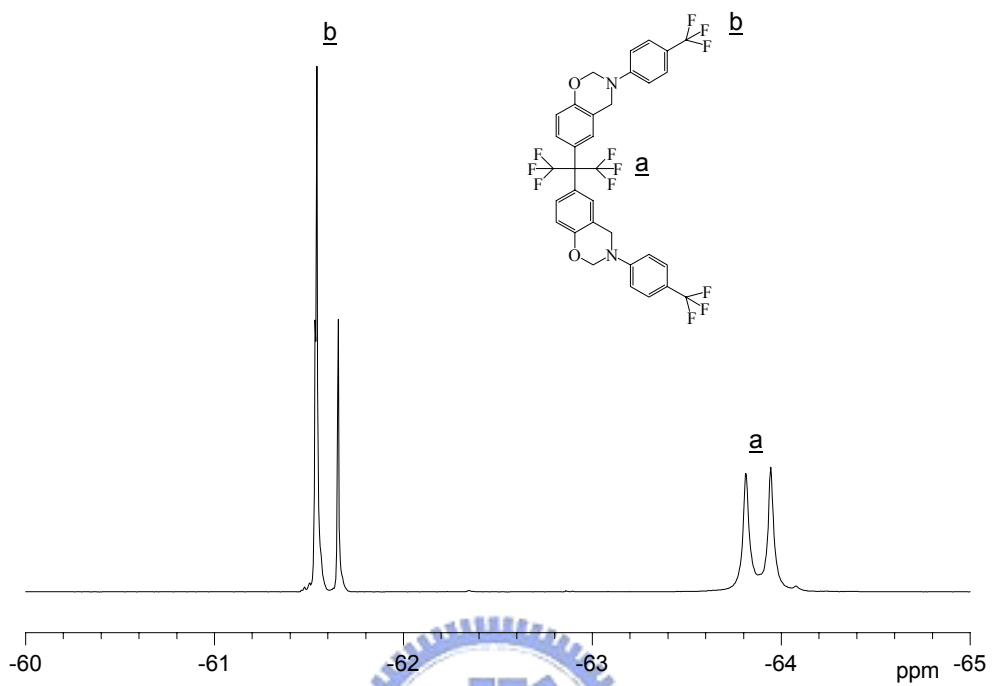


Figure 5-3. The ^{19}F -NMR spectrum of F-1 benzoxazine

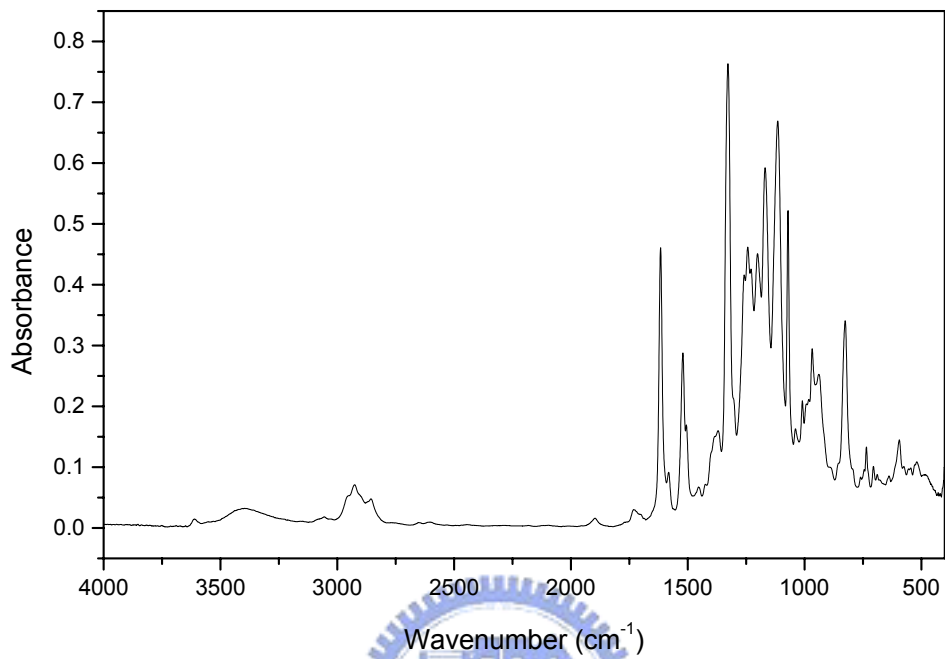


Figure 5-4. The FT-IR spectrum of F-1 benzoxazine

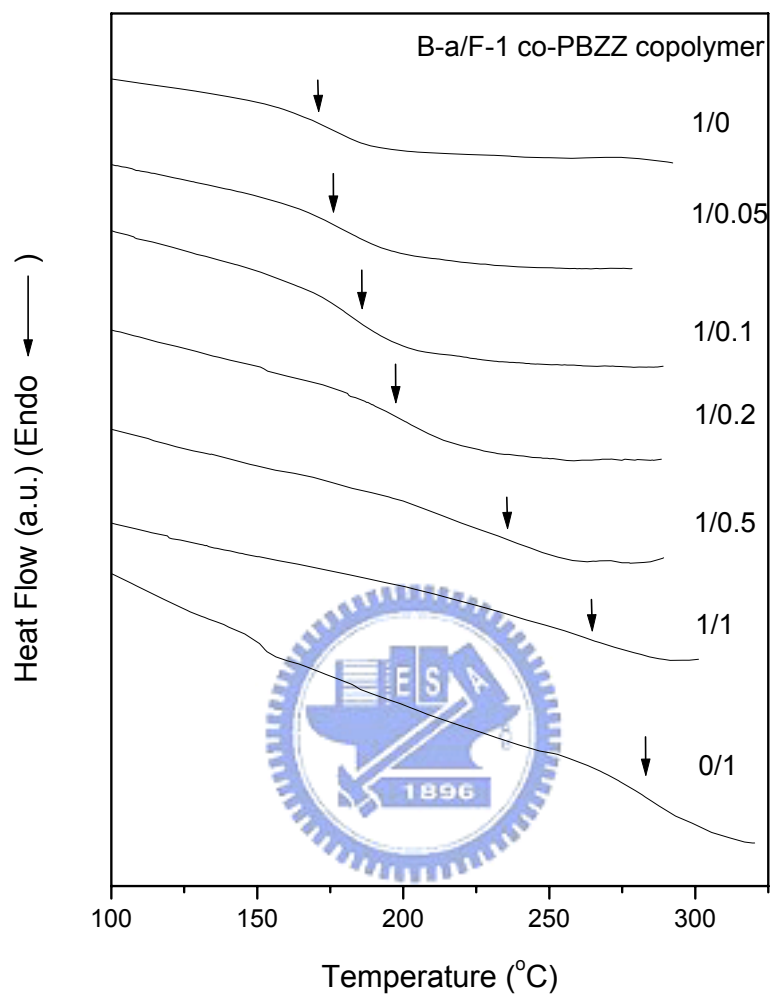


Figure 5-5. The DSC scans of B-a/F-1 co-PBZZ copolymers with different composition

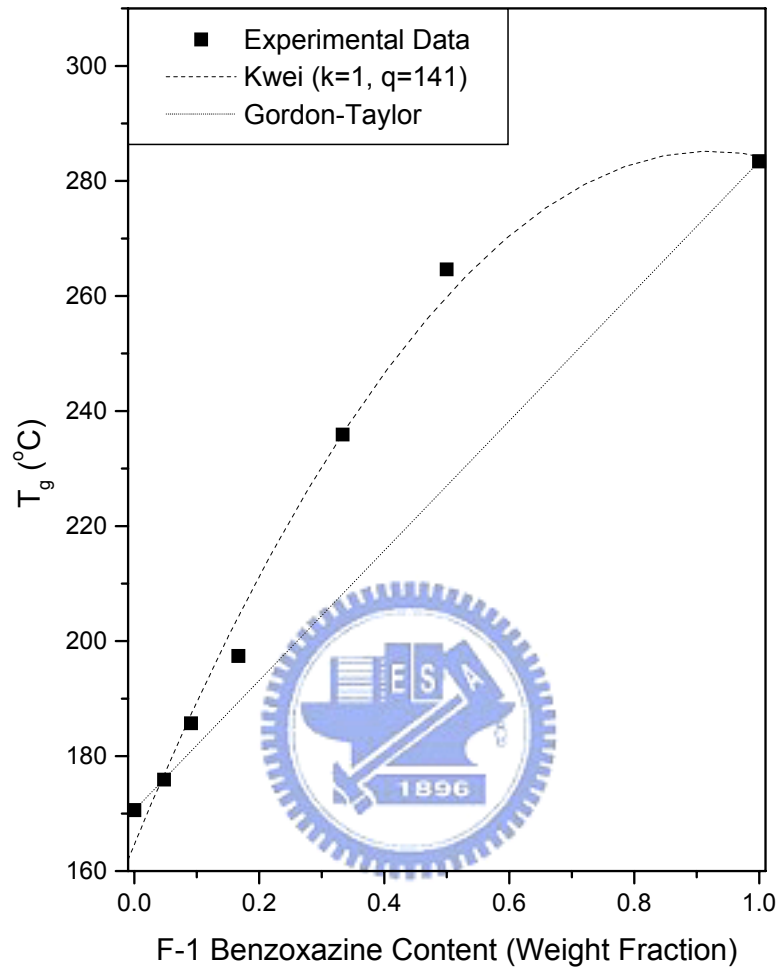


Figure 5-6. T_g versus composition curved base on B-a/F-1 co-PBZZ copolymers

Chapter 6

Study of the Morphologies and Dielectric Constants of Nanoporous Materials Derived from Benzoxazine-Terminated Poly(ϵ -caprolactone)/Polybenzoxazine Copolymers

Abstract

We have generated porous polybenzoxazine (PBZZ) materials by using a B-a type PBZZ as the matrix and various molecular weights of poly (ϵ -caprolactone) (pa-PCL) as the labile constituent. The slight degree of hydrogen bonding that exists between the two polymers results in micro-phase separation without an excess degree of aggregation occurring. The porous structures form after hydrolysis of the PCL domains; we characterized them using a variety of techniques, including FT-IR spectroscopy, DSC, TGA, FE-SEM, and DEA. At 298 K and 10^5 Hz, we obtained a thin, transparent, and nanoporous film that has a very low dielectric constant (1.95).

6.1 Introduction

As feature sizes in microelectronic devices are driven to sub-100-nm dimensions, device performance will no longer be on the scale it has been in the past because of a substantial increase in interconnect delays (*RC* delay) [1-4] caused by the increased line resistance, capacitive coupling, and cross talk that occurs between smaller and more closely spaced metal lines. Fluorinating polymers and forming porous structures are two major directions that have been followed in the course of developing materials that have low dielectric constants (low *k*) [1,2, 5-7]. Recently, there has been a demand for low-dielectric-constant materials that can decrease the *RC* delay, power consumption, and cross-talk noise; this demand has stimulated intense efforts in the exploration and applicability of porous materials, especially nanoporous materials [8-11].

Nanoporous and mesoporous materials have potential or are used in many devices, which include sensors, photonic crystals, waveguides, and dielectrics [12-13]. It is becoming increasingly more important to be able to control the pore structures and understand their properties on nano- and micrometer length scales. It is well known that reducing the dielectric constant can be achieved simply by replacing the polymer with air [14-15], which has a dielectric constant of 1. Therefore, increasing the pore density will lead to lower-dielectric-constant materials. The size of the voids,

however, must be substantially smaller than both the film thickness and any microelectronic features for the gain in the dielectric constant to be realized [1,2]. Suitable porous structures can be prepared from copolymers comprising a thermally stable or solvent-stable material and a thermally labile or solvent-labile material [12,16,17]; the latter system constitutes a dispersed phase. The greatest challenge in the future will be to reduce the pore size at an even distribution while maintaining the strength within a range acceptable for mechanical and electronic applications.

In this study, we prepared a porous material having a low value for its dielectric constant by treating poly(ϵ -caprolactone) (PCL) with B-a type polybenzoxazine (PBZZ), which act as the labile and stable constituents, respectively. PCL is a highly crystalline polymer that becomes miscible with several amorphous polymers through the formation of hydrogen bonds [18-20]. A variety of catalysts have been investigated for the ring-opening polymerization (ROP) of ϵ -caprolactone (ϵ -CL) to PCL. Copolymers of PCL are useful because of their biodegradability and polymer blend compatibility. The miscibility of PCL blends or copolymers depends on self- and inter-association that arises through hydrogen bonding with donor polymers. In addition, PBZZ contains a high density of hydroxyl groups [21-24] that interact with the carbonyl groups of PCL through hydrogen bonding. To prepare a microporous material, it is essential to prepare a well-dispersed microphase-separated

labile constituent within a stable matrix. Hence, we modified the PCL's end group to decrease the degree of phase separation.

As shown in Schemes 6-1 and 6-2, pa-PCL forms covalent bonds with the PBZZ backbone because these pa-PCL compounds possess similar benzoxazine structures. We generated a porous structure by preparing a copolymer between the matrix phase (PBZZ) and a minor phase that consisted of a solvent (basic)-labile polymer (PCL). We synthesized copolymers of pa-PCL and PBZZ having different molecular weights. Films of the copolymers were cast and then heated to effect annealing, which resulted in the nanoscale microphase separation of these two dissimilar blocks. We removed the labile constituent selectively through hydrolysis using NaHCO_3 , which created pores having the shape of the original copolymer's morphology. Using this approach, we obtained a porous material having a low dielectric constant.

6.2 Experimental

6.2.1 Materials

4-Hydroxybenzyl alcohol, ϵ -caprolactone and tin(II) 2-ethylhexanoate were purchased from the Acros Chemical Company (USA). Formaldehyde and aniline were purchased from the Aldrich Chemical Company (USA).

6.2.2 Synthesis of (3-phenyl-3,4-dihydro-2H-1,3-benzoxazin-6-yl)methanol (pa-OH)

The benzoxazine was prepared according to Scheme 6-2. 37% Aqueous formaldehyde solution (6.53 g, 0.08 mol) and dioxane (10 mL) were mixed for 10 min under nitrogen in a three-necked flask placed in an ice bath. Then, the aniline (3.75 g, 0.04 mol) dissolved in dioxane (10 mL) was added slowly using a dropping funnel. The mixture was stirred magnetically for 10 min before 4-hydroxybenzyl alcohol (5 g, 0.04 mol) in dioxane (10 mL) was added. The reaction temperature was raised to 100 °C and the mixture was heated under reflux for 6 hr. The solvent was then evaporated under reduced pressure to yield a light-yellow powder. This crude product was dissolved in ethyl ether and washed sequentially with 1 N NaOH and water for three times; the organic phase was dried by magnesium sulfate and the solvent evaporated under reduced pressure. The residue was purified by column chromatography on silica gel (hexane/ethyl acetate, 6:1) to gives pa-OH as a light-yellow liquid which solidified to a pale-yellow powder upon drying (87.5 %).

6.2.3 Syntheses of *pa-OH* terminated PCL (*pa-PCL*)

Hydroxyl groups [24-26] act as initiators for the polymerization of ϵ -CL polymerization in presence of $\text{Sn}(\text{Oct})_2$ [27,28]. In the case of controlled/living polymerization, the molecular weight of *pa-PCL* can be predicted from the ϵ -CL/*pa-OH* molar ratio, as indicated in Table 6-1. The ring opening polymerization was performed at 120 °C over 24 h as shown in Scheme 6-2. Various quantities of ϵ -CL to *pa-OH* were added under nitrogen into a two-necked flask, equipped with a dry stirring bar, and mixed for 10 min. The flask was placed into an oil bath maintained at 120 °C and the contents were stirred vigorously for ca. 5 min. A certain amount of $\text{Sn}(\text{Oct})_2$ in dry toluene was added to the mixture. The crude sample was cooled after 24 h and then dissolved in THF; the solution was poured dropwise into an excess of hexane. The purified polymer was dried in a vacuum oven until constant weight; the yield was determined gravimetrically.

6.2.4 Preparation of Reactants

Mixtures of *pa-PCL* (25 wt %) and B-a type benzoxazine (75 wt %) having several different molecular weights (see Table 6-2) were prepared by solution blending. The mixture was dissolved by stirring in THF; the solution was left to evaporate slowly at 50 °C for 1 day and then cured at 180 °C for 4hr under vacuum to ensure total curing of the co-polybenzoxazine (co-PBZZ). After curing, we obtained a

smooth, stiff, hazel-to-brown film. The cured sample was stirred and heated reflux in 0.3 N aqueous NaHCO₃ at 90 °C for 24 hr to remove the ester group of the labile constituent (PCL). The porous structures were obtained after drying under vacuum in an oven.

6.2.5 Nuclear Magnetic Resonance (NMR)

¹H NMR spectra were recorded on a Varian Unity Inova 500 FT NMR Spectrometer operating at 500 MHz; chemical shifts are reported in parts per million (ppm). Deuterated chloroform was used as the solvent.

6.2.6 Fourier Transform Infrared Spectroscopy (FT-IR)

FT-IR spectroscopic measurements were conducted on a Nicolet Avatar 320 FT-IR Spectrophotometer; 32 scans were collected with a spectral resolution of 1 cm⁻¹. Infrared spectra of the copolymers were obtained using the conventional NaCl method. The film used in this study was thin enough to obey the Beer-Lambert law. To maintain a dry film, the sample chamber was purged with nitrogen during the measurement process.

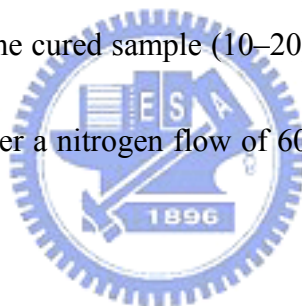
6.2.7 Differential Scanning Calorimetry (DSC)

The calorimetric measurement was performed using a TA Instruments Differential Scanning Calorimeter (DSC-2010) and conducted under a nitrogen flow of 25 mL/min. The sample was preheated at a scan rate of 20 °C/min from 30 to 240

°C and then maintained at 240 °C for 2 min. The measurement was made using 5–10 mg of sample in a DSC sample cell by cooling to –120 °C quickly from the melt of the first scan. The second scan was conducted at a rate of 20 °C/min from –120 to 250 °C and the value of T_g was taken as the midpoint of the heat capacity transition between the upper and lower points of deviation from the extrapolated liquids and glass lines. Furthermore, we also obtained the values of T_m and ΔH_m .

6.2.8 Thermogravimetric Analysis (TGA)

The thermal stability of the cured sample was investigated using a TA Instruments Q50 apparatus. The cured sample (10–20) mg was placed in a Pt cell and heated from 30 to 800 °C under a nitrogen flow of 60 mL/min at a heating rate of 20 °C/min.

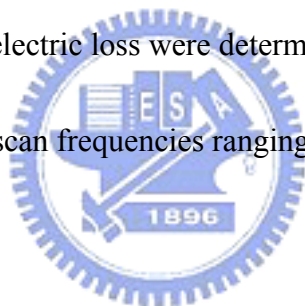


6.2.9 Field Emission Scanning Electron Microscopy (FE-SEM)

The samples of the porous pa-PCL/PBZZ copolymers were fractured using liquid nitrogen and their cross-sectional morphologies were observed by low-voltage FE-SEM. SEM images were recorded at high magnifications under high vacuum using a TOSHIBA S4700I field emission microscope working at 5 kV with a beam current of 1×10^{-10} A. To increase the resolution of the FE-SEM image, a thin layer of Pt was spun onto the surface of the sample to increase its conductivity; the thickness of this Pt layer was controlled to ca. 10 nm to avoid affecting the actual images.

6.2.10 Dielectric Analysis

Dielectric relaxation data were obtained using a TA Instruments DEA-2970 apparatus, which incorporated a parallel plate cell arrangement and a computer-controlled furnace to ensure that good electrical contact was made between the electrodes and the sample. A flat film is required to increase the accuracy of the measurement of the dielectric constant and, thus, we used the automatic scraper to form such a flat film. The experiment was conducted under a nitrogen flow of 90 mL/min and the thickness of sample was controlled to between 0.125 and 0.75 mm. The dielectric constant and dielectric loss were determined between 0 to 50 °C using a heating rate of 2 °C/min with scan frequencies ranging from 1 to 10⁵ Hz.



6.3 Results and Discussion

6.3.1 Nuclear Magnetic Resonance Analyses

After the cyclization of the oxazine, we observed the characteristic benzoxazine peaks (Ar-CH₂-N and N-CH₂-O units) using ¹H NMR spectroscopy. Figure 6-1 provides the ¹H NMR spectrum (CDCl₃, 500 MHz) of pa-OH: δ (ppm) 4.54 (s, 2H, Ar-CH₂-N), 4.60 (s, 2H, Ar-CH₂-OH), 5.38 (s, 2H, N-CH₂-O), 6.76–7.26 (8H, Ar). Furthermore, Figure 6-2 provides the ¹H NMR spectrum (CDCl₃, 500 MHz) of pa-PCL(Mn=24000, **1c**): δ (ppm) 1.35 (m, 2H, -CH₂-, poly), 1.62 (m, 2H, -CH₂-, poly), 1.62 (m, 2H, -CH₂-, poly), 2.28 (t, 2H, -O(O)CCH₂-, poly), 3.66 (q, 2H, -CH₂OH-, ω-end), 4.03 [t, 2H, -CH₂OC(O)-, poly]. We observed similar results for the other pa-PCL compounds (Mn=3000, **1a**; Mn=14800, **1b**). Therefore, based on these ¹H NMR spectra, we confirmed the successful synthesis of pa-OH and pa-PCL derivatives of various molecular weights.

6.3.2 Fourier Transfer Infrared Spectroscopy Analyses

Figures 6-3 (a)–(f) display the carbonyl stretching region (1680–1780 cm⁻¹) of the IR spectra, measured at room temperature, of pa-PCL and the pa-PCL/PBZZ copolymers. The carbonyl stretching for pure pa-PCL is split into two bands at 1734 and 1724 cm⁻¹, as indicated in Figures 6-3 (a)–(c), which correspond to absorptions by

the amorphous and crystalline conformations, respectively. The crystalline conformation at 1724 cm^{-1} of pa-PCL was destroyed substantially after incorporating pa-PCL into the PBZZ backbone as shown in Figures 6-3 (d)–(f). A small amount of the crystalline conformation at 1724 cm^{-1} of pa-PCL is still present, however, which indicates that pa-PCL and PBZZ are not fully miscible. We assign another band, which appears at ca. 1705 cm^{-1} to the pa-PCL carbonyl groups that are hydrogen bonded to the PBZZ hydroxyl groups. The carbonyl stretching frequency splits into only two major bands at 1732 and 1705 cm^{-1} , which correspond to the free and hydrogen-bonded carbonyl groups, that fit well to the Gaussian function. We calculated the fraction of hydrogen-bonded carbonyl groups using the following equation [29]:

$$f_b^{C=O} = \frac{A_b / 1.5}{A_b / 1.5 + A_f} \quad (1)$$

where A_f and A_b are the peak areas corresponding to the free and hydrogen-bonded carbonyl groups, respectively. The conversion coefficient 1.5 is the ratio of these two bands, the free and hydrogen-bonded carbonyl groups. Table 6-2 summarizes the results from curve fitting. The fraction of the hydrogen-bonded carbonyl groups decreases upon increasing the relative molecular weight of the pa-PCL. In other words, a lower-molecular-weight pa-PCL has better miscibility with PBZZ.

In addition, Figures 6-4 (a)–(c) present the region from 1400 to 1800 cm^{-1} in

the IR spectra, measured at room temperature, of pa-PCL(Mn=3000, **1a**), pa-PCL(Mn=3000)/PBZZ copolymer (**2a**), and porous PBZZ (**3a**), respectively. It is clear that the carbonyl groups of pa-PCL disappear after the hydrolysis of the pa-PCL/PBZZ copolymer using NaHCO₃. Meanwhile, the characteristic peaks of PBZZ are still present in Figure 6-4 (c). In other words, a porous PBZZ structure had formed and we confirmed its components by obtaining these FTIR spectra.

6.3.3 Differential Scanning Calorimetry Analyses

Figures 6-5 (A)–(C) and Table 6-3 display the values of T_g , T_m , and ΔH_m of the various pa-PCL, pa-PCL/PBZZ, and pure PBZZ systems. The pa-PCL/PBZZ copolymers (**2a**, **2b**, and **2c**) possess two glass transition temperatures, representing pa-PCL and PBZZ, respectively, which is a phenomenon that indicates that pa-PCL and PBZZ are not totally miscible in the amorphous region. Meanwhile, the value of T_m of pa-PCL shifts to higher temperature gradually as it becomes incorporated into the PBZZ matrix, presumably because the crosslinking structure of PBZZ hinders the transfer of heat to the crystalline region of pa-PCL. The crystalline pa-PCL was destroyed substantially, however, upon the DSC measurement as shown in Figure 6-5 (B) and Table 6-3; these results are consistent with those obtained from the FTIR spectra. The DSC results show that these copolymers were micro-phase separated,

which is a prerequisite for forming porous low-dielectric-constant materials.

6.3.4 Thermogravimetric Analyses

Figure 6-6 displays TGA thermograms of (a) pa-PCL, (b) pa-PCL/PBZZ, and (c) pa-PCL/PBZZ after hydrolysis, as a function of the various molecular weights of pa-PCL; Table 6-4 summarizes the results, including the 5 wt % loss temperatures and char yields. As can be seen, increasing the molecular weight of pa-PCL increase the decomposition temperature in Figure 6-6 (a). Furthermore, the opposite result of char yield was observed because of the higher or lower content of the terminal end group of the pa benzoxazine. The 5 wt % loss temperatures of the various pa-PCL/PBZZ mixtures are close as shown in Figure 6-6 (b), but the tendency of the char yield is similar to that observed for pa-PCL for the same reason suggested for Figure 6-6 (a). Moreover, after the hydrolysis process, which removes the PCL segment of pa-PCL, the decomposition temperatures increased and are close to that of PBZZ as shown in Figure 6-6 (c) and Table 6-4. In other words, these results indicate that the PCL domains were completely removed from the pa-PCL/PBZZ copolymers after hydrolysis.

6.3.5 Scanning Electron Microscopy Analysis

We also investigated the pore morphologies of the pa-PCL/PBZZ copolymers by FE-SEM after removal of the pa-PCL segment. Figures 6-7 (a)–(f) present SEM micrographs of fracture surfaces (cross-sections) of the pa-PCL/PBZZ copolymers, which were frozen in liquid nitrogen after hydrolysis of the PCL segments using NaHCO_3 . Each of these systems possesses a pa-PCL content of 25 wt %, but notable variations in morphology occur as a result of their different molecular weights. We observe heterogeneous morphologies in Figures 6-7 (a)–(f), i.e., the copolymers were micro-phase separated after the pa-PCL segment was incorporated into the PBZZ matrix. For the pa-PCL($M_n=3000$)/PBZZ system in Figures 6-7 (a) and (b), it can be seen that the pores are dispersed uniformly in the continuous matrix, and these pores have diameters that are < 50 nm. Furthermore, we attribute these voids to the pa-PCL rich phase whereas the continuous phase is the PBZZ matrix. Upon increasing the molecular weight of pa-PCL from $M_n=3000$ to 14800 and 24000, the porous structures display remarkably different morphologies as shown in Figures 6-7 (c)–(f). These morphologies incorporate pore sizes that vary in the range from tens to hundreds of nanometer as these voids began to aggregate, interconnect, and exhibit irregular shapes. Meanwhile, the pore size distribution became broader on the cross-sectional surface. The results of these morphological studies reveals that the

pa-PCL having $M_n=3000$ is the one most suitable for forming the most evenly distributed porous minor phase within the PBZZ matrix. Most importantly, it also gives the lowest degree of pore interconnection; a closed or isolated pore structure is usually preferred to an open or connected pore structure because connected pores may create current path leakage and result in solvent absorption during wet cleaning processes, which allows damaging gases to penetrate deep into the film during the etching and dry resist stripping processes.

6.3.6 Dielectric Analysis

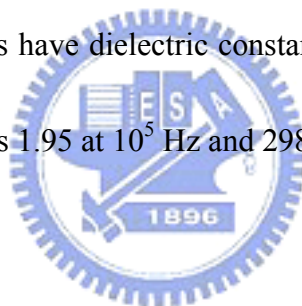
Because the dielectric constants of gases are not much different from that of a vacuum ($k=1$), the incorporation of free space or pores is an attractive method for decreasing the dielectric constants of films, even though porous and low-density materials pose greater challenges in both characterization and integration. The key to determining a material's properties depends directly on integration issues, including porosity, pore size, and size distribution, and the extent of interconnection. Increasing the porosity decreases the dielectric constant, but it tends to reduce the material's mechanical properties. In general, the maximum porosity is controlled to between 25 and 30 %. The average pore size must be substantially smaller, and the size distribution (uniform or random) may affect the mechanical properties of the film.

Therefore, it is necessary to control the frequency of large pores, which would constitute void defects between metal lines. Furthermore, the pa-PCL(Mn=3000)/PBZZ (**3a**) system possesses a relative closed and well-distributed pore structure, as evidenced from the FE-SEM images, which implies that it is most suitable for applications as a low-dielectric-constant material.

The PBZZ porous structure was created after removing the PCL segment from the pa-PCL/PBZZ copolymer, the value of its dielectric constant is lower than that of virgin PBZZ. In Figure 6-8 (a), we observe that the dielectric constant of the PBZZ decreases from 3.56 to 1.95 upon varying the pa-PCL molecular weight at a constant pa-PCL loading (25 wt %). Based on the DEA measurement, pa-PCL(Mn=3000)/PBZZ (**3a**) gives the lowest value of k . Figure 6-8 (b) displays the dielectric constant of different pa-PCL(Mn=3000) loading in the PBZZ matrix. As would be expected, the decrease in the value of k from 3.56 to 1.95 occurred as the pa-PCL content was increased from 0 to 25 wt % after hydrolysis.

6.4 Conclusions

We have developed a new class of nanoporous PBZZ material that has a substantially lower dielectric constant by using the pa-PCL as the labile constituent. FE-SEM images show that the labile polymer micro-phase separates in the PBZZ matrix with domain sizes that depend upon the molecular weight of pa-PCL used. These pores were generated when the pa-PCL was eliminated by hydrolysis of the pa-PCL/PBZZ copolymer. A transition from isolated to interconnected pores was observed when the molecular weights of pa-PCL were increased from $M_n=3000$ to 24000. These porous materials have dielectric constants, relative to that of the virgin PBZZ (3.56), that are as low as 1.95 at 10^5 Hz and 298 K.



References

- [1] Ho, P. S.; Leu, J.; Lee, W. W. In *Low Dielectric Constant Materials for IC Application*; New York: Springer, 2002.
- [2] Maier, G. *Prog. Polym. Sci.* **2001**, 26, 3.
- [3] Nalwa, H. S., Ed. In *Handbook of Advanced Electronic and Photonic Materials and Devices*, Vol. 4; San Diego: Academic Press, 2001.
- [4] Treichel, H.; Ruhl, G.; Ansmann, P.; Wurl, R.; Muller, C. H.; Dietlmeier, M. *Microelectronic Eng.* **1998**, 40, 1.
- [5] Yang, P.; Zhao, D.; Chmelka, B. F.; Stucky, G. D. *Chem. Mater.* **1998**, 10, 2033.
- [6] Charlier, Y.; Hedrick, J. L.; Russell, T. P.; Jonas, A.; Volksen, W. *Polymer* **1995**, 36, 987.
- [7] Hedrick, J. L.; Carter, K.R.; Cha, H. J.; Hawker, C. J.; DiPietro, R. A.; Labadie, J. W.; Miller, R. D.; Russel, T. P.; Sanchez, M. I.; Volksen, W.; Yoon, D. Y.; Mecerreyes, D.; Jerome, R.; McGrath, J. E. *Reactive & Functional Polymers* **1996**, 30, 43.
- [8] Kim, H. C.; Volksen, W.; Miller, R. D. *Chem. Mater.* **2003**, 15, 609.
- [9] Nguyen, C.V.; Carter, K. R.; Hawker, C. J.; Hedrick, J. L.; Jaffe, R. L.; Miller, R. D.; Remenar, J. F.; Rhee, H. W.; Rice, P. M.; Toney, M. F.; Trollsås, M.; Yoon, D.Y et al. *Chem. Mater.* **1999**, 11, 3080.

- [10] Carter, K. R.; Dipietro, R. A.; Sanchez, M. I.; Russell, T. P. *Chem. Mater.* **1997**, *9*, 105.
- [11] Carter, K. R.; Dipietro, R. A.; Sanchez, M. I.; Swanson, S. A. *Chem. Mater.* **2001**, *13*, 213.
- [12] Yang, S.; Mirau, P. A.; Pai, C. S.; Nalamasu, O.; Reichmanis, E.; Lin, E. K.; Lee, H. J.; Gidley, D. W.; Sun, J. *Chem. Mater.* **2001**, *13*, 2762.
- [13] Yang, S.; Mirau, P. A.; Pai, C. S.; Nalamasu, O.; Reichmanis, E.; Pai, J. C.; Obeng, Y. S.; Seputro, J.; Lin, E. K.; Lee, H. J.; Sun, J.; Gidley, D. W.. *Chem. Mater.* **2002**, *14*, 369.
- [14] Hung, Q. R.; Volksen, W.; Huang, E.; Toney, M.; Frank, C. W.; Miller, R. D. *Chem. Mater.* **2002**, *14*, 3676.
- [15] Hung, Q. R.; Kim, H. C.; Huang, E.; Mecerreyes, D.; Hedrick, J. L.; Volksen, W.; Frank, C. W.; Miller, R. D. *Macromolecules* **2003**, *36*, 7661.
- [16] Kim, H. C.; Wilds, J. B.; Hinsberg, W. D.; Johnson, L. R.; Volksen, W.; Magbitang, T.; Lee, V. Y.; Hedrick, J. L.; Hawker, C. J.; Miller, R. D. *Chem. Mater.* **2002**, *14*, 4628.
- [17] Hedrick, J. L.; Russell, T. P.; Labadie, J.; Lucas, M.; Swanson, S. **1995**, *Polymer*, *36*, 2685.
- [18] Lezcano, E. G.; Coll, C. S.; Prolongo, M. G. *Polymer* **1996**, *37*, 3603.



- [19] de Juana, R.; Cortazar, M. *Macromolecules* **1993**, *26*, 1170.
- [20] Kuo, S. W.; Chang, F. C. *Macromolecules* **2001**, *34*, 7737.
- [21] Ishida, H.; Sanders, D. P. *Macromolecules* **2000**, *33*, 8149.
- [22] Wang, Y. X.; Ishida, H. *Macromolecules* **2000**, *33*, 2839.
- [23] Su, Y. C.; Chang, F. C. *Polymer* **2003**, *44*, 7989.
- [24] Ning, X.; Ishida, H. *J. Polym. Sci., Part B: Polym. Phys.* **1994**, *32*, 921.
- [25] Ydens, I.; Rutot, D.; Degee, P.; Six, J. L.; Dellacherie, E.; Dubois, P.
Macromolecules **2000**, *33*, 6713.
- [26] Jeon, O.; Lee, S. H.; Kim, S. H.; Lee, Y. M.; Kim, Y. H. *Macromolecules* **2003**,
36, 5585.
- [27] Nederberg, F.; Bowden, T.; Hilborn, J. *Macromolecules* **2004**, *37*, 954.
- [28] Shuai, X.; Merdan, T.; Unger, F.; Wittmar, M.; Kissel, T. *Macromolecules* **2003**,
36, 5751.
- [29] Coleman, M. M.; Graf, J. F.; Painter, P. C. In *Specific Interactions and the
Miscibility of Polymer Blends*; Technomic: Lancaster, PA, 1991.

Table 6-1. Results of the Homopolymerization of ϵ -Caprolactone (CL) with Various

Amounts of pa-OH in the Bulk at 120 °C and $[CL]/[Sn(Oct)_2] = 1000$;

Polymerization Time: 24 h

Entry	[M]/[I]	$M_{n,GPC}$	$M_{n,NMR}$	M_w/M_n	Yield (%)
1a	30	3,000	5,100	1.15	95.5
1b	120	14,800	28,700	1.54	94.4
1c	200	24,000	41,600	1.71	90.5

Table 6-2. Curve fitting of fraction of hydrogen-bonding results of the pa-PCL/PBZZ copolymers at room temperature

Pa-PCL/PBZZ	Free C=O		H-Bonded C=O		
	ν (cm^{-1})	A_f (%)	ν (cm^{-1})	A_b (%)	f_b (%)
pa-PCL($M_n=3000$), 2a	1733.5	32.71	1708.4	67.29	57.83
pa-PCL($M_n=14800$), 2b	1732.2	67.36	1705.7	32.64	24.42
pa-PCL($M_n=24000$), 2c	1731.5	73.51	1704.8	26.49	19.37

f_b = fraction of hydrogen bonding

Table 6-3. Glass transition temperatures, melting temperatures, and heats of melting of different pa-PCL/PBZZ composites

component	T_g (°C)	T_m (°C)	ΔH_m (J/g)
pa-PCL(Mn=3000), 1a	-45	51	85.2
pa-PCL(Mn=14800), 1b	-54	57	81.4
pa-PCL(Mn=24000), 1c	-58	59	80.9
pa-PCL(Mn=3000)/PBZZ, 2a	-47, 198	55	16.5
pa-PCL(Mn=14800) /PBZZ, 2b	-47, 203	59	17.3
pa-PCL(Mn=24000) /PBZZ, 2c	-41, 212	61	18.0
PBZZ	171	-	-

Table 6-4. The 5 wt % Weight-loss temperatures of different pa-PCL composites recorded under a N₂ environment

Component	5 wt % Weight loss (°C)	Char yield (%) at 800 °C
pa-PCL(Mn=3000), 1a	270	3.6
pa-PCL(Mn=14800), 1b	326	1.2
pa-PCL(Mn=24000), 1c	334	0.9
pa-PCL(Mn=3000)/PBZZ, 2a	328	23.3
pa-PCL(Mn=14800) /PBZZ, 2b	329	22.2
pa-PCL(Mn=24000) /PBZZ, 2c	330	21.4
pa-PCL(Mn=3000)/PBZZ after hydrolysis, 3a	343	23.4
pa-PCL(Mn=14800)/PBZZ after hydrolysis, 3b	343	22.0
pa-PCL(Mn=24000)/PBZZ after hydrolysis, 3c	337	22.1
PBZZ	340	30.1

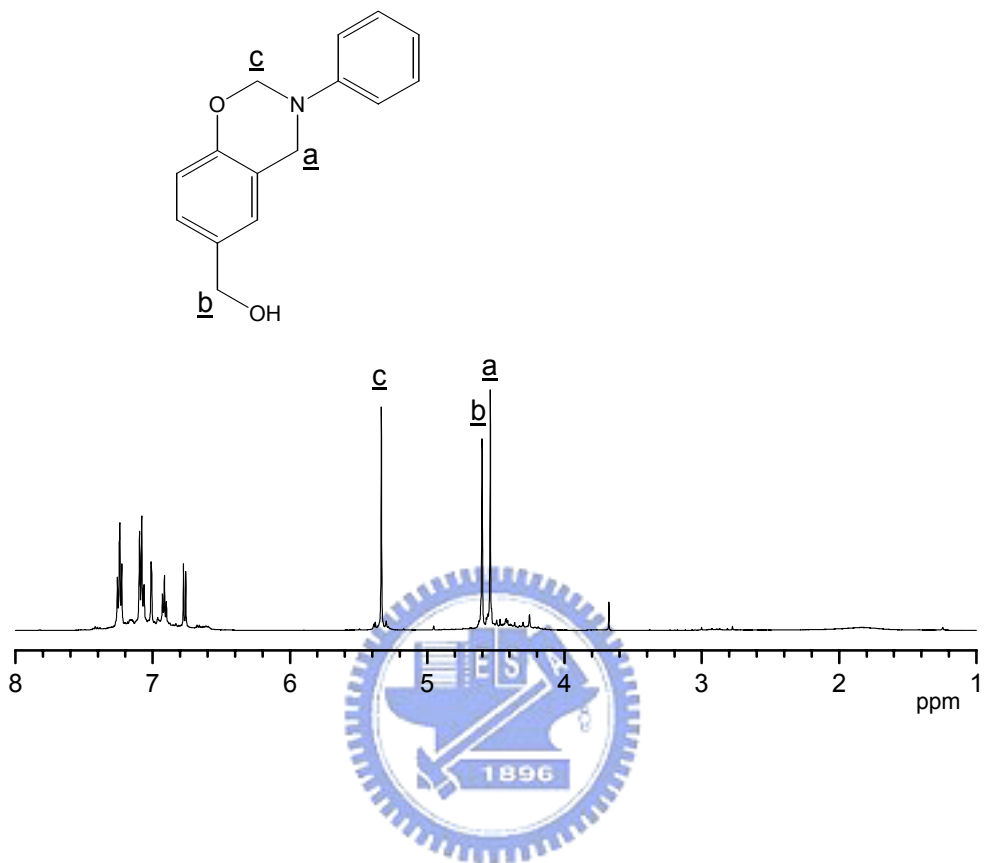


Figure 6-1. ^1H NMR spectra of *pa*-OH

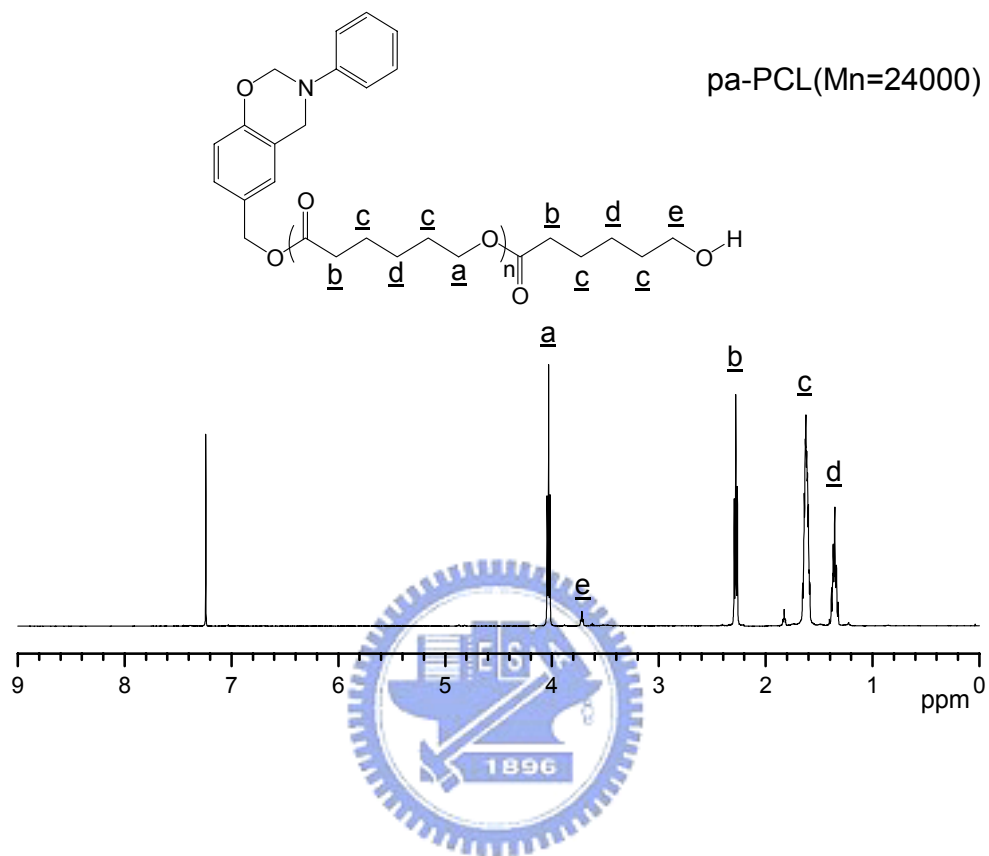


Figure 6-2. ^1H NMR spectra of pa-PCL ($M_n=24000$)

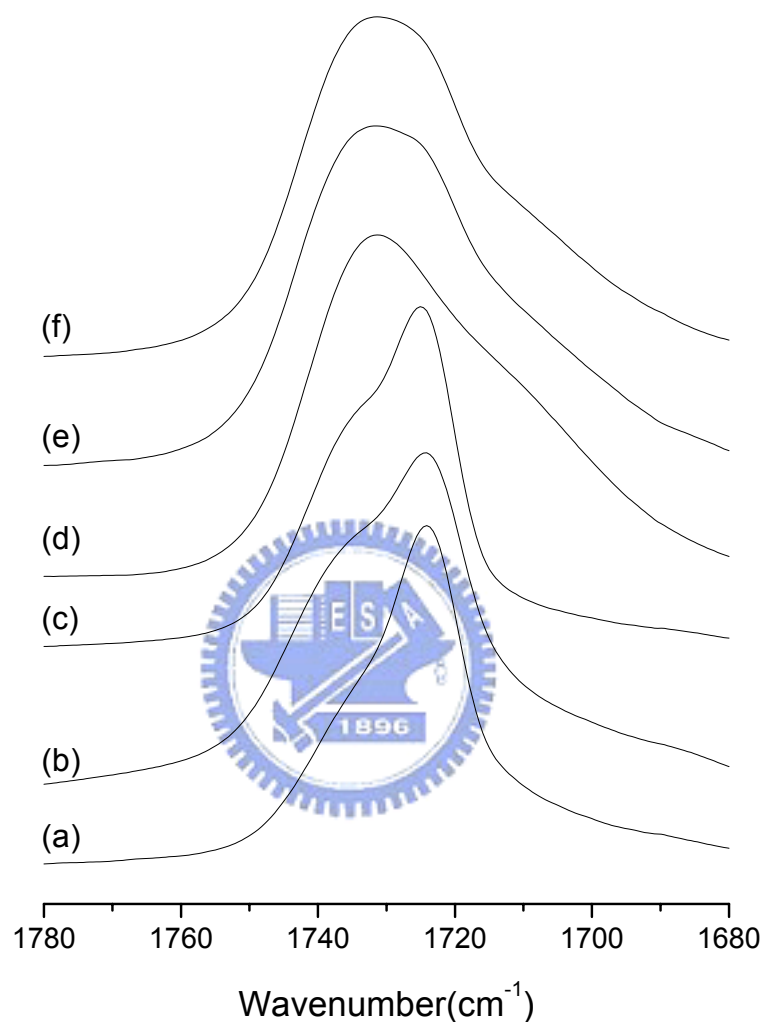


Figure 6-3. FTIR spectra of (a) pa-PCL(Mn=3000, **1a**), (b) pa-PCL(Mn=14800, **1b**), (c) pa-PCL(Mn=24000, **1c**), (d) pa-PCL/PBZZ (Mn=3000, **2a**), (e) pa-PCL/PBZZ (Mn=14800, **2b**), (f) pa-PCL/PBZZ (Mn=24000, **2c**) recorded at room temperature between 1680-1780 cm⁻¹

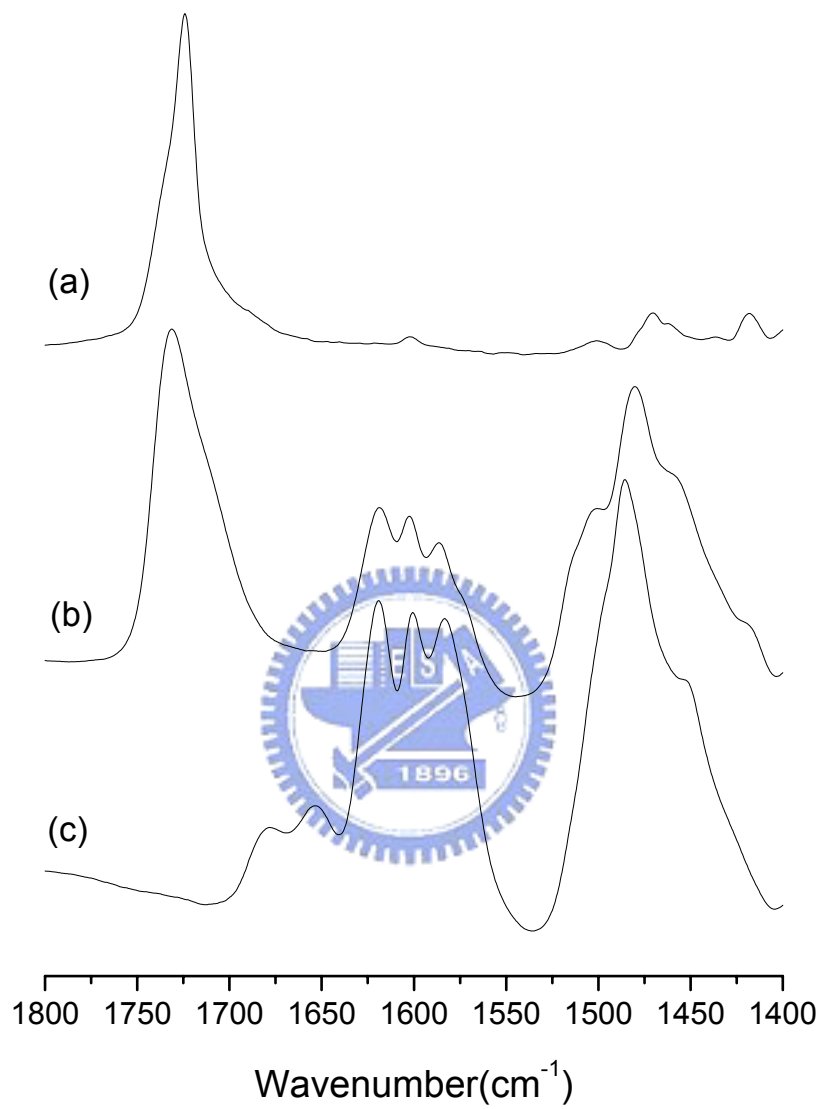


Figure 6-4. FTIR spectra of (a) pa-PCL (Mn=3000, **1a**), (b) pa-PCL/PBZZ (Mn=3000, **2a**), (c) porous PBZZ (Mn=3000, **3a**) recorded at room temperature between 1400 to 1800 cm⁻¹

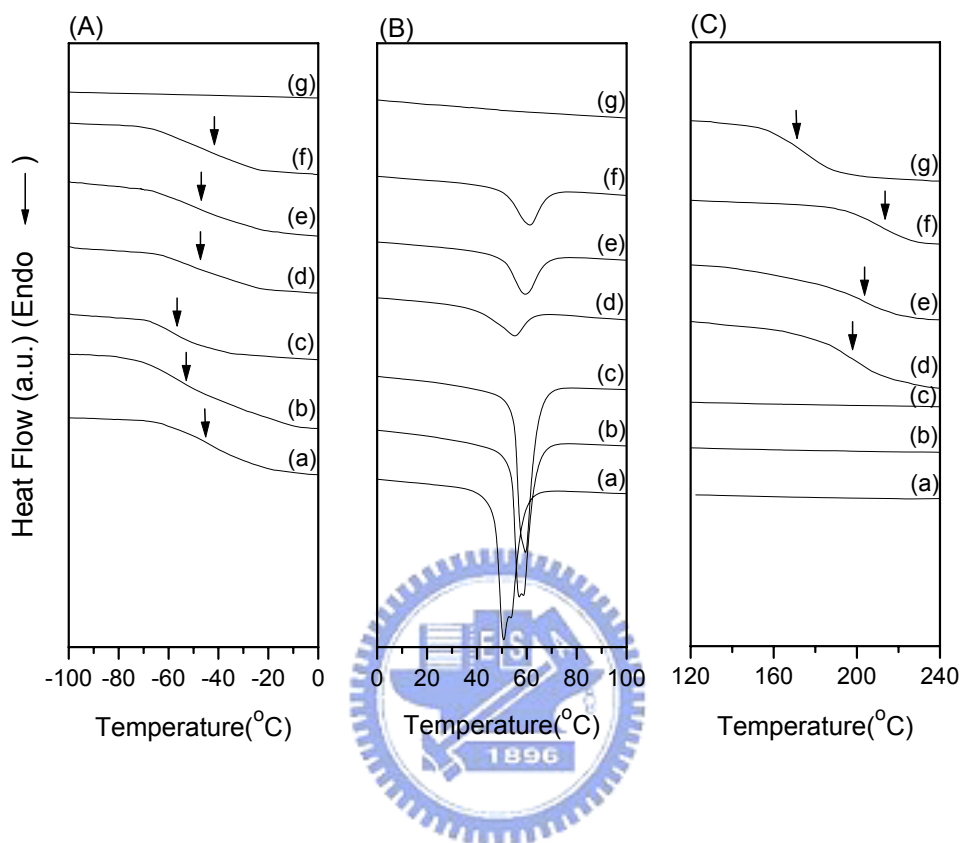


Figure 6-5. DSC scans in the ranges from (A) -120 to 0 °C, (B) 0 to 100 °C, and (C) 120 to 240 °C of (a) pa-PCL($M_n=3000$, **1a**), (b) pa-PCL($M_n=14800$, **1b**), (c) pa-PCL($M_n=24000$, **1c**), (d) pa-PCL/PBZZ ($M_n=3000$, **2a**), (e) pa-PCL/PBZZ ($M_n=14800$, **2b**), (f) pa-PCL/PBZZ ($M_n=24000$, **2c**), (g) pure PBZZ

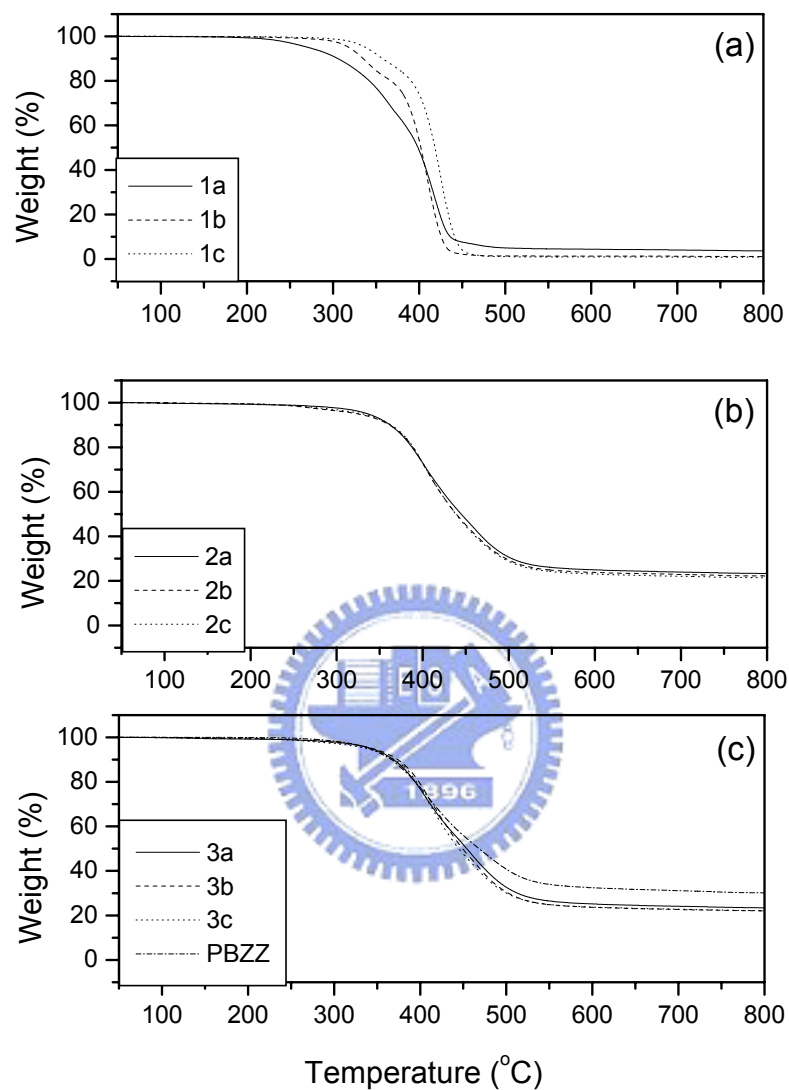
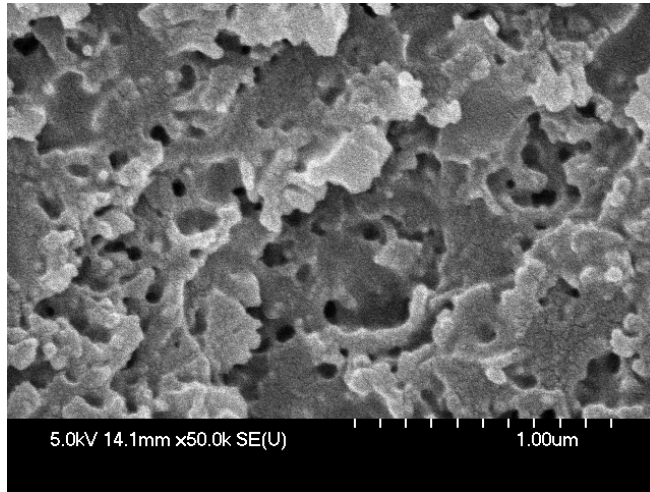
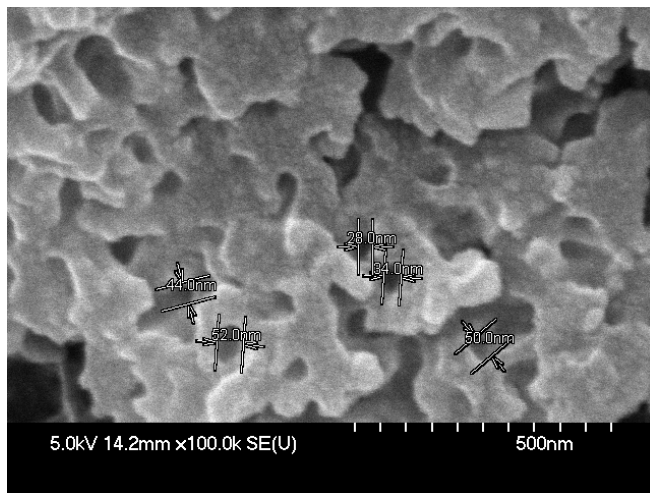


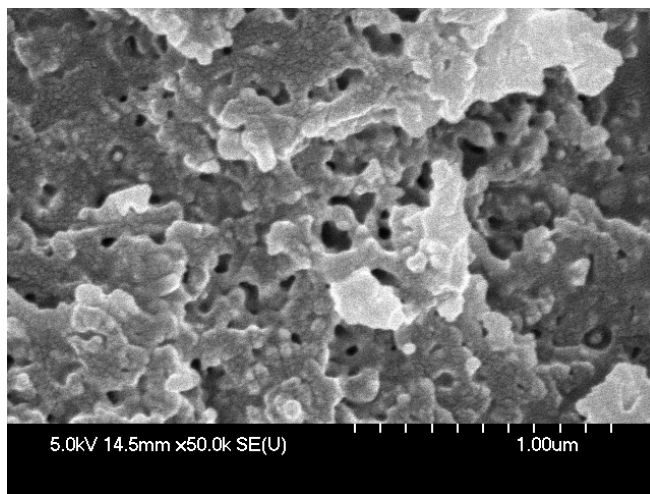
Figure 6-6. TGA thermograms of (a) pa-PCL, (b) pa-PCL/PBZZ, and (c) pa-PCL/PBZZ after hydrolysis, as a function of the molecular weight of pa-PCL



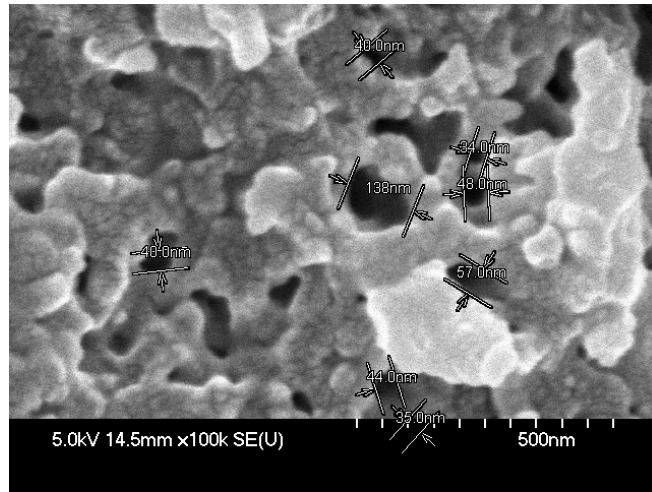
(a)



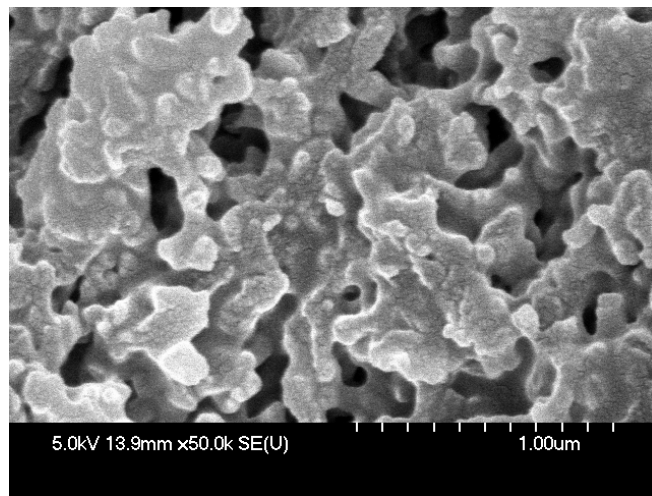
(b)



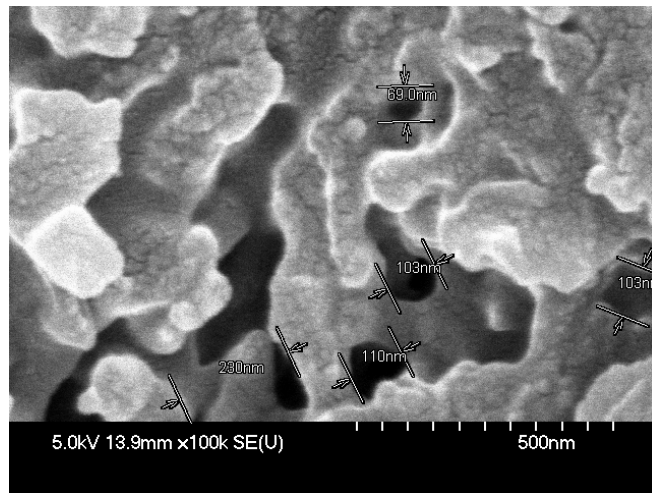
(c)



(d)



(e)



(f)

Figure 6-7. FE-SEM images of cross-sections of pa-PCL/PBZZ after hydrolysis recorded at high magnifications: (a) (3a, 50KX), (b) (3a, 100KX), (c) (3b, 50KX), (d) (3b, 100KX), (e) (3c, 50KX), (f) (3c, 100KX).

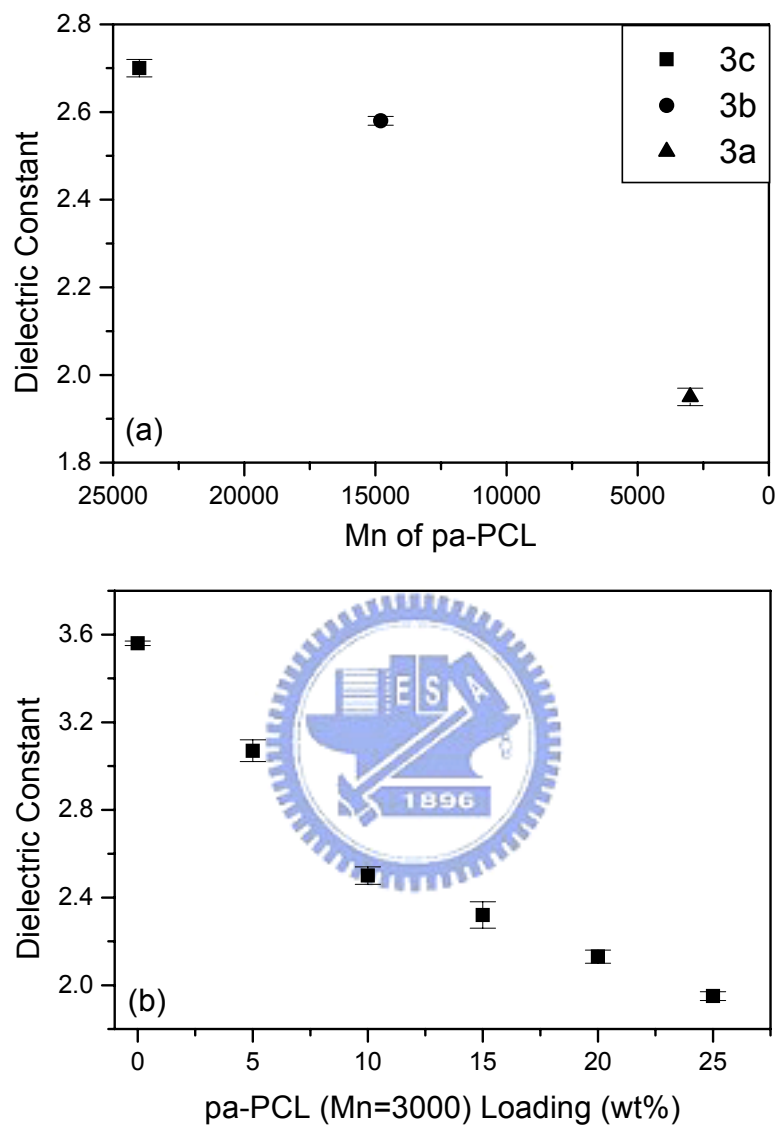


Figure 6-8. Dielectric constants of PBZZ materials obtained using (a) pa-PCL of different molecular weights at a constant loading of 25 wt % at 10^5 Hz and 298 K and (b) different loading percentages of the pa-PCL(Mn=3000).

Chapter 7

Synthesis and Characterization of Novel Adamantane-Modified Polybenzoxazine

Abstract

Two novel structures of adamantane-modified benzoxazines were synthesized from the 4-(1-Adamantyl)phenol by incorporating adamantane as a pendant group into the polybenzoxazines backbone. Both $^1\text{H-NMR}$ and FT-IR spectra have been used to characterize these structures. The rigid structure of the adamantane tends to hinder the chain mobility (boat anchor effect), and enhances the thermal properties substantially including glass transition temperature and decomposition temperature, especially in the poly(3 benzoxazine) case. In the poly(2 benzoxazine) system, on the contrary, a opposite result in glass transition temperature was observed that can be interpreted as lower crosslinking density. The phenyl group is more bulky than the methyl group and the movement of the molecular chain is hindered between bridging points during curing process, and results in a lower crosslinking density and lower glass transition temperature than that of the poly(3 benzoxazine).

7.1 Introduction

Benzoxazines are cyclic heterocycles generated by the Mannich-like condensation reaction, and their chemistry and oligomeric products have been reported recently [1-3]. Benzoxazine polymerizes via a thermally induced ring-opening reaction to form a phenolic-like structure by a Mannich base bridge (-CH₂-NR-CH₂-) [4,5], but it has overcome the shortcomings of the traditional phenolic resins [6]. Polybenzoxazines (PBZZs), as a class of thermosetting resins, offer a number of outstanding properties including low melt viscosity, no release of volatiles during curing, no need for catalysts, low water absorption, relatively low dielectric constant, high glass transition temperature (T_g), high thermal stability (T_d), good mechanical properties, and a wide molecular design flexibility [3,4,6].

In general, a polymer containing a linear n-alkyl substitute tends to decrease its T_g value, a longer substitute is expected to result in lower T_g . On the other hand, a cyclic alkyl substitute tends to raise its T_g [7,8]. In addition, positioning the mass center of the substitute closer to the polymer backbone will increase the bulkiness of the substitute and thus become more effective for T_g increasing. Besides, the introduction of a sterically hindered bridged or fused ring structure to the polymer chain results in T_g higher than the predicted ones. Adamantane is a symmetric tricyclic hydrocarbon with three fused chair-form cyclohexane rings [9] in a diamond lattice structure which is thermodynamically very stable. It possesses a high melting point (268 °C) and high thermal stability because of its rigid and spherical structure [10]. It contains four bridgehead positions that can be easily substituted using the Friedel-Craft chemistry. The adamantane moiety has been introduced into the main chains or side chains of various polymers [9-16]. These adamantane derivative polymers show unique properties, such as high thermal stability, high glass transition

temperature, high thermal oxidative stability, and great chain stiffness. It is intuitive that large pendant groups tend to have such an effect due to the reduced chain mobility (boat anchor effect), and the magnitude of increase is surprisingly high for adamantane.

This study concentrates primarily on synthesizing adamantane-modified PBZZ. By incorporating adamantane as a pendant group into the PBZZ structure, it is expected to form a more stable and further performance enhanced polymer.

7.2 Experimental

7.2.1 Materials

Both 1-bromoadamantane and methylamine were purchased from Aldrich Chemical Company of USA. Phenol was purchased from SHOWA Chemical Company of Japan. Formaldehyde, aniline and Iron (III) chloride were purchased from Aldrich Chemical Company of USA.

7.2.2 Synthesis of 4-(1-Adamantyl)phenol (**1**) [10]

According to Scheme 7-1, a 150 mL round-bottomed flask was charged with 1-bromoadamantane (6.00 g, 27.89 mmol), phenol (39.37 g, 0.418 mol), and FeCl₃ (0.05 g, 3.39 mmol). The flask was fitted with a reflux condenser and an outlet leading to a beaker with a NaOH solution to trap the HBr evolved during reaction. The reaction was carried out by stirring at 80 °C for 16 h under nitrogen environment. The excess phenol was removed by washing the product by hot water 3 times. The product was dried under vacuum, and the crude product was crystallized from methanol to afford 1.78 g (28 %) of white crystals.

7.2.3 Synthesis of 6-adamantyl-3-phenyl-3,4-dihydro-2H-1,3-benzoxazine

(2 benzoxazine)

The 2 benzoxazine was prepared according to Scheme 7-2 (a) [15]. 37% formaldehyde aqueous solution (0.71 g, 8.76 mmol) and 5 mL dioxane were mixed in a three-necked flask with nitrogen in an ice bath for 10 min. Then, the aniline (0.4079 g, 4.38 mmol) dissolved in 5 mL dioxane was added slowly by a dropping funnel. The mixture was stirred magnetically for 10 min before adding 4-(1-Adamantyl)phenol (1g, 4.38mmol) in 10 mL dioxane. The reaction temperature was raised to 100 °C and allowed to reflux for 24 hr. The solvent was then removed by reducing pressure, and the white powder product was obtained. The crude product was dissolved in ethyl ether and washed with 1N NaOH and water in sequence for three times, and the product solution was dried by magnesium sodium and distilled by reducing pressure. Finally, a light white powder product, 2 benzoxazine, in 87.5 % yield was obtained.

7.2.4 Synthesis of 6-adamanty -3-methyl-3,4-dihydro-2H-1,3-benzoxazine

(3 benzoxazine)

The 3 benzoxazine have also been synthesized by the same method as 2 benzoxazine shown in Scheme 7-2 (b) by using 37% formaldehyde aqueous solution (0.533g, 6.57mol), 40 % methylamine (0.255g, 3.285 mmol), and 4-(1-Adamantyl)phenol (0.75g, 3.285 mmol) to synthesize 3 benzoxazine. A white powder with 64.5 % yield was obtained in this system.

7.2.5 Nuclear Magnetic Resonance (NMR)

¹H NMR spectra were recorded on a Varian Unity Inova 500 FT NMR Spectrometer operating at 500 MHz with chemical shift reported in parts per million (ppm). Deuterium chloroform was used as solvent.

7.2.6 Fourier Transform Infrared Spectroscopy (FT-IR)

FT-IR measurement was recorded on a Nicolet Avatar 320 FT-IR Spectrophotometer, 32 scans were collected with a spectral resolution of 1 cm^{-1} . Infrared spectra of the benzoxazine were obtained using the conventional NaCl method. The film used in this study was thin enough to obey the Beer-Lambert law. The sample chamber was purged with nitrogen during process of measurement in order to maintain sample film drying.

7.2.7 Differential Scanning Calorimetry (DSC)

The calorimetric measurement was performed using a TA Instruments Differential Scanning Calorimeter (DSC-2010) conducted under a nitrogen flow of 25 mL/min. The sample was preheated with a scan rate of $20\text{ }^{\circ}\text{C}/\text{min}$ from $30\text{ }^{\circ}\text{C}$ to $260\text{ }^{\circ}\text{C}$ and maintained at $260\text{ }^{\circ}\text{C}$ for 2 min. The measurement was made using 5-10 mg sample in a DSC sample cell by cooling to $30\text{ }^{\circ}\text{C}$ quickly from the melt of the first scan. The second scan rate was $20\text{ }^{\circ}\text{C}/\text{min}$ from 30 to $300\text{ }^{\circ}\text{C}$ and the T_g was taken as the midpoint of the heat capacity transition between the upper and lower points of deviation from the extrapolated liquids and glass lines.

7.2.8 Thermogravimetric Analysis (TGA)

Thermal stability of the cured sample was investigated by a TA Instruments (Q 50). The cured sample of 10-20 mg was placed in a Pt cell and heated at a heating rate of $10\text{ }^{\circ}\text{C}/\text{min}$ from 30 to $700\text{ }^{\circ}\text{C}$ at a nitrogen flow of 60 mL/min.

7.3 Results and Discussion

7.3.1 Nuclear Magnetic Resonance Analyses

Figure 7-1 shows the $^1\text{H-NMR}$ (CDCl_3 , 500 M Hz) of the 4-(1-Adamantyl)phenol (**1**): δ 1.72 ppm (q, 6H, adamantane), δ 1.85 ppm (d, 6H, adamantane), δ 2.06 ppm (s, 3H, adamantane), δ 4.64 ppm (s, 1H, hydroxyl), δ 6.77 ppm (d, 2H, Ar), and 7.22 ppm (t, 2H, Ar). After the cyclization of the oxazine, the benzoxazine characteristic peaks $\text{Ar}-\underline{\text{CH}_2}-\text{N}$ and $\text{N}-\underline{\text{CH}_2}-\text{O}$ can be observed by the proton NMR [5,6]. Figure 7-2 shows the $^1\text{H-NMR}$ (CDCl_3 , 500 M Hz) of the **2** benzoxazine: δ 1.72 ppm (q, 6H, adamantane), δ 1.85 ppm (d, 6H, adamantane), δ 2.06 ppm (s, 3H, adamantane), δ 4.62 ppm (s, 2H, $\text{Ar}-\underline{\text{CH}_2}-\text{N}$), δ 5.33 ppm (s, 2H, $\text{N}-\underline{\text{CH}_2}-\text{O}$), and δ 6.67 ~ 7.23 ppm (7H, Ar). Figure 7-3 shows the $^1\text{H-NMR}$ (CDCl_3 , 500 M Hz) of the **3** benzoxazine: δ 1.72 ppm (q, 6H, adamantane), δ 1.85 ppm (d, 6H, adamantane), δ 2.06 ppm (s, 3H, adamantane), δ 2.59 ppm (s, 3H, methyl), δ 3.94 ppm (s, 2H, $\text{Ar}-\underline{\text{CH}_2}-\text{N}$), δ 4.75 ppm (s, 2H, $\text{N}-\underline{\text{CH}_2}-\text{O}$), and δ 6.71 ~ 7.24 ppm (3H, Ar). Based on these $^1\text{H-NMR}$ results, we confirmed that 4-(1-Adamantyl)phenol, **2** benzoxazine and **3** benzoxazine have been successfully synthesized in the study.

7.3.2 Fourier Transfer Infrared Spectroscopy Analyses

Figures 7-4(a) and (b) show FT-IR spectra of **2** benzoxazine and poly(**2** benzoxazine) where bands of 753 cm^{-1} and 693 cm^{-1} corresponding to the monosubstituted benzene are still present even after curing. However, the characteristic absorption band of the oxazine ring at 948 cm^{-1} is disappeared, and the absorptions at 1512 cm^{-1} from the trisubstituted benzene ring and at 1246 cm^{-1} from the CH_2 wagging are both decreased. A new absorption band appears at 1502 cm^{-1}

from the tetrasubstituted benzene ring mode. Besides, the absorptions at 1031 and 1235 cm^{-1} , corresponding to the symmetric and asymmetric C—O—C bonds of the benzoxazine, disappear after the curing process. Furthermore, a broad hydroxyl band is formed between 3096 and 3640 cm^{-1} due to the ring opening process.

Figures 7-5(a) and (b) show FT-IR spectra of **3** benzoxazine and poly(**3** benzoxazine). The bands of neither 753 cm^{-1} nor 693 cm^{-1} (referred to monosubstituted benzene) appears in comparing with the **2** benzoxazine. In addition, similar absorption bands at 965, 1513, 1254, 1484, 1040 and 1231 cm^{-1} appear corresponding to the characteristic absorption bands of the **2** benzoxazine. The FT-IR spectra of Figures 7-4 (a) and 5 (a) agrees well with $^1\text{H-NMR}$ results, again confirmed the structures of **2** and **3** benzoxazines. Furthermore, FT-IR spectra of Figures 7-4 (b) and 5 (b) interpreted the variation of **2** and **3** benzoxazines before and after curing.

7.3.3 Glass Transition Temperature Analyses

Adamantane has been incorporated into many polymers over the past several years due to the unusual physical and thermal properties of the multicyclic cage structure. It's rigid and spherical structure result in a very high melting point and excellent thermal stability for the parent molecule. In this study, the adamantane unit was incorporated into the PBZZ as a pendant group. Figure 7-6 shows the DSC thermograms of p-a type PBZZ, poly(/**2** benzoxazine), p-m type PBZZ, and poly(/**3** benzoxazine). The poly(**3** benzoxazine) (188.8 $^{\circ}\text{C}$) possesses a higher glass transition temperature than the poly(**2** benzoxazine) (109.4 $^{\circ}\text{C}$) since the phenyl group is more bulky than the methyl group and hinders the molecular chain movement chiefly between bridging points of the cured resin. Therefore, the poly(**2** benzoxazine) has lower crosslinking density and lower glass transition temperature. Similar

phenomenon has also been reported in B-a type and B-m type PBZZ [17]. Surprisingly, the T_g of p-m type PBZZ is increased from 164.4 °C to 188.8 °C for the poly(3 benzoxazine) while the T_g of p-a type PBZZ is decreased from 128.3 °C to 109.4 °C for the poly(2 benzoxazine). The reason will be discussed in more details during next section. Scheme 7-3 shows various benzoxazine systems including p-a, p-m, B-a, and B-m types.

In order to better understand the observed unexpected glass transition temperature behavior between poly(2 benzoxazine) and poly(3 benzoxazine), blends with several different compositions were prepared by solution blending as shown in Table 7-1. The monomer mixture was stirred and dissolved in acetone, then the solution was allowed to evaporate slowly at 50 °C for 1 day. Afterwards, it was cured at 180 °C for 4 hr under vacuum to ensure total curing of the benzoxazine. Figure 7-7 and Figure 7-8 show the DSC thermograms of p-a/2 benzoxazine and p-m/3 benzoxazine co-PBZZs where only single T_g are present from all composition. A single T_g strongly implies that all these p-a/2 benzoxazine and p-m/3 benzoxazine co-PBZZs are homogenous.

In the p-m/3 benzoxazine co-PBZZs system, greater mobility of methyl group of p-m and 3 benzoxazine is expected during ring-opening process and results in higher crosslinking density. Therefore, the incorporation of more content of the 3 benzoxazine results in product with higher crosslinking density and higher glass transition temperature than the original p-m type PBZZ as shown in Figure 7-8. Figure 7-9 (a) plots T_g versus 3 benzoxazine content showing a positive deviation which is fitted well by the Kwei equation [18]. It describes the effect of hydrogen bonding interaction on T_g between polymers or a copolymer as shown in equation (1):

$$T_g = \frac{W_1 T_{g1} + kW_2 T_{g2}}{(W_1 + kW_2)} + qW_1W_2 \quad (1)$$

where W_1 and W_2 are weight fractions of the components, T_{g1} and T_{g2} represent the component glass transition temperatures. The large positive q value of 98 reveals that the observed positive T_g deviation is caused by the pendant group effect and the hydrogen bonding (OH...OH) between p-m and **3** benzoxazine co-PBZZs. More free hydroxyl groups of the p-m type PBZZ are available to bond with hydroxyl groups of the poly(**3** benzoxazine), and thus result in a positive deviation of glass transition temperature. Furthermore, it also explained why the ladder form, poly(**3** benzoxazine), has a glass transition temperature (188.8 °C) even higher than B-a and B-m type PBZZs with crosslinking structure [17].

In the p-a/**2** benzoxazine system, the bulky phenyl group present in the p-a type benzoxazine and **2** benzoxazine during ring-opening process results in lower mobility, lower crosslinking density and lower thermal properties comparing to the p-m/**3** benzoxazine system. Increasing the **2** benzoxazine content results in T_g decrease with a negative $q = -14$ as shown in Figure 7-9 (b).

Essentially, it is a competition between T_g increase due to bulky pendant group and T_g decrease due to lower crosslinking density. In the p-a/**2** benzoxazine system, the lower crosslinking density appears to play a more dominated role than the bulky pendant group effect and results in lower T_g .

7.3.4 Thermogravimetric Analyses

Figure 7-10 shows TGA thermograms of (a) p-m type PBZZ (b) p-a type PBZZ (c) poly(**3** benzoxazine) (d) poly(**2** benzoxazine). As can be seen, p-a type (b) and p-m (a) type PBZZs have substantially lower initial decomposition temperatures

than poly(2 benzoxazine) (d) and poly(3 benzoxazine) (c) due to the presence of the adamantane group in their polymer chains. In particular, the poly(3 benzoxazine) shows a extremely high in 5 wt % loss temperature at 399 °C as shown in Figure 7-10 and Table 7-2. On the other hand, char yields of these non-admantane types, p-a type PBZZ and p-m type PBZZ, are significantly higher than poly(2 benzoxazine) and poly(3 benzoxazine). Higher crosslinking density results in higher char yield and those adamantane-containing polymers, in general, give lower crosslinking density.



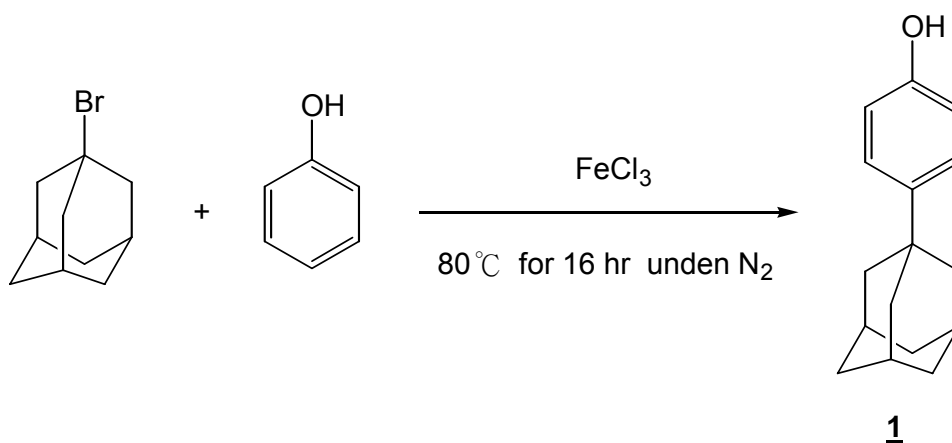
7.4 Conclusions

Two novel adamantane-modified benzoxazines were synthesized from 4-(1-Adamantyl)phenol, which were polymerized via a thermally induced ring-opening process. The steric hindrance is evident by the incorporating the adamantane group into the PBZZ backbone during curing and results in lower crosslinking density, especially in the poly(2 benzoxazine) system. Therefore, the poly(3 benzoxazine) has higher crosslinking density, higher glass transition temperature and higher decomposition temperature than that of the poly(2 benzoxazine). Furthermore, it also makes the p-a/2 benzoxazine system with a negative T_g deviation while the p-a/3 benzoxazine blends possessing a positive T_g deviation.

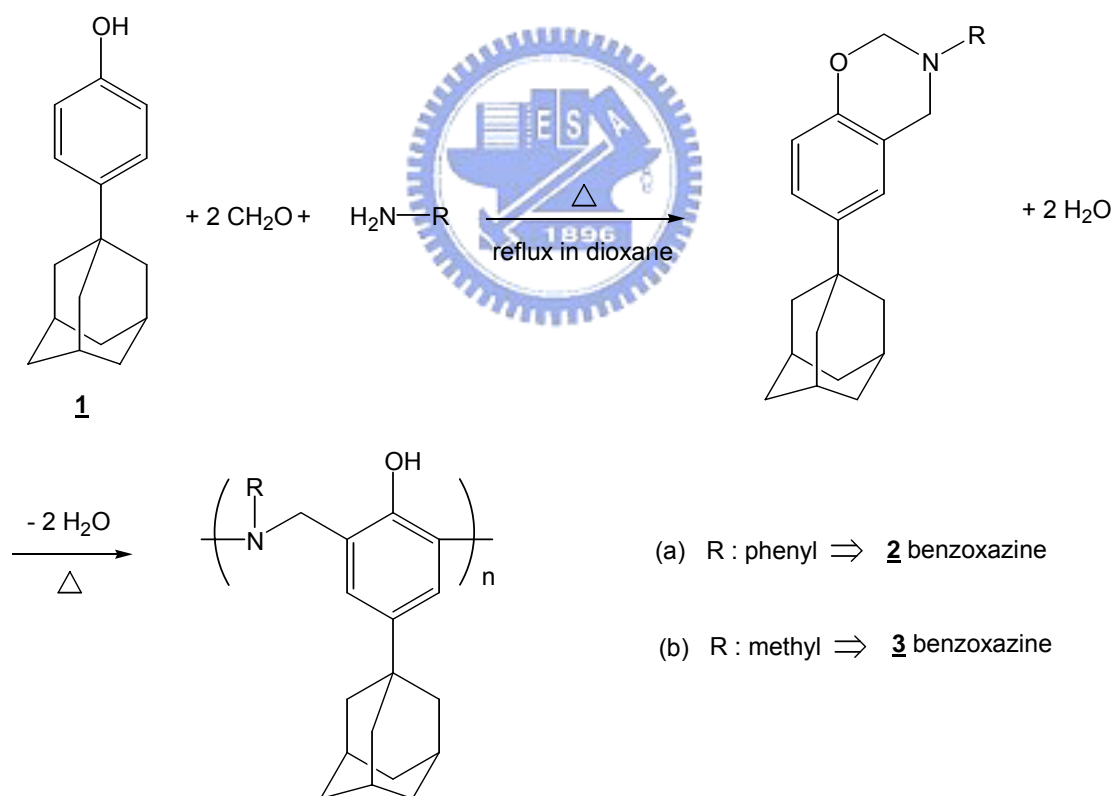


References

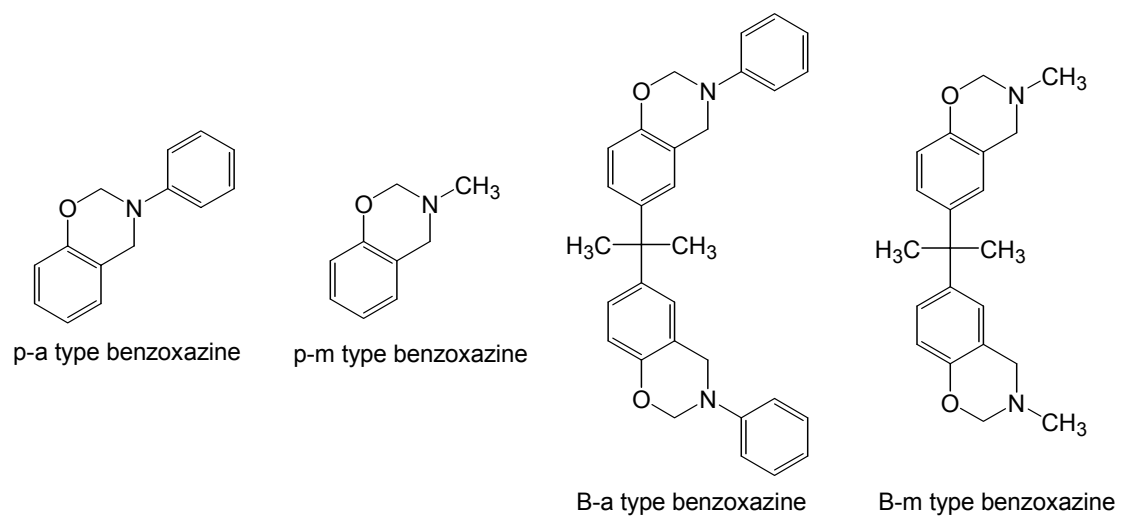
- [1] Wang, Y. X.; Ishida, H. *Macromolecules* **2000**, *33*, 2839.
- [2] Ishida, H.; Krus, C. M. *Macromolecules* **1998**, *31*, 2409.
- [3] Ishida, H.; Low, H. Y. *Macromolecules* **1997**, *30*, 1099.
- [4] Ishida, H.; Sanders, D. P. *Macromolecules* **2000**, *33*, 8149.
- [5] Laobuthee, A.; Chirachanchai, S.; Ishida, H.; Tashiro, K. *J. Am. Chem. Soc.* **2001**, *123*, 9947.
- [6] Agag, T.; Takeichi, T. *Macromolecules* **2001**, *34*, 7257.
- [7] Moine, L.; Cammas, S.; Amiel, C.; Guerin, P.; Seville, B. *Polymer* **1997**, *38*, 3121.
- [8] Mays, J. W.; Kioulafa, E. S.; Hadjichristidis, N. *Macromolecules* **1990**, *23*, 3530.
- [9] Cypcar, C. C.; Camelio, P.; Lazzeri, V.; Mathias, L. J.; Waegell, B. *Macromolecules* **1996**, *29*, 8954.
- [10] Fort, R. C. Jr.; Schleyer, P. V. R. *Chem. Rev.* **1964**, *64*, 277.
- [11] Mathias, L. J.; Tullos, G. L. *Polymer* **1996**, *37*, 3771.
- [12] Chern, Y. T.; Shiue, H. C. *Macromolecules* **1997**, *30*, 4646.
- [13] Jensen, J. J.; Grimsley, M.; Mathias, L. J. *J. Polym. Sci., Part A: Polym. Chem.* **1996**, *34*, 397.
- [14] Teraguchi, M.; Masuda, T. *J. Polym. Sci., Part A: Polym. Chem.* **1999**, *37*, 4546.
- [15] Mathias, L. J.; Lewis, C. M.; Wiegel, K. N. *Macromolecules* **1997**, *30*, 5970.
- [16] Acar, H. Y.; Jensen, J. J.; Thigpen, K.; McGowen, J. A.; Mathias, L. J. *Macromolecules* **2000**, *33*, 3855.
- [17] Ishida, H.; Allen, D. J. *J. Polym. Sci., Part B: Polym. Sci.* **1996**, *34*, 1019.
- [18] Kwei, T. K. *J. Polym. Sci. Polym. Lett. Ed.* **1984**, *22*, 307.



Scheme 7-1. The synthesis of 4-(1-Adamantyl)phenol



Scheme 7-2. The synthesis of **2** benzoxazine, **3** benzoxazine and their polymerization



Scheme 7-3. The structures of p-a, p-m, B-a and B-m type PBZZs



Table 7-1. The compositions and T_g s of p-a/2 benzoxazine and p-m/3 benzoxazine co-PBZZs

p-a/ <u>2</u> benzoxazine (weight ratio)	100/0	80/20	60/40	40/60	20/80	0/100
T_g (°C)	128.3	123.7	118.5	112.3	110.5	109.4
p-m/ <u>3</u> benzoxazine (weight ratio)	100/0	80/20	60/40	40/60	20/80	0/100
T_g (°C)	164.4	189.6	192.6	205.6	202.4	188.8

Table 7-2. The weight loss and char yield of poly(2 benzoxazine) and poly(3 benzoxazine) under N_2 environment

	5 wt % loss (°C)	10 wt % loss (°C)	char yield (%) at 700°C
p-a type PBZZ	224	264	43.2
p-m type PBZZ	245	268	52.2
poly(<u>2</u> benzoxazine)	335	365	24.2
poly(<u>3</u> benzoxazine)	399	439	30.8

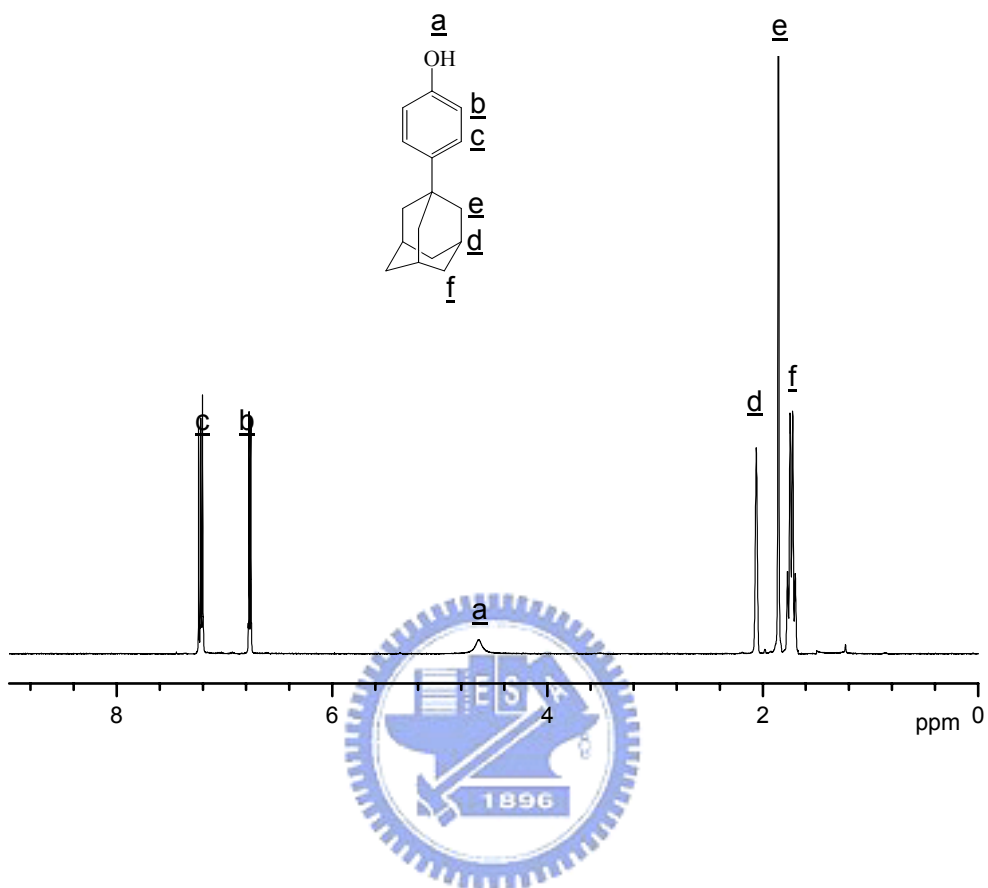


Figure 7-1. The ¹H-NMR spectrum of 4-(1-Adamantyl)phenol

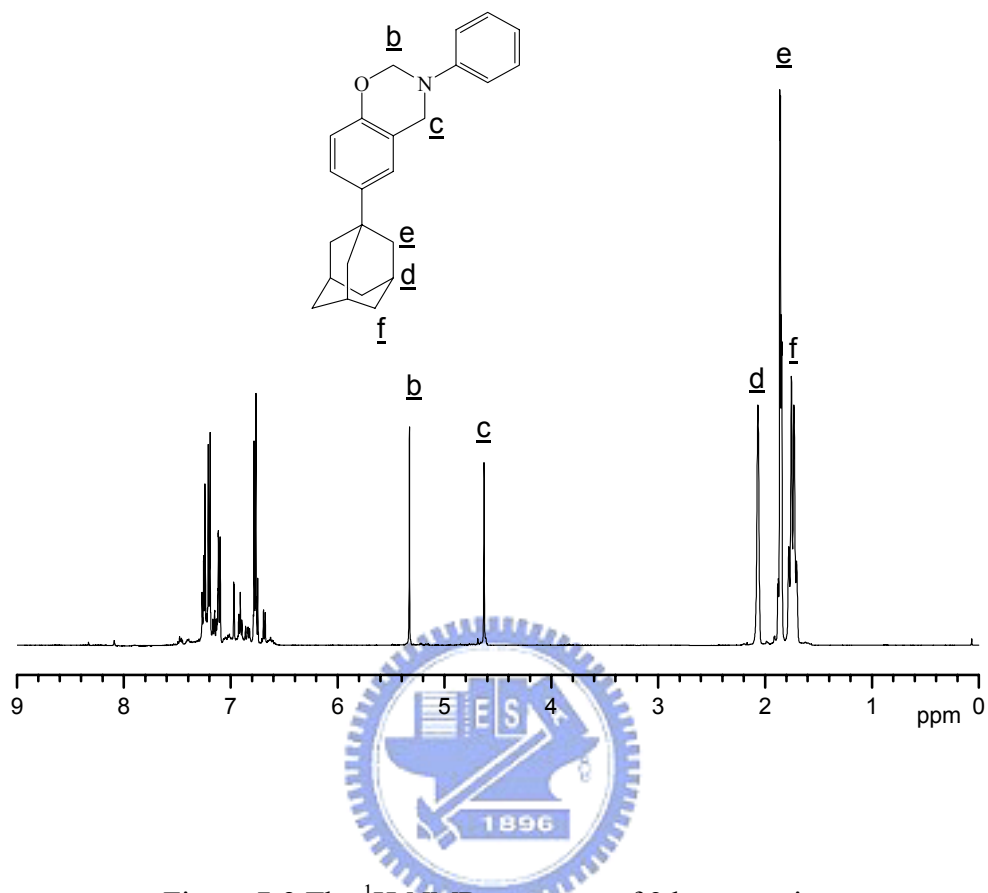


Figure 7-2 The ¹H-NMR spectrum of 2 benzoxazine

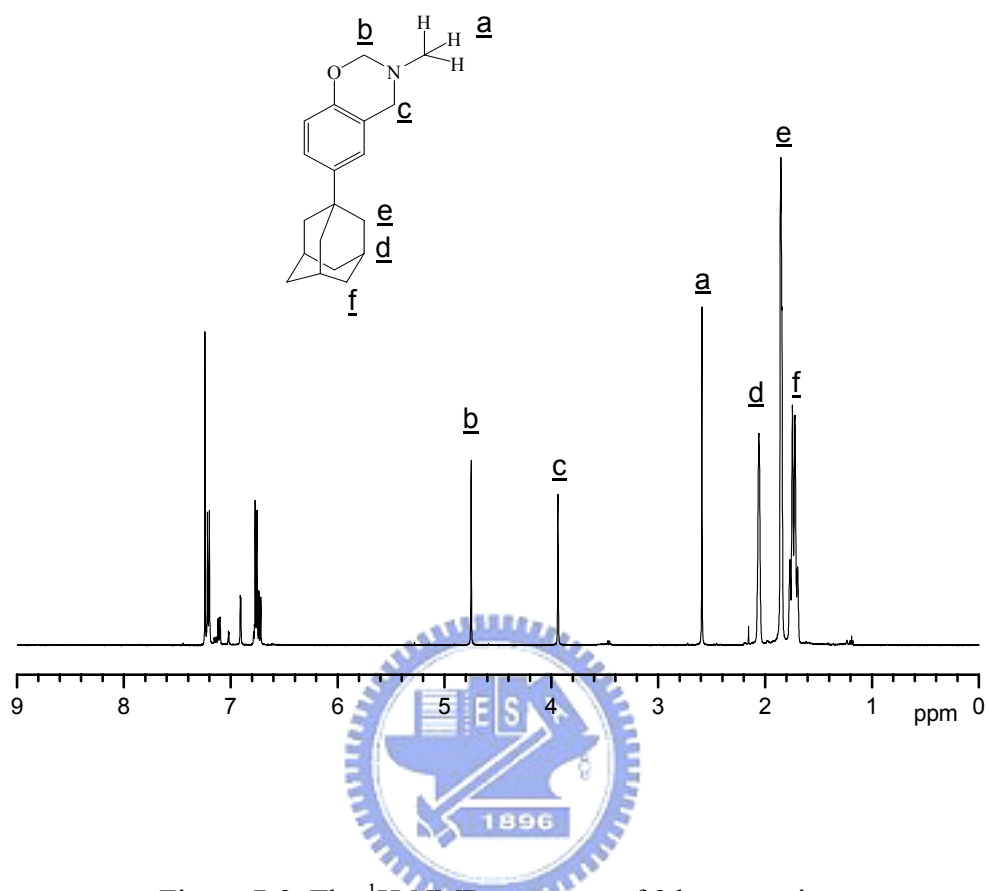


Figure 7-3. The ¹H-NMR spectrum of **3** benzoxazine

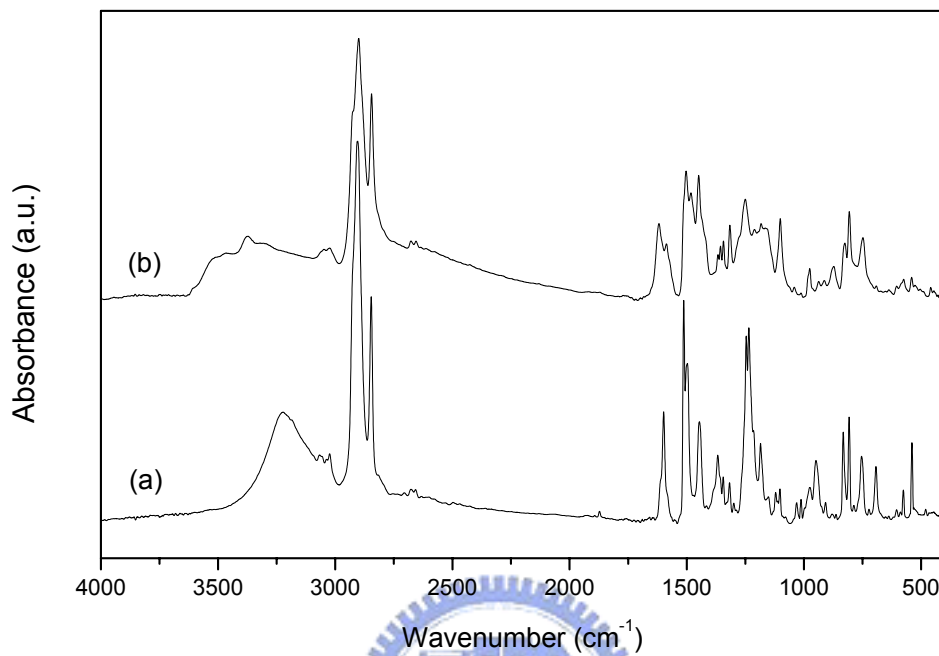


Figure 7-4. The FT-IR spectra of (a) 2 benzoxazine and (b) poly(2 benzoxazine)

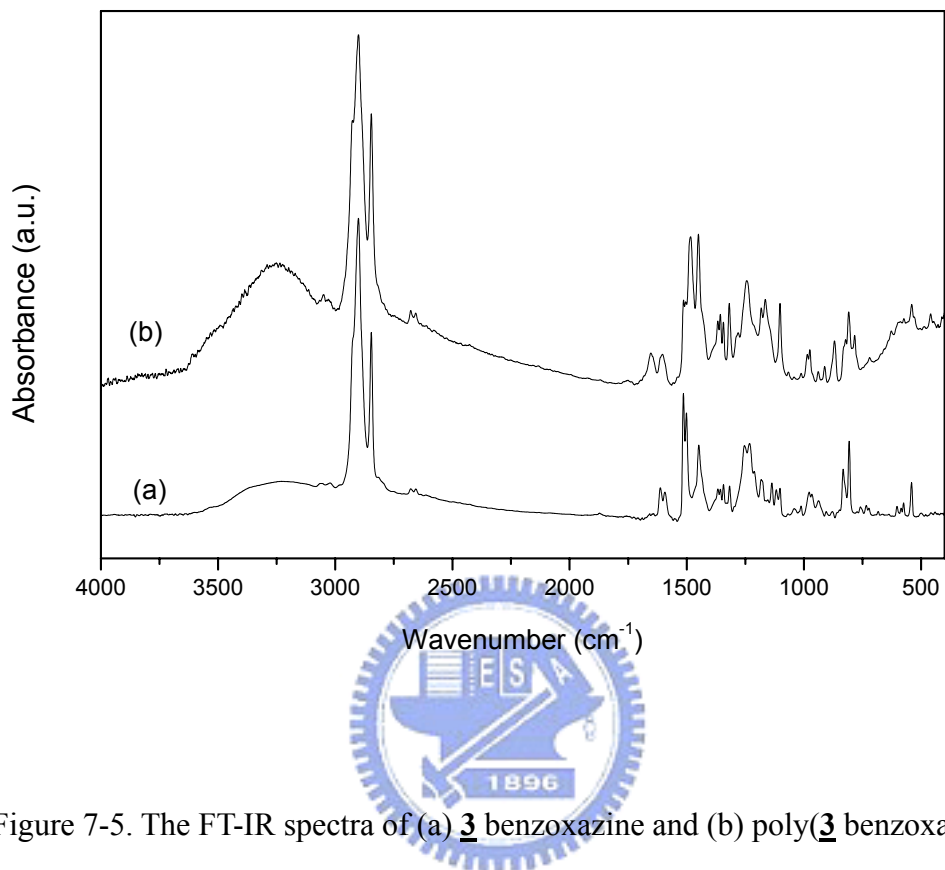


Figure 7-5. The FT-IR spectra of (a) **3** benzoxazine and (b) poly(**3** benzoxazine)

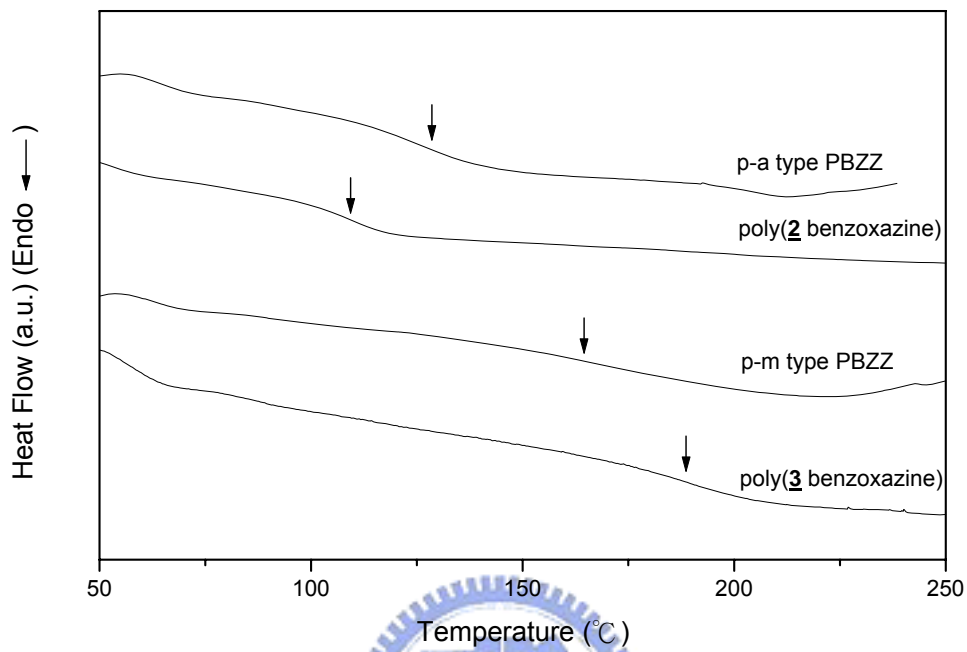


Figure 7-6. The DSC scans of p-a type PBZZ, poly(2 benzoxazine), p-m type PBZZ, and poly(3 benzoxazine)

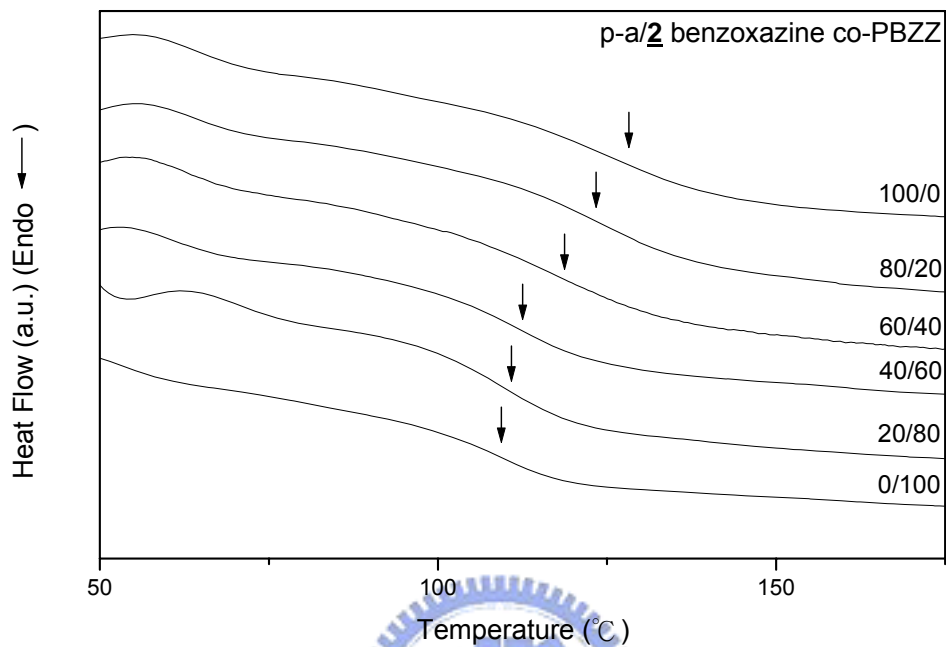


Figure 7-7. The DSC scans of p-a/2 benzoxazine co-PBZZ copolymers with different composition

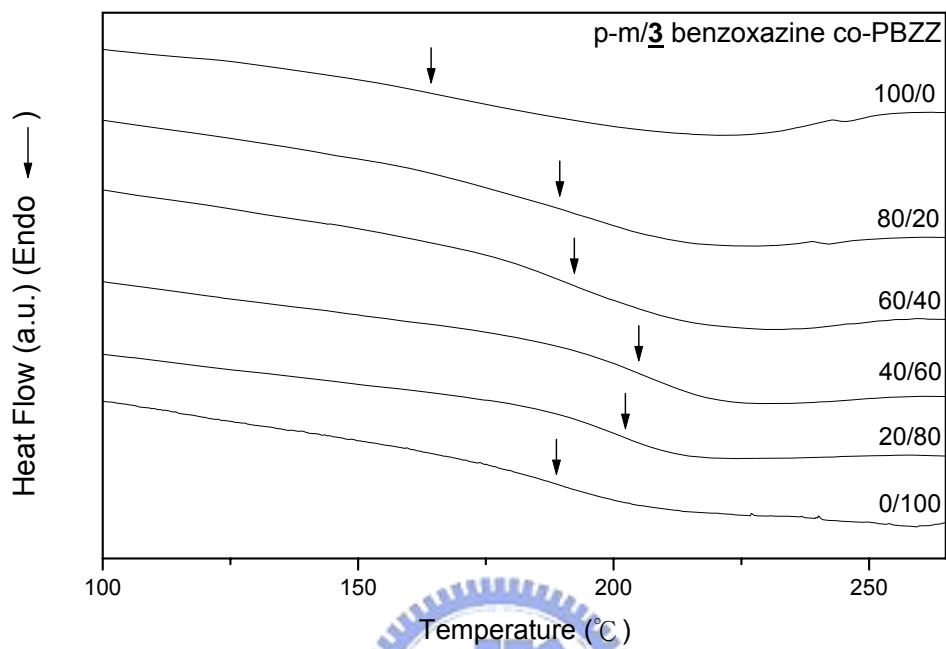


Figure 7-8. The DSC scans of p-m/3 benzoxazine co-PBZZ copolymers with different composition

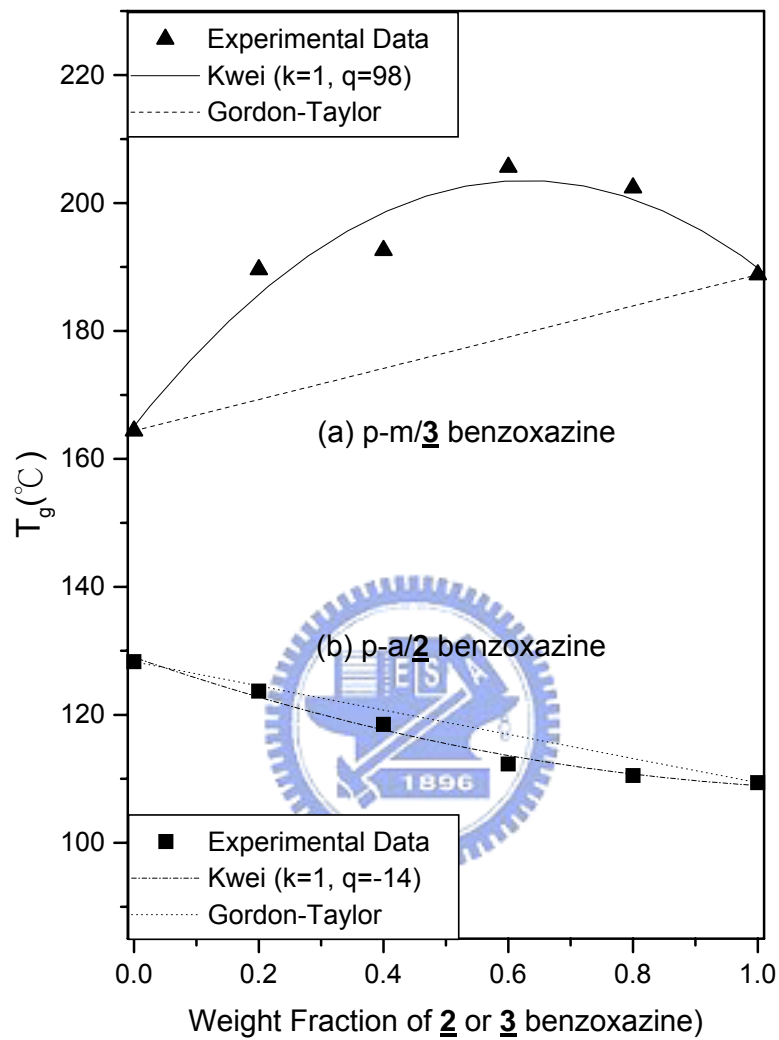


Figure 7-9. T_g versus composition curved base on (a) p-m/3 benzoxazine and (b) p-a/2 benzoxazine PBZZs copolymers

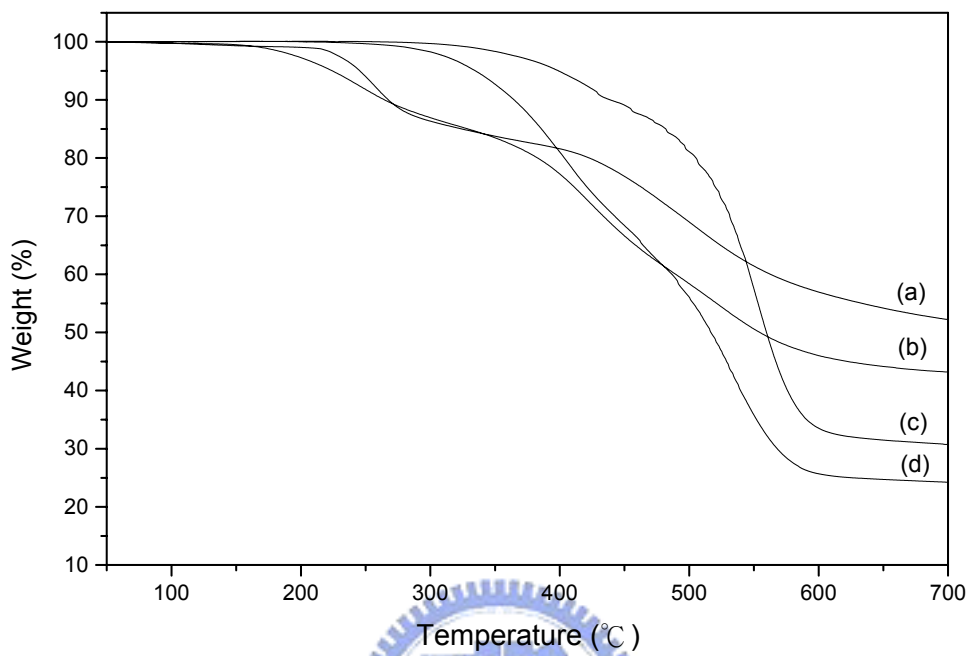


Figure 7-10. The TGA thermogram of (a) p-m type PBZZ (b) p-a type PBZZ (c) poly(3 benzoxazine) (d) poly(2 benzoxazine) under N₂ environment

Chapter 8

Preparation and Characterization of Polypseudorotaxanes Based on Adamantane-Modified Polybenzoxazines and β -Cyclodextrin

Abstract

β -Cyclodextrin (β -CD) forms inclusion complexes (ICs) with the adamantane-modified benzoxazines (**2** benzoxazine and **3** benzoxazine). These benzoxazines readily penetrate into the CD's hydrophobic cavity, causing turbidity of their solutions, from which fine crystalline powders are obtained. We characterized these complexes by powder X-ray diffraction, ^1H NMR spectroscopy, ^{13}C and ^{13}C CP/MAS NMR spectroscopies, DSC, and TGA. The X-ray diffraction and solid-state ^{13}C CP/MAS NMR spectroscopy studies indicate that the IC domains of the polypseudorotaxanes maintain their channel-type structures after the ring-opening curing reactions have occurred. ^1H NMR spectroscopy indicates that the pseudorotaxane structure is indeed formed, with the adamantane-modified benzoxazines units existing in the ICs. Furthermore, DSC measurements indicate that complexing the adamantane-modified benzoxazine units with β -CDs result in stiffer main chains and, thus, higher glass transition temperatures. TGA also indicates that the inclusion complexes have enhanced thermal stability.

8.1 Introduction

Cyclodextrins (CDs) are water-soluble, homochiral, cyclic oligosaccharides containing six, seven, or eight α -1, 4-linked D-glucopyranose units (α -, β -, and γ -cyclodextrins, respectively) and have pore sizes ranging from 4.9 to 7.9 Å (Scheme 1) [1-5]. Moreover, the C₂-OH group of one glucopyranoside unit can form a hydrogen bond with the C₃-OH group of its adjacent glucopyranose unit; in β -CD molecule, a complete secondary belt is formed by these hydrogen bonds, and, therefore, this molecules has a rather rigid structure. Such intramolecular hydrogen bond formation is probably responsible for β -CD having the lowest water solubility among all CDs. The hydrogen bond belt is incomplete in the α -CD molecule because the glucopyranose units are distorted; as a consequence, only four of the six possible intramolecular H-bonds can be fully established in α -CD. Although γ -CD is quite nonpolar, it has more flexible structure, therefore, it is the most soluble of these three CDs [5-7].

The most interesting property of these CDs is that they can include a wide range of guest molecules selectively within their cavities. These internal cavities are rather hydrophobic and can accommodate suitably sized hydrophobic molecules. Because primary and secondary –OH groups are positioned at the upper and lower rims of CD's, these rims are, therefore, hydrophilic [5,8]. In the presence of hydrophobic species, the water molecules that usually are associated with the CDs are readily expelled to allow the guest molecules to penetrate into the empty cavity. As a result, inclusion complexes are formed that are stabilized thermodynamically by relevant hydrophobic interactions. In addition, the water molecules reentering the aqueous phase results in an overall positive ΔS contribution [9]. Besides being used as carriers, CDs have also been applied as components of supramolecular assemblies

[10] for the creation of novel molecular materials; additionally, they are capable of forming supramolecular nano-objects [11] with almost all kinds of polymers (e.g., alkanes, ethers, amines, and esters). The kinetics and the yield of such processes depend on the structure of both the CD and the polymer, the polymer's molecular weight, the temperature, the solvent, and the nature of other solutes present in the solution [1].

When CD's form complexes with low-molecular-weight guests, the aggregates of these ICs have either channel or cage structures [12]. In the channel structure, the CD rings are stacked on top of one another to produce extended cylindrical central cavities. In the cage structure, the cavity of one CD molecule is closed on both sides by adjacent molecules. Because of the long chain lengths of polymers, polymer-CD complexes are expected to possess channel-type crystal structures. The formation of polymer-CD complexes also provides a unique opportunity to study single polymer chains isolated from their neighboring chains. Such studies may eventually provide valuable insight into the single-chain electrical and optical properties of polymers in the solid state.

The polymer-CD inclusion complexes that have been reported to date have belonged mainly to classes of main-chain polypseudorotaxanes and polyprotaxanes. In this study, we focused on the formation and characterization of side-chain polypseudorotaxanes. In an earlier publication, we reported the successful synthesis of two adamantane-modified benzoxazines, which are presented in Scheme 2 (a) [13]. A unique feature of this present study is the self-assembly of β -CD with the adamantane-modified benzoxazines. We selected the adamantane unit because it fits precisely into the slightly polar β -CD cavity [14,15]. In an aqueous solution, water molecules in the CD cavity are energetically unstable and are readily substituted by a

less-polar guest molecule having appropriate dimensions [16].

8.2 Experimental

8.2.1 Materials

1-Bromoadamantane, methylamine and β -cyclodextrin were purchased from the Acros Chemical Company (USA). Formaldehyde and aniline were purchased from the Aldrich Chemical Company (USA).

8.2.2 Nuclear Magnetic Resonance (NMR)

^1H and spectra were recorded on a Varian Unity Inova 500 FT NMR Spectrometer operating at 500 MHz; chemical shifts are reported in parts per million (ppm). High-resolution solid-state ^{13}C NMR spectroscopy experiments were carried out at room temperature using a Bruker DSX-400 Spectrometer operating at a resonance frequency of 100.47 MHz. The high-resolution solid-state ^{13}C NMR spectra were acquired by using the cross-polarization (CP)/magic-angle spinning (MAS)/high-power dipolar decoupling technique, using a 90° pulse width of 3.9 ms, a 3 s pulse delay time, and an acquisition time of 30 ms with 2048 scans. A magic-angle sample-spinning rate of 5.4 kHz was used to avoid absorption overlapping. The proton spin-lattice relaxation time in the rotating frame $T_{1\rho}^H$ was determined indirectly via carbon observation using a $90^\circ-\tau$ -spin lock pulse sequence prior to CP. The data acquisition was performed using delay time (τ) ranging from 0.1 to 15 ms.

8.2.3 Wide Angle X-ray Diffraction (WAXD)

Wide-angle X-ray diffraction patterns of powder samples were obtained at ambient conditions on a Siemens type-F X-ray Diffractometer equipped with a nickel-filtered Cu $K\alpha$ radiation source (wavelength = 1.54 Å). The supplied voltage

and current were set to 50 kV and 200 mA, respectively. Samples were mounted on a sample holder with Scotch tape and the diffracting intensities were recorded every 0.02 from 2θ scans in the range 3.5–50°.

8.2.4 Differential Scanning Calorimetry (DSC)

Calorimetric measurements were performed using a TA DSC-2010 Differential Scanning Calorimeter and were conducted under a nitrogen flow of 25 mL/min and a heating rate of 20 °C/min. The sample was preheated from 30 to 260 °C and maintained at 260 °C for 2 min. The measurement was made using 5–10 mg of sample in a DSC sample cell by cooling to 30 °C quickly from the melt of the first scan. The second scan involved heating the sample from 30 to 300 °C and the value of T_g was taken as the midpoint of the heat capacity transition between the upper and lower points of deviation from the extrapolated rubbery and glassy lines.

8.2.5 Thermogravimetric Analysis (TGA)

The thermal stability of the cured sample was investigated using a TA Instruments Q 50 apparatus. The cured sample of (10–20 mg) was placed in a Pt cell and heated from 30 to 700 °C under a nitrogen flow of 60 mL/min and a heating rate of 10 °C/min.

8.2.6 Synthesis of the β -CD/2 benzoxazine inclusion complex

We have synthesized and characterized 4-(1-Adamantyl)phenol, 2 benzoxazine and 3 benzoxazine in Chapter 7 [13]. The β -CD/2 benzoxazine inclusion complex was prepared by the sonication method according to Scheme 2 (b). Both 2 benzoxazine (0.1 g was dissolved in 35.5 mL acetone) and saturated aqueous β -CD solution [5,7] (0.657 g was dissolved in 35.5 mL water) were kept in room temperature. The solution of 2 benzoxazine was added slowly over 2 hr to the β -CD solution while sonicating. The mixture rapidly became turbid and a white precipitate

was formed subsequently. After filtration, the white powder was washed with water and acetone several times to remove any uncomplexed β -CD and the free 2 benzoxazine. Finally, the white powder was dried in a vacuum oven at 60 °C for 12 hr.

8.2.7 Synthesis of the β -CD/3 benzoxazine inclusion complex

A similar method, illustrated in Scheme 2 (b), was adopted for the synthesis of the β -CD/3 benzoxazine inclusion complex as that described above for the β -CD/2 benzoxazine complex, except that we employed solutions of 3 benzoxazine (0.1g was dissolved in 43.24 mL acetone) and saturated aqueous β -CD solution (0.8 g was dissolved in 43.24 mL water). After proceeding through same purification process, the β -CD/3 benzoxazine inclusion complex was obtained as a white powder.



8.3 Results and Discussion

8.3.1 Wide Angle X-ray Diffraction Analysis

The inclusion complexes of CDs with low-molecular-weight compounds can be classified as having either “cage-type” or “channel-type” structures. Figures 8-1 (a)-(c) and Figures 8-2 (a)-(c) present the WAXD patterns of β -CD, 2 benzoxazine, and the β -CD/2 benzoxazine inclusion complex and of β -CD, 3 benzoxazine, and the β -CD/3 benzoxazine inclusion complex, respectively. These patterns indicate that both of these complexes are crystalline and that they are completely different from those of β -CD and the benzoxazines. The appearance of two sharp peaks in both the β -CD/2 benzoxazine and β -CD/3 benzoxazine inclusion complexes at ca. $2\theta=11.6^\circ$ ($d=7.62 \text{ \AA}$) and 17.9° ($d=4.95 \text{ \AA}$) is the key feature that serves as a fingerprint to indicate the channel-type structures of these β -CD/polymer inclusion complexes [17]. These benzoxazine complexes of β -CD exhibit packing different from that of the free β -CD and possess channel structures similar to those of other β -CD based polypseudorotaxanes [8,17].

Figures 8-1 (d) and 8-2 (d) display the WAXD patterns of poly(β -CD/2 benzoxazine) and poly(β -CD/3 benzoxazine) obtained after thermal curing of the ICs at $180 \text{ }^\circ\text{C}$ for 4 hr. These inclusion complexes become transformed into side-chain polypseudorotaxanes, as indicated in Scheme 2 (c). The intensities of the characteristic peaks of the channel-type structure at ca. $2\theta=11.6^\circ$ ($d=7.62 \text{ \AA}$) and 17.9° ($d=4.95 \text{ \AA}$) become smaller as some features of the crystal structures are destroyed during the curing process. These observations indicate that the channel-type structures of the inclusion complexes remain essentially intact, despite the occurrence of the ring-opening curing reaction.

8.3.2 Nuclear Magnetic Resonance Analysis

Solid-state ^{13}C NMR spectroscopic studies, conducted by ^{13}C cross-polarization magic-angle spinning (CP/MAS), can provide information regarding the structures of CD complexes [18-20]. Figures 8-3 (a)-(c) display the ^{13}C CP/MAS NMR spectra of β -CD and the β -CD/2 benzoxazine and β -CD/3 benzoxazine inclusion complexes, respectively. β -CD assumes a less-symmetrical conformation in the crystal because it does not possess a guest compound included in its cavity. Figure 8-3 (a) displays resolved resonances for the C_1 and C_4 nuclei of each of the α -1,4-linked glucose residues. Two peaks appear at 94.2 and 96.7 ppm, which are assigned as the conformationally strained glycosidic linkages [21]. These two peaks, however, disappear in the spectra of the β -CD/2 benzoxazine and β -CD/3 benzoxazine inclusion complexes. Furthermore, ^{13}C resonances of β -CD give multiple lines because of the asymmetric glucopyranosyl conformations, but each carbon of the glucose of β -CD/adamantane-modified benzoxazine inclusion complexes can be observed in a sharp single peak of the complexes in the ^{13}C CP/MAS NMR. The C_1 - C_6 nuclei of β -CD appear as distinct, but unresolved, resonances in Figures 8-3 (b) and 3(c), indicating that, in the ICs, the β -CD units adopt more-symmetrical conformations in which each glucose unit of β -CD exists in a similar environment. It is known, from a previous X-ray crystallographic study on single crystals, that β -CD adopts a symmetrical conformation when it includes including a guest into its cavity [22]. Hence, our ^{13}C CP/MAS NMR spectra of the complexed and uncomplexed cyclodextrins are consistent with the prior results from the X-ray crystallography, and, therefore, the adamantane units of 2 and 3 benzoxazines are indeed included within the cavity of the β -CD.

The compositions of these β -CD/adamantane-modified benzoxazine

pseudorotaxanes were investigated by ^1H NMR spectroscopy ($\text{d}_6\text{-DMSO}$, 500 MHz). Figures 8-4 (b) and 8-4 (c) present the spectra of the pseudorotaxanes $\beta\text{-CD}/\underline{\mathbf{2}}$ benzoxazine and $\beta\text{-CD}/\underline{\mathbf{3}}$ benzoxazine compared with their respective precursors as shown in experimental section, and Figure 8-4 (a) provides the ^1H NMR spectrum of $\beta\text{-CD}$ [23]. The characteristic peaks of $\beta\text{-CD}$ and $\underline{\mathbf{2}}$ benzoxazine are both present in Figure 8-4(b), [$\underline{\mathbf{2}}$ benzoxazine: δ (ppm) 1.70 (q, 6H, adamantane), 1.78 (d, 6H, adamantane), 2.07 (s, 3H, adamantane), 4.63 (s, 2H, $\text{Ar}-\underline{\text{CH}}_2-\text{N}$), 5.38 (s, 2H, $\text{N}-\underline{\text{CH}}_2-\text{O}$), 6.62–7.22 (8H, Ar)]. In Figure 8-4(c), we observe the characteristic peaks of both $\beta\text{-CD}$ and $\underline{\mathbf{3}}$ benzoxazine [$\underline{\mathbf{3}}$ benzoxazine: δ (ppm) 1.70 (q, 6H, adamantane), 1.78 (d, 6H, adamantane), 2.44 (s, 3H, methyl), 3.85 (s, 2H, $\text{Ar}-\underline{\text{CH}}_2-\text{N}$), 4.68 (s, 2H, $\text{N}-\underline{\text{CH}}_2-\text{O}$), 6.64–7.08 (3H, Ar)]. These ^1H NMR spectra indicate that the pseudorotaxane structure is indeed formed, and that the adamantane-modified benzoxazines exist in the ICs.



8.3.3 Proton $T_{1\rho}^H$ Relaxation Time Analysis

Solid-state NMR spectroscopy is often used to study the length scale of phase separation in semicrystalline polymers and blends because the rate of magnetization transfer via proton spin diffusion is on the correct time scale to measure phase separation over a length scale of 5–200 Å. The length scale of phase separation is of interest in many polymeric systems, and several methods have been developed to measure domain sizes using proton spin diffusion. In the present study, we have used the proton $T_{1\rho}^H$ relaxation rates to measure the magnetization exchange between the guest polymer and the CDs [6,24]. If there is efficient magnetization exchange on a length scale of 20 Å or less, an averaged relaxation time can be observed between the

polymer and the host CD. The magnetization of the resonance is expected to decay according to the following exponential function for a model spin-locking mode:

$$\ln(M_\tau / M_0) = -\tau / T_{1\rho}^H \quad (1)$$

where $T_{1\rho}^H$ is the spin-lattice relaxation time in the rotating frame, τ is the delay time used in the experiment, and M_τ is the corresponding resonance. $T_{1\rho}^H$ can be obtained from the slope of a plot of $\ln(M_\tau / M_0)$ vs. τ .

Figure 8-5 presents the results of the proton $T_{1\rho}^H$ relaxation measurements for β -CD, β -CD/2 benzoxazine and β -CD/3 benzoxazine ICs. We observed slightly longer relaxation times (8.13 and 8.82 ms) for the β -CD/2 benzoxazine and β -CD/3 benzoxazine ICs relative to that of the pure β -CD (8.06 ms). Instead of large variations in the relaxation times, the difference is only slight because the guests, adamantane-modified benzoxazines, are not macromolecular. Nevertheless, the slight differences observed indicate that some spin diffusion exists between the host and the guest. In any case, we conclude that the environments before curing are similar for the β -CD and the β -CD/ adamantane-modified benzoxazine ICs.

8.3.4 Glass Transition Temperature Analysis

We performed differential scanning calorimetry (DSC) to obtain the glass transition temperatures of the adamantane-modified polybenzoxazines and their polypseudorotaxanes formed with β -CD. The side chains of the β -CD/adamantane-modified polybenzoxazine inclusion complexes are included into the CD molecules, which is a situation that we expected would affect the mobility of the polybenzoxazine main chain segments. Figure 8-6 displays the DSC curves of the two polybenzoxazines and the two inclusion complexes: all show poorly defined

single glass transition temperatures. The value of T_g of poly(2 benzoxazine) and poly(3 benzoxazine) are 109.4 and 188.8 °C, respectively, as indicated in Figures 8-6 (a) and 8-6 (c). Furthermore, Figures 8-6 (b) and 8-6 (d) present the DSC traces of poly(β -CD/2 benzoxazine IC) and poly(β -CD/3 benzoxazine IC). In comparison, the values of T_g of these polyseudorotaxanes are increased significantly, from 109.4 to 216.6 °C and from 188.8 to 243.4 °C, respectively. These results are reasonable because the larger steric congestion existing in the complexes will cause the polybenzoxazine's main chains to become relatively stiffer, which is a situation that results in higher glass transition temperatures.

8.3.5 Thermogravimetric Analysis

We investigated the thermal stabilities of β -CD and the polyseudorotaxanes by thermogravimetric analysis (TGA). Figure 8-7 and Table 8-1 display the initial decomposition temperatures, temperatures of maximum weight loss rate, and char yields of β -CD, poly(β -CD/2 benzoxazine IC), and poly(β -CD/3 benzoxazine IC) under nitrogen atmospheres. The pure β -CD and the polymeric inclusion complexes being to decompose (5 wt %) in the range from 323 to 340 °C as shown in Figures 8-7 (a)-(c). Furthermore, Figures 8-7 (d)-(f) display the traces of the derivative weight per degree C (%/°C) of β -CD, poly(β -CD/2 benzoxazine IC), and poly(β -CD/3 benzoxazine IC). Instead of only a slight increase in the 5 wt % weight loss temperature, the temperature of maximum weight loss rate of β -CD is increased substantially from 335 °C to 376 °C and 385 °C for poly(β -CD/2 benzoxazine IC) and poly(β -CD/3 benzoxazine IC), respectively. In other words, these results indicate that the thermal stability of the CD is enhanced by the formation of inclusion complexes.

8.4 Conclusions

β -CD forms stoichiometric complexes with 2 benzoxazine and 3 benzoxazine. This is a new finding that the β -CD is able to form a complex with adamantane-modified benzoxazine. X-ray diffraction and solid-state ^{13}C CP/MAS NMR spectroscopic studies indicate that the IC domains of the resulting polypseudorotaxanes have channel-type structures even through the ring opening curing process occurred at high temperature. DSC measurements indicate that the inclusion of the adamantane-modified benzoxazines into β -CD units results in stiffer of the main chains and, thus, higher glass transition temperatures. TGA analyses also indicate that the thermal stability of the inclusion complexes is enhanced.



References

- [1] Easton, C. J.; Lincoln, S. F. *Modified Cyclodextrins*; Imperial College Press: London, 1999.
- [2] Ogoshi, T.; Chujo, Y. *Macromolecules* **2003**, *36*, 654.
- [3] Wulff, M.; Alden, M.; Tegenfeldt, J. *Bioconjugate Chem.* **2002**, *13*, 240.
- [4] Asanuma, H., A.; Hishiya, T.; Komiyama, M. *Adv. Mater.* **2000**, *12*, 1019.
- [5] Szejtli, J. *Chem. Rev.* **1998**, *98*, 1743.
- [6] Lu, J.; Mirau, P. A.; Tonelli, A. E. *Macromolecules* **2001**, *34*, 3276.
- [7] Okumura, H.; Kawaguchi, Y.; Harada, A. *Macromolecules* **2001**, *34*, 6338.
- [8] Harada, A. *Adv. Polm. Sci.* **1997**, *133*, 141.
- [9] Nostro, P. L.; Santoni, I.; Bonini, M.; Baglioni, P. *Langmuir* **2003**, *19*, 2313.
- [10] Becheri, A.; Nostro, P. L.; Ninham, B. W.; Baglioni, P. *J. Phys. Chem. B* **2003**, *107*, 3979
- [11] Liu, J.; Alvarez, J.; Kaifer, A. E. *Adv. Mater.* **2000**, *12*, 1381.
- [12] Huang, L.; Allen, E.; Tonelli, A. E. *Polymer* **1998**, *39*, 4857.
- [13] Su, Y. C.; Chen, W. C.; Chang, F. C. *J. Appl. Polym. Sci.*, submitted.
- [14] Sandier, A.; Brown, W.; Mays, H. *Langmuir* **2000**, *16*, 1634.
- [15] Chamberlain, R. V., II; Slowinska, K.; Majda, M. *Langmuir* **2000**, *16*, 1388.
- [16] Eftink, M. R.; Andy, M. L.; Bystrom, K.; Perlmutter, H. D.; Kristol, D. S. *J. Am. Chem. Soc.* **1989**, *111*, 6765.
- [17] Jiao, H.; Goh, S. H.; Valiyaveetil, S. *Macromolecules* **2002**, *35*, 3997.
- [18] Jiao, H.; Goh, S. H.; Valiyaveetil, S. *Macromolecules* **2001**, *34*, 8138.
- [19] Li, J.; Ni, X.; Zhou, Z.; Leong, K. W. *J. Am. Chem. Soc.* **2003**, *125*, 1788.
- [20] Jiao, H.; Goh, S. H.; Valiyaveetil, S. *Macromolecules* **2002**, *35*, 1980.
- [21] Harada, A.; Okada, M.; Li, J.; Kamachi, M. *Macromolecules* **1995**, *28*, 8406.

[22] Harding, M. M.; MacLennan, J. M.; Paton, R. M. *Nature* **1978**, *274*, 621.

[23] Auzély-Velty, R.; Rinaudo, M. *Macromolecules* **2002**, *35*, 7955.

[24] McBrierty, V. J.; Douglass, D. C.; Kwei, T. K. *Macromolecules* **1978**, *11*, 1265.



Table 8-1. Weight losses temperatures, temperatures of maximum weight losses rates, and char yields of (a) β -CD, (b) poly(β -CD/2 benzoxazine IC) and (c) poly(β -CD/3 benzoxazine IC) under N_2 atmospheres.

Code	Temp. ($^{\circ}C$)		Char yield (%) at 700 $^{\circ}C$
	5 wt % loss	max. weight loss rate	
(a) β -CD	323	335	11.6
(b) poly(β -CD/ <u>2</u> benzoxazine IC)	330	376	10.8
(c) poly(β -CD/ <u>3</u> benzoxazine IC)	340	385	11.8

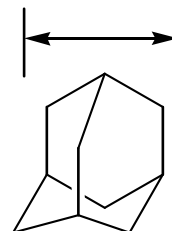
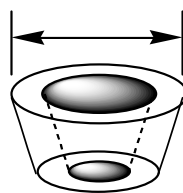
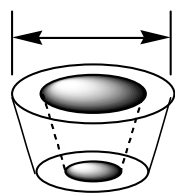
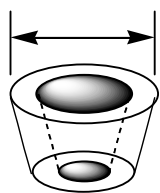


4.5–5.3 Å

6.0–7.0 Å

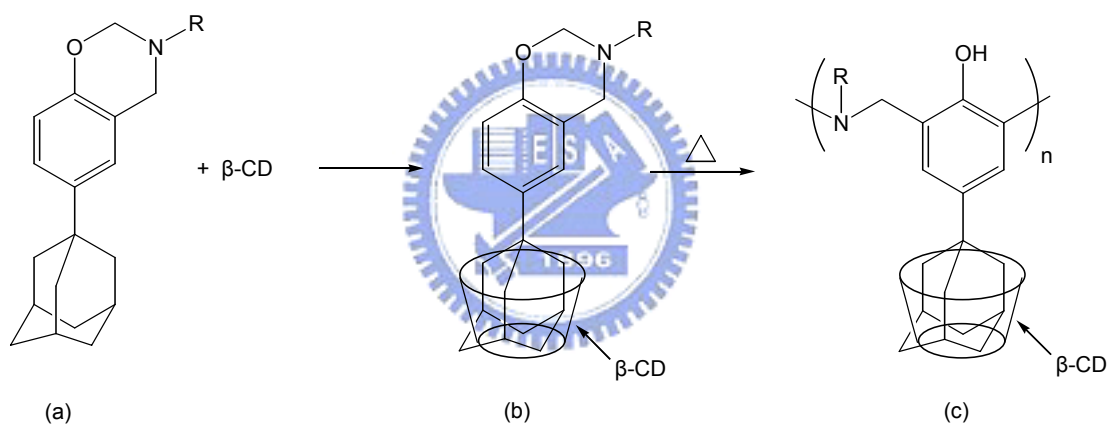
7.5–8.5 Å

6.5 Å

 α -CD β -CD γ -CD

adamantane

Scheme 8-1. Structure and dimensions of α -, β -, and γ - CD and the guest molecule, adamantane.



R : phenyl \Rightarrow 2 benzoxazine

R : methyl \Rightarrow 3 benzoxazine

Scheme 8-2. Synthesis of β -CD/2 benzoxazine IC, β -CD/3 benzoxazine IC, poly(β -CD/2 benzoxazine IC), and poly(β -CD/3 benzoxazine IC).

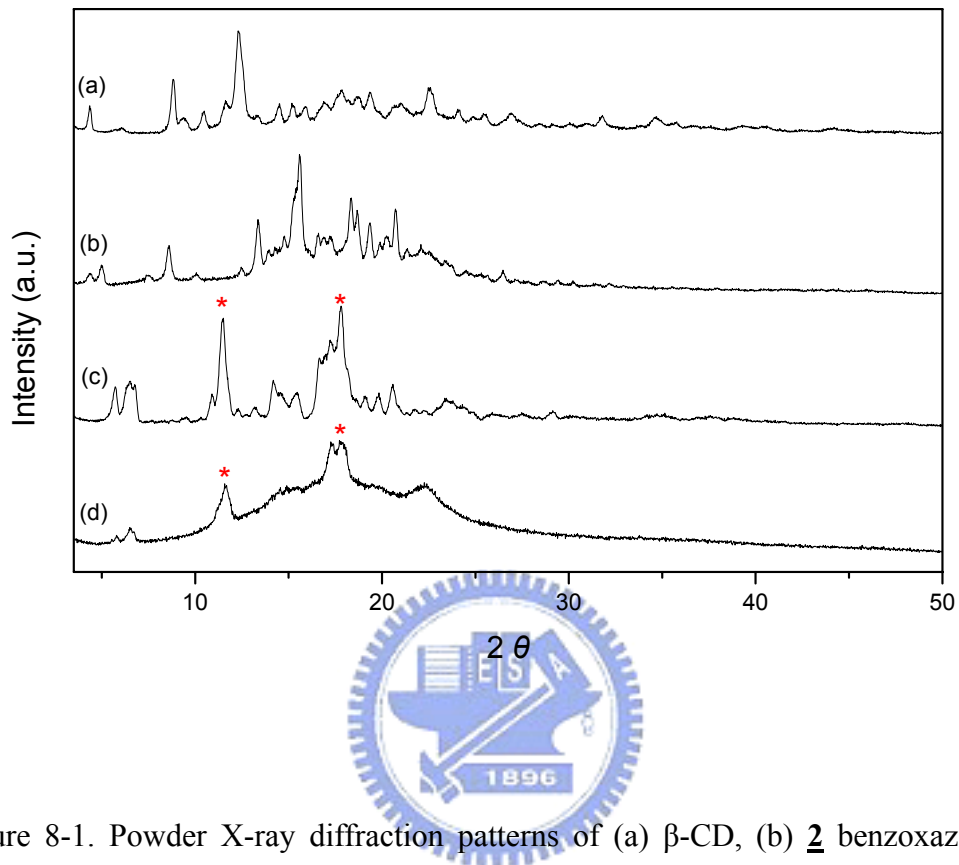


Figure 8-1. Powder X-ray diffraction patterns of (a) β -CD, (b) 2 benzoxazine, (c) β -CD/2 benzoxazine IC, and (d) poly(β -CD/2 benzoxazine IC).

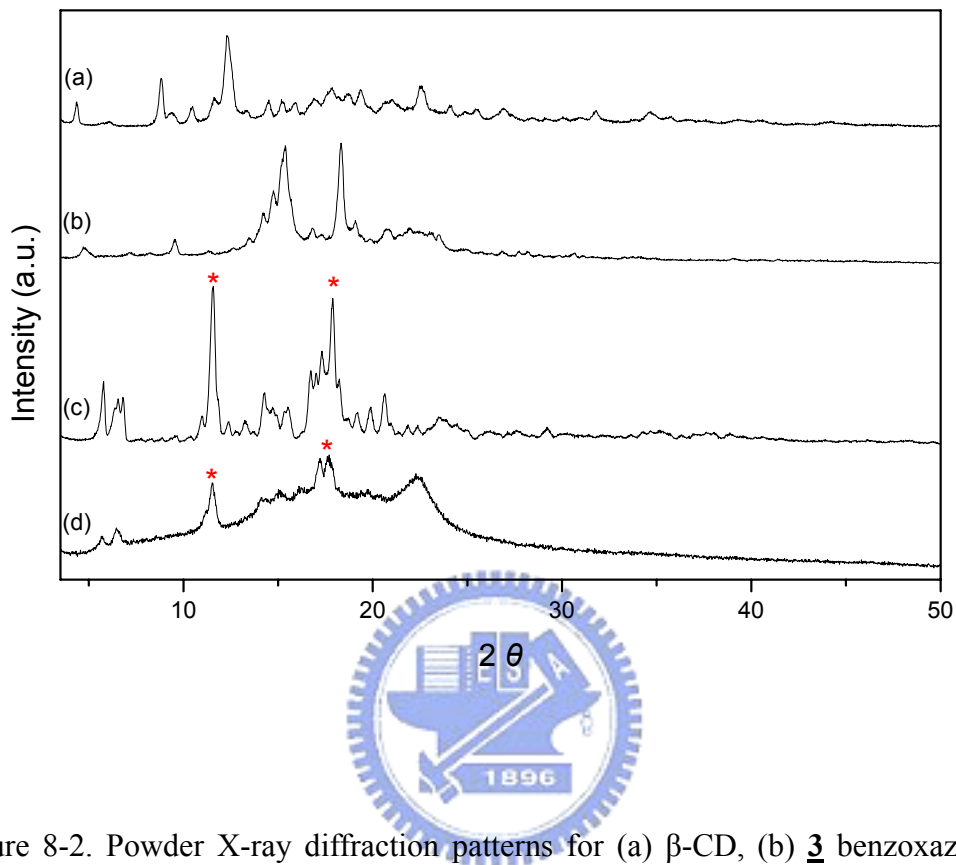


Figure 8-2. Powder X-ray diffraction patterns for (a) β -CD, (b) 3 benzoxazine, (c) β -CD/3 benzoxazine IC, and (d) poly(β -CD/3 benzoxazine IC).

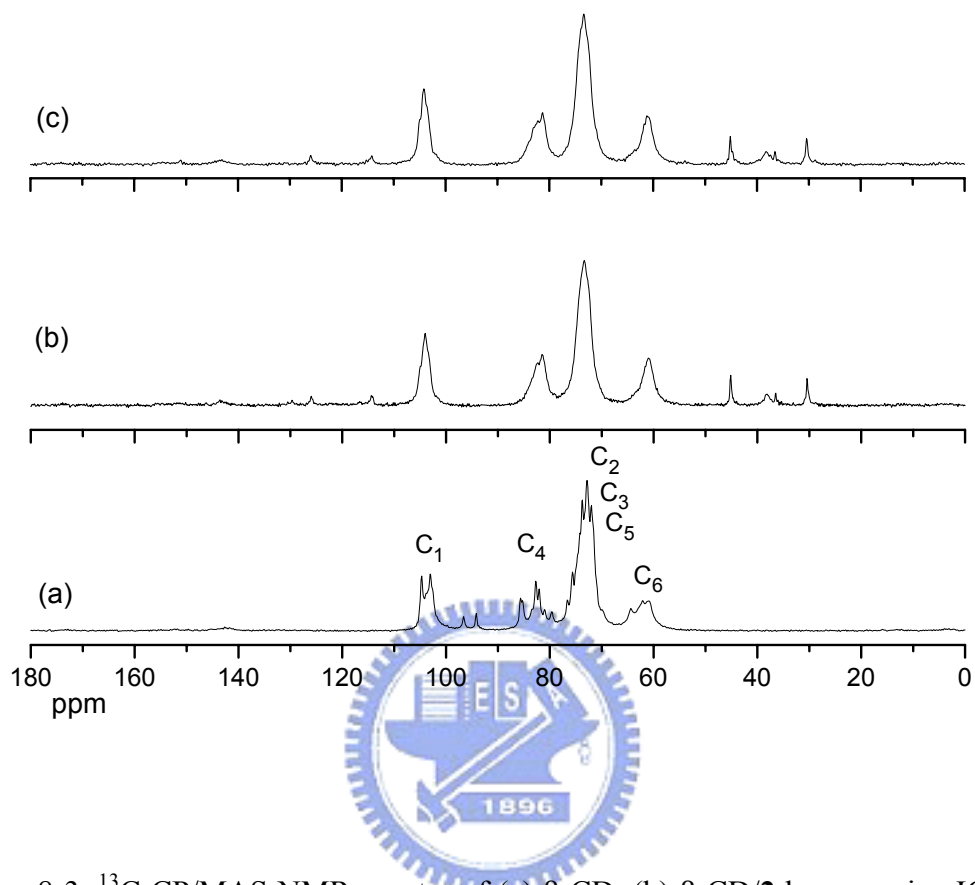


Figure 8-3. ^{13}C CP/MAS NMR spectra of (a) β -CD, (b) β -CD/2 benzoxazine IC, and (c) β -CD/3 benzoxazine IC.

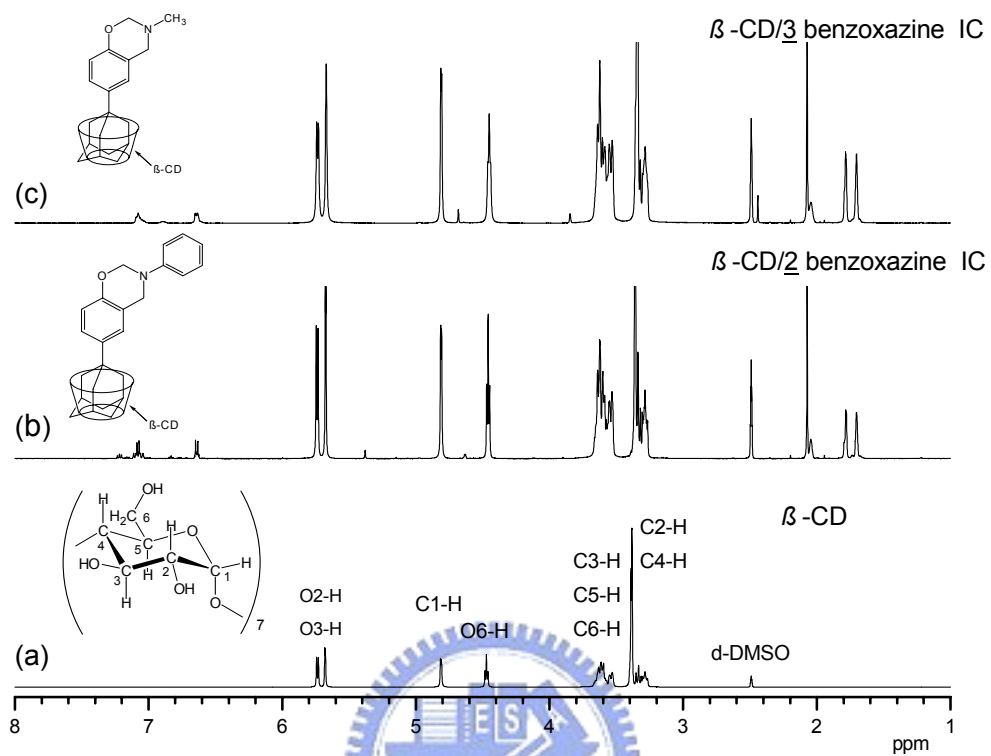


Figure 8-4. ^1H NMR spectra of (a) β -CD, (b) β -CD/2 benzoxazine IC, and (c) β -CD/3 benzoxazine IC.

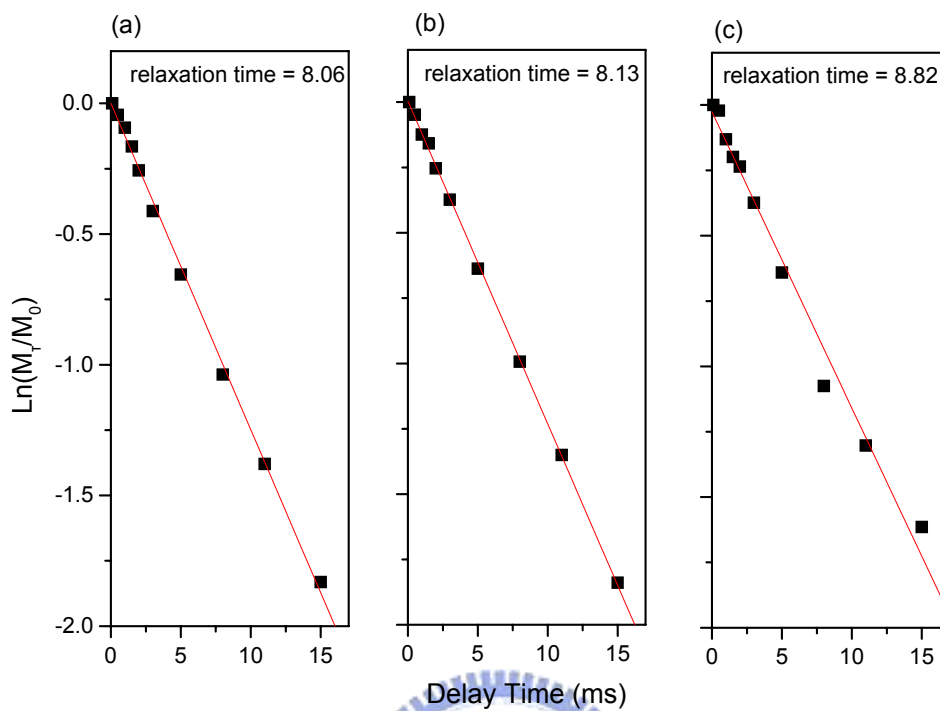


Figure 8-5. Proton $T_{1\rho}^H$ relaxations of (a) β -CD, (b) β -CD/2 benzoxazine IC, and (c) β -CD/3 benzoxazine IC.

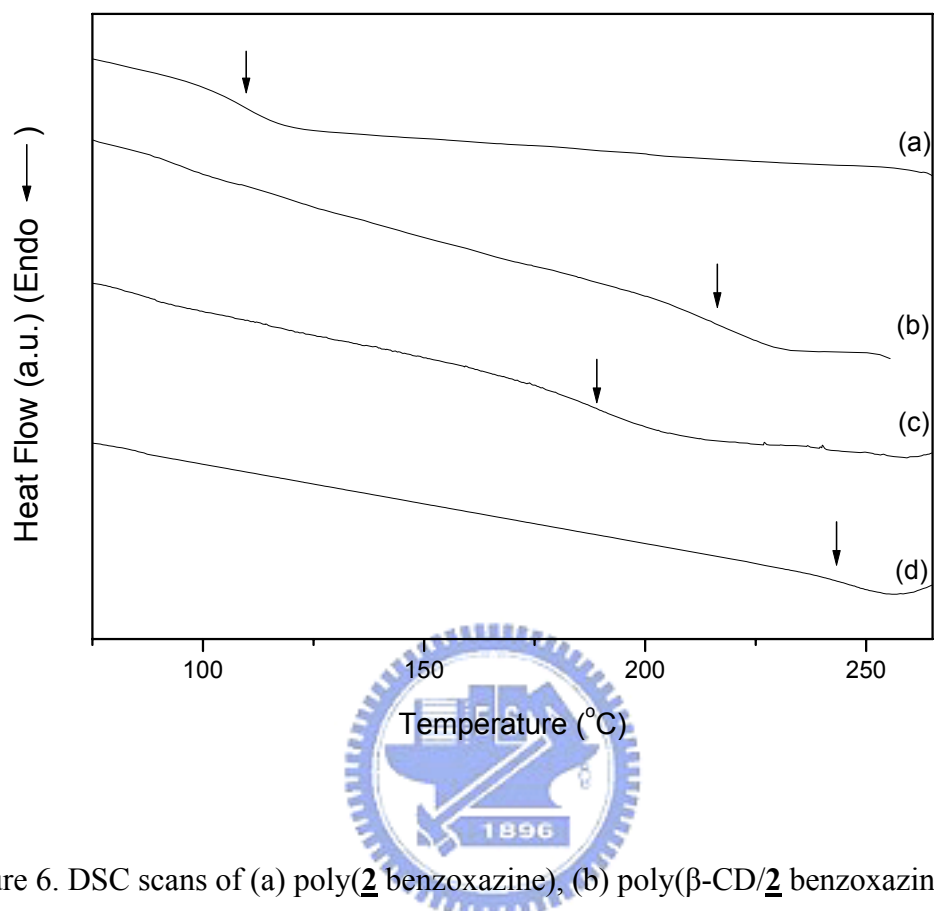


Figure 6. DSC scans of (a) poly(2 benzoxazine), (b) poly(β -CD/2 benzoxazine IC), (c) poly(3 benzoxazine), (d) poly(β -CD/3 benzoxazine IC).

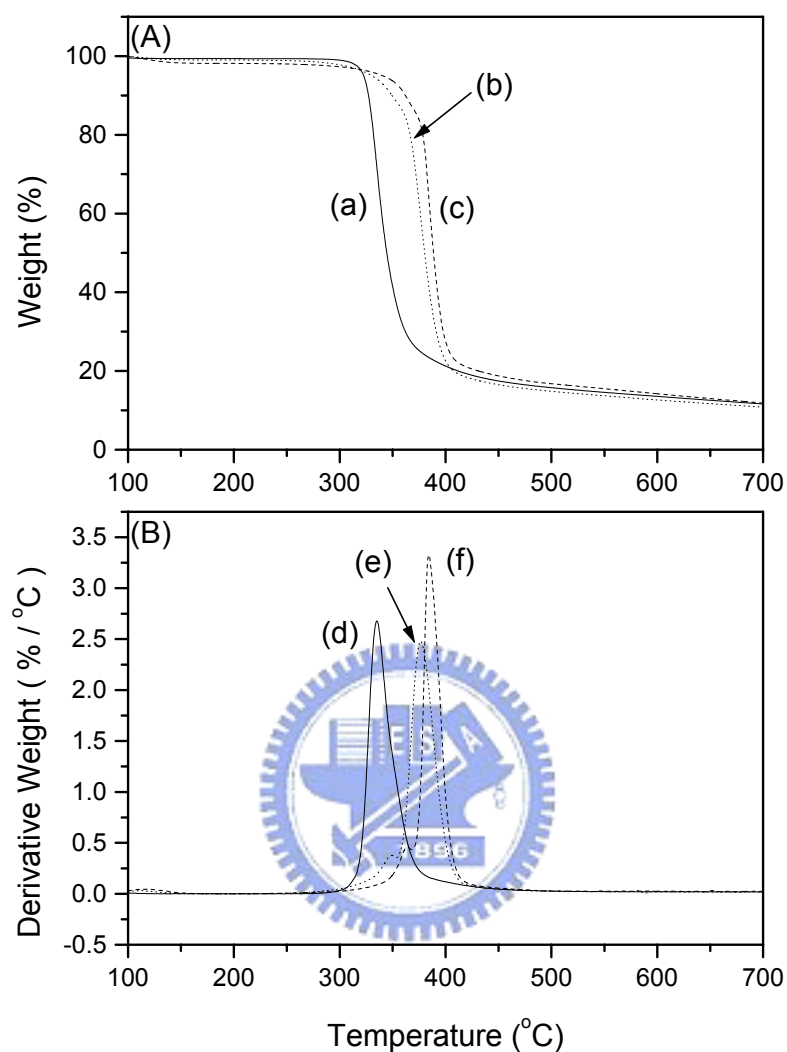


Figure 8-7. (A) The TGA trace of (a) β -CD, (b) poly(β -CD/2 benzoxazine IC), and (c) poly(β -CD/3 benzoxazine IC). (B) Plots of derivative weight per degree C of (d) β -CD, (e) poly(β -CD/2 benzoxazine IC) and (f) poly(β -CD/3 benzoxazine IC) under N_2 atmospheres.

Chapter 9

Conclusions and Future Outlook

In the discussion of the thermal properties and hydrogen bonding behavior of PBZZ (B-a type)/PVP blends. The PBZZ is completely miscible with PVP in the amorphous phase and results in T_g positive deviation based on Kwei equation over entire compositions mainly due to formation of hydrogen bonding between PBZZ hydroxyl and PVP carbonyl. The strength of hydrogen bonding interaction is in the order of inter-association between the hydroxyl group of PBZZ and the carbonyl group of PVP ($K_A=594 \text{ Lmol}^{-1}$) > self-association between the hydroxyl group of pure PBZZ ($K_B=72.6 \text{ Lmol}^{-1}$) > inter-association between the hydroxyl and the Mannich-based bridge of pure PBZZ ($K_C < 10 \text{ Lmol}^{-1}$).

In the discussion of the thermal properties and curing behavior of B-a type and P-a type co-PBZZ, the copolymer gives a single glass transition temperature and the T_g depends upon ratio of B-a/P-a benzoxazine, curing temperature and curing time. The isothermal curing process of the co-PBZZ precursor involves an autocatalytic type curing mechanism. In the dynamic experiments, the activation energy is 72.11 KJ/mol based on Kissinger method and 84.06 KJ/mol based on Flynn-Wall-Ozawa method. Furthermore, in the isothermal experiments, the activation energy and Arrhenius preexponential are 50.3 KJ/mol and 7959 based on Kamal method, and the total order of reaction is between 2.66 and 3.03, depending on the isothermal curing temperature.

In this preparation of low dielectric constant materials, we have synthesized a series of co-PBZZ with different B-a/F-1 (fluorinated PBZZ) ratios. A large positive deviation based on Kwei equation in the T_g versus composition diagram, implies that strong hydrogen bonding interactions exist within B-a/F-1 co-PBZZ. The fluorination

on PBZZ is able to reduce dielectric constant and increase thermal properties. The co-PBZZ with B-a/F-1=1/1 gives low dielectric constant at 2.36 and $\tan \delta$ at 0.0044. Furthermore, we have also developed a new class of nanoporous PBZZ material that has a substantially lower dielectric constant by using the pa-PCL as the labile constituent. FE-SEM images show that the labile polymer micro-phase separates in the PBZZ matrix with domain sizes that depend upon the molecular weight of pa-PCL used. These pores were generated when the pa-PCL was eliminated by hydrolysis of the pa-PCL/PBZZ copolymer. These porous materials have dielectric constants, relative to that of the virgin PBZZ (3.56), that are as low as 1.95 at 10^5 Hz and 298 K.

In the preparation of polypseudorotaxanes, two novel adamantane-modified benzoxazines (2 benzoxazine and 3 benzoxazine) were synthesized from 4-(1-Adamantyl)phenol, and β -CD forms stoichiometric complexes with 2 benzoxazine and 3 benzoxazine. This is a new finding that the β -CD is able to form a complex with adamantane-modified benzoxazine. X-ray diffraction and solid-state ^{13}C CP/MAS NMR spectroscopic studies indicate that the IC domains of the resulting polypseudorotaxanes have channel-type structures even through the ring opening curing process occurred at high temperature. DSC measurements indicate that the inclusion of the adamantane-modified benzoxazines into β -CD units results in stiffer of the main chains and, thus, higher glass transition temperatures. TGA analyses also indicate that the thermal stability of the inclusion complexes is enhanced.

In the future, we will extend controlled free radical polymerization on block copolymer synthesis based on thermoplasting polymer-*block*-thermosetting polymer (poly(polybenzoxazine), such as PMMA-*b*-poly(polybenzoxazine), PS-*b*-poly(polybenzoxazine), and PHEMA-*b*-poly(polybenzoxazine). In the PMMA-*b*-poly(polybenzoxazine) system, a series block copolymers were synthesized

in sequence including PMMA-*b*-PAS (poly(4-Acetoxy styrene)), PMMA-*b*-PVPh (poly(4-vinylphenol)), PMMA-*b*-polybenzoxazine, and PMMA-*b*-poly(polybenzoxazine). A detail discussion will be made in the next study. Furthermore, a very low surface energy was observed in the cured PBZZ surface after an appropriate curing temperature and curing time. The surface energy of PBZZ could be dropped even lower than the one of Teflon. The detail studies of morphologies and surface compositions will also be made, and it will benefit us to understand why the PBZZ surfaces possess such low surface energy property and extend its applications.



List of Publications

1. **Yi-Che Su**, Shiao-Wei Kuo, Ding-Ru Yei, Hongyao Xu, and Feng-Chih Chang ”*Thermal Properties and Hydrogen Bonding in Polymer Blend of Polybenzoxazine/Poly (N-vinyl-2-pyrrolidone)*”, *Polymer*, **2003**, *44*, 2187-2191.
2. **Yi-Che Su**, and Feng-Chih Chang “*Synthesis and Characterization of Fluorinated Polybenzoxazine Material with Low Dielectric Constant*”, *Polymer*, **2003**, *44*, 7989-7996.
3. Dar-Jong Lin, Ching-Chung Chen, Cheng-Liang Chang, **Yi-Che Su**, and Liao-Ping Cheng “*Observation of Nano-Particles in Silica/poly(HEMA) Hybrid by Electron Microscopy*”, *Journal of Polymer Research*, **2002**, *9*, 115-118.
4. **Yi-Che Su**, Ding-Ru Yei, and Feng-Chih Chang ”*The Kinetics of B-a and P-a Type Copolybenzoxazine via Ring Opening Process*”, *Journal of Applied Polymer Science*, **2004**, accepted.
5. **Yi-Che Su**, Wan-Chun Chen, and Feng-Chih Chang ”*Investigation of Thermal Properties of Novel Adamantane-Modified Polybenzoxazine*”, *Journal of Applied Polymer Science*, **2004**, in press.
6. Ding-Ru Yei, Shiao-Wei Kuo, **Yi-Chi Su**, and Feng-Chih Chang “*Enhanced Thermal Properties of PS Nanocomposites formed from Inorganic POSS-Treated Montmorillonite*”, *Polymer*, **2004**, *45*, 2633-2640.

7. Yuan-Jyh Lee, Shiao-Wei Kuo, Yi-Chi Su, Jem-Kun Chen, and Feng-Chih Chang
“Syntheses, Thermal Properties, and Phase Morphologies of Novel Benzoxazine Functionalized with Polyhedral Oligomeric Silsesquioxane (POSS) Nanocomposites”, *Polymer*, **2004**, accepted.
8. Yi-Che Su, Wan-Chun Chen, and Feng-Chih Chang *”Preparation and Characterization of Polyseudorataxanes Based on Adamantane-Modified Polybenzoxazines and β -Cyclodextrin”*, *Polymer*, revised.
9. Yi-Che Su, Wan-Chun Chen, Kai-Lin OU, and Feng-Chih Chang *”Study of the Morphologies and Dielectric Constants of Nanoporous Materials Derived from Benzoxazine-Terminated Poly(ϵ -caprolactone)/Polybenzoxazine Copolymers”*, *Chem. Mater.*, submitted.
10. Yi-Che Su, Chih-Feng Huang, Wan-Chun Chen, and Feng-Chih Chang
“Synthesis and Thermal Properties of Miscible Block Copolymer: Poly(methyl methacrylate)-block-Poly(4-vinylphenol) via Atom Transfer Radical Polymerization”, in preparation.
11. Chih-Feng Wang, Yi-Che Su, Feng-Chih Chang *”Evolution of Surface Free Energy during Polymerization of Polybenzoxazine”*, in preparation.



Introduction to Author

English name: Yi-Che Su

Chinese name: 蘇一哲

Birthday: 1976 March 1

Address: No.75, Dexie Rd., Yanpu Shiang, Pingtung County 907, Taiwan (R.O.C.)



Education:

1995.09~1999.06 **B.S.**, Department of Chemical Engineering, Tam Kang University, Taipei, Taiwan.

1999.09~2001.06 **M.S.**, Department of Chemical Engineering, Tam Kang University, Taipei, Taiwan.

2001.09~2004.09 **Ph.D.**, Institute of Applied Chemistry, National Chiao Tung University, Hsinchu, Taiwan.

